THE COORDINATION OF MOVEMENT FROM MOTOR UNITS TO MUSCLE SYNERGIES

by

DANIEL FRANCIS FEENEY

B.S., University of Delaware, 2012

M.S., University of Delaware, 2015

A thesis submitted to the

Faculty of the Graduate School of the

University of Colorado in partial fulfillment

of the requirement for the degree of

Doctor of Philosophy

Department of Integrative Physiology

2018

This thesis entitled:
The coordination of muscle force from motor units to muscle synergies
written by Daniel Francis Feeney
has been approved for the Department of Integrative Physiology

Roger M. Enoka, Ph.D., Committee Chair

Alaa Ahmed, Ph.D

Rodger Kram, Ph.D

Francois Meyer, Ph.D

Alena Grabowski, Ph.D

Date

The final copy of this thesis has been examined by the signatories, and we find that both the content and the form meet acceptable presentation standards of scholarly work in the above mentioned discipline.

IRB protocol # 14-0356, 15-0568, 15-0719, 16-0782, 17-0064

Abstract

Feeney, Daniel Francis (Ph.D., Integrative Physiology)

The coordination of muscle force from motor units to multijoint synergies

Thesis directed by Professor Roger M. Enoka

This dissertation comprises computational and experimental studies that examined the neuromuscular factors underlying differences in manual dexterity and mobility in health and disease.

The first two studies developed models of motor unit force production. The first model used a Proportional-Integral-Derivative (PID) control algorithm to activate a pool of motor units to simulate the force trajectory during force-matching tasks. The second model comprised a probabilistic state-space model to estimate the common synaptic input to motor neurons based on the discharge times of action potentials by activated motor units. The state-space model demonstrated superior sensitivity compared with previous models.

The next three studies examined manual dexterity and begin with the use of the state-space model to quantify variability in common synaptic input for young and older adults during isometric contractions, and how this variability related to performance on a pegboard test of manual dexterity. Variability in common synaptic input was significantly associated with the coefficient of variation for force during steady contractions (force steadiness) and with pegboard times in older adults. The source of the force fluctuations was evaluated by comparing force steadiness during voluntary and electrically evoked contractions. Force steadiness was worse for old adults than young adults during voluntary contractions, but there was no difference between age groups during the electrically evoked contractions. Thus, differences in force steadiness must arise from signal transduction in the central nervous system and not the periphery. The plasticity of pegboard performance was examined by comparing peg-manipulation characteristics of persons with multiple sclerosis to healthy controls. Grooved pegboard time for individuals with MS was most associated with the time to select a peg, whereas times for healthy controls were most related to peg transportation and selection.

The last two studies examine the influence of an orthopedic problem (sacroiliac joint dysfunction) on movement patterns. These individuals exhibited a compromised muscle synergy when walking and greater movement asymmetries during a sit-to-stand task.

This dissertation explored how common synaptic input influences force steadiness and manual dexterity, how multiple sclerosis alters manual dexterity, and how individuals with sacroiliac joint dysfunction differ from healthy controls during walking and sit-to-stand tasks.

Dedication

This dissertation is dedicated to my fiancée, Melissa, and my Mom

for without them, I would not be where I am today.

Acknowledgments

A gracious thank you goes to my mentor, Roger Enoka. It has been a great privilege and honor to do my doctoral training in your laboratory, and I am grateful for all that I have learned from you both scientifically and personally. I will never forget your adage, "it is not about the science we do but about enjoying who we are working with."

Thank you to all my lab colleagues for the support and friendship. It has been a great pleasure to work with you over the years. I cherish the many discussions, happy hours, and conferences with you all.

A thank you to my committee members, Drs. Alaa Ahmed, Rodger Kram, Francois Meyer, and Alena Grabowski, the guidance over the years and the intellectual and personal growth you have helped me achieve.

Lastly, thank you to my fiancée, Melissa, for all the adventures we have and will continue to take.

Contents

Tables

Figures

Chapter I

Review of the Literature

Introduction

Movement is the result of coordinated interactions between the nervous system and muscles pulling on the skeleton. Muscles are excited by electrical signals known as action potentials that pass from the central nervous system to muscle fibers, thereby enabling a muscle contraction. The force produced by each muscle is controlled by hundreds of motor neurons, each of which innervate varying numbers of muscle fibers. Furthermore, each motor neuron receives many inputs—both excitatory and inhibitory—from descending centers as well as afferent receptors. The ability to produce force is the result of the cumulative output of these motor neurons and the response of the activated muscle fibers. This relatively simple framework is complicated by the abundant degrees of freedom available to perform any movement. Bernstein (1938) first hypothesized that the infinite degrees of freedom to perform a task pose a challenge to controlling movement and that, "The co-ordination of a movement is the process of mastering redundant degrees of freedom of the moving organ, in other words its conversion to a controllable system."

While it may seem to impose a burden on the nervous system to choose a single combination of activation signals for a given task, the physiological properties of the neuromuscular system determine a convenient pattern of activation predicted by physical laws. Recent evidence indicates that a common signal to all motor neurons innervating a muscle—and possibly synergistic muscles—may be used to simplify the control of voluntary actions. The mathematical and physiological nature of this common signal is still a matter of debate, but eventually could provide the basis for advanced rehabilitation techniques, such as human-computer interfaces to control various devices.

Motor units are the basic force-producing element of the nervous system; as such, they

are critical in controlling voluntary actions. To understand movement, it is necessary to know how the nervous system controls motor unit activity and coordinates the infinite degrees of freedom involved with any task. The goals of this introduction are to describe how motor units are controlled, and in turn how the muscles acting about adjacent joints are coordinated to accomplish activities of daily living, such as hand movements and walking.

1. Motor Units

1.1 Properties of Motor Neurons

A motor unit comprises the dendritic projections of a motor neuron in the spinal cord, its axon projecting to the muscle, and the muscle fibers that it innervates (Liddell and Sherrington, 1925; Duchateau and Enoka, 2011; Heckman and Enoka, 2012). Because motor neurons integrate many synaptic inputs received by its dendrites and send a final signal to the muscle, the motor unit is known as the "final common pathway" in the production of muscle force (Liddell and Sherrington, 1925; Duchateau and Enoka, 2011). The force generated by a muscle is modulated by the number of motor units that are recruited and the rates at which they discharge action potentials (Adrian and Bronk, 1929; Bigland and Lippold, 1954; Monster and Chan, 1977; Heckman and Enoka, 2012).

The nervous system controls muscle force by providing inhibitory and excitatory inputs to motor neuron pools. Motor neurons receive thousands of synaptic inputs on their dendrites that are conducted and integrated at the trigger zone, which is located near the soma. The net synaptic current is the sum of excitatory and inhibitory currents received by the neuron and ultimately determines when it discharges an action potential. Once voltage threshold is exceeded, an action potential is generated at the axon hillock (distal to the soma) and propagates along the axon to the neuromuscular junction where it engages the processes involved in excitation-

contraction coupling and elicits a subsequent muscle contraction.

Morphological features common to all motor units allow for the effective transmission of the activation signal from the nervous system to the muscle. The nucleus of a motor neuron is surrounded by a lipid bilayer that is well suited for storing a potential difference, which establishes the resting membrane potential. The input conductance of the neuron (g_{in}) quantifies the ability of a neuron to conduct current, and is a function of both the density of ion channels and the size of the neuron (Heckman and Enoka, 2012). Ohm's Law describes the relation between potential difference (V_m) across a capacitor (the membrane), synaptic current (I), and the input conductance of a neuron:

$$V = \frac{I}{g_{in}} \quad (1)$$

Because input conductance varies as a function of neuron size, smaller neurons experience a greater change in membrane potential in response to a given synaptic current.

The motor neurons within a given motor nucleus exhibit a wide range of physiological features. Burke and colleagues characterized the physiological properties of alpha motor neurons innervating hindlimb muscles in anesthetized cats. A laminectomy was performed on the cats, and an intracellular electrode was used to stimulate single ventral root filaments. Using intracellular stimulation electrodes and strain gauges on the appropriate tendons, they found larger diameter neurons have faster axonal conduction velocities, longer afterhyperpolarization durations, and greater input conductance when compared with small neurons (Burke, 1967; Burke and Tsairis, 1973). Burke and colleagues also classified motor units into three distinct types based on fatigability and sag. Units were first classified by the shape of their unfused tetanus; if the force output of the unit did not increase monotonically to stimuli delivered at 1.25

x the contraction time of the motor unit, the unit was said to exhibit "sag," and was classified as a fast-twitch unit. Units that did not exhibit sag were classified as slow twitch. The fast-twitch units were further differentiated with a fatigability protocol, where units were stimulated for 6 min at 40 Hz for 330 ms. Units with a greater decline in force (below 25% initial force) were classified as fast-to-fatigue (type FF) and units with a lesser decline were classified as fatigue resistant (type FR) (Burke, 1967; Burke et al., 1973; Burke et al., 1974). Contrary to this classification scheme, the analysis of motor unit force as a function of twitch contraction time (Burke and Tsairis, 1974) and the distributions of twitch torque within a motor nuclei (Van Cutsem et al., 1997) indicate that motor units have a continuous distribution of twitch characteristics that does not allow for classification into distinct fast, slow, or fatigable units (Macefield et al., 1996; Heckman and Enoka, 2012). Rather, the more precise approach is to characterize motor units based on recruitment threshold and twitch force.

The synaptic current required for motor neurons to begin and sustain discharging action potentials depends on the physiological characteristics of the neurons. Individual motor neurons will begin discharging action potentials at irregular intervals once a minimal current specific to the neuron—known as rheobase—is reached (Gustafsson and Pinter, 1984). The rheobase of a neuron increases with neuron size and is inversely proportional to afterhyperpolarization duration, indicating that smaller neurons are recruited at lower currents and initially discharge action potentials at lower rates (Gustafsson and Pinter, 1984). As the current increases, motor neurons discharge action potentials at an increasing and less variable rate (Person and Kudina, 1972). Kernell and Monster (1981) found that the current required to maintain repetitive discharge for individual motor units is greater for larger neurons that innervate the medial gastrocnemius muscle of cats. These physiological properties indicate that the activation of

motor neurons in response to synaptic currents varies as a function of neuron size.

1.2 Properties of Motor Nuclei

The motor nucleus consists of all motor neurons innervating a single muscle and the cumulative activity of these neurons ultimately determines the force output. The neurons in a motor nucleus are found within a relatively limited region in the ventral horn of the spinal cord and are topographically close to motor nuclei of synergistic muscles (Dasen et al., 2003; Demireva et al., 2011). The contractile properties of the motor units associated with a motor nucleus range from slow contracting and weak to fast contracting and strong (Van Cutsem et al., 1997; Heckman and Enoka, 2012). Whereas a motor nucleus refers to the group of motor neurons within the spinal cord innervating a single muscle, a motor unit pool also includes the muscle fibers associated with the motor nucleus.

The locations of motor neurons within the spinal cord is linked to the position of its synaptic target (Dasen et al., 2003; Demireva et al., 2011). Animal models demonstrate that the motor neurons for muscles that produce specific biomechanical functions cluster within the same transverse location of the spinal cord and their axons are contained within 2-3 adjacent dorsal roots. The motor nuclei for trunk muscles cluster medially within the ventral horn of the spinal cord, whereas those of the extremities are located more laterally. Genetic disruption of the beta- and gamma-catenin proteins scramble the spinal location of the neurons in a mouse model and causes motor impairments in rats (Demireva et al., 2011). This finding indicates that catenin proteins act as surface adhesion receptors for functionally linked motor neurons, and the motor nucleus is clustered within a close region of the spinal cord.

Motor nuclei contain from 90 to 4,150 motor neurons that innervate the constitutive fibers of a muscle (Feinstein et al., 1955; Jenny and Inukai, 1983). The innervation number for

motor units varies exponentially within a muscle, with the majority of units innervating few muscle fibers. The specific number of muscle fibers innervated by the i^{th} motor unit can be estimated by the exponential function:

$$IN_i = a * e^{\frac{\ln(R)}{n} * i} \quad (2)$$

where IN_i is the innervation number of the i^{th} motor unit, a is the innervation number for the smallest motor unit, R is ratio of innervation numbers for largest to the smallest unit, and *n* is the total number of motor units. Equation 2 indicates that most motor units exert lower torques due to smaller innervation numbers, and relatively few motor units produce large torques (McPhedran et al., 1965; Milner-Brown et al., 1973; Monster and Chan, 1977).

Muscle force gradation is modulated by increasing or decreasing the amount of net synaptic current sent to the motor nucleus, which recruits more motor units and increases the rate at which they discharge action potentials with greater synaptic current. When individuals repeated isometric contractions, Pennybacker and Denny-Brown (1938) found the recruitment order of two motor units was relatively invariant and hypothesized that motor units are recruited in a fixed order. Subsequently, Henneman (1957) examined the recruitment order of motor axons when stimulating the ventral roots of spinal nerves in cats to evoke reflexes that were observed in the dorsal roots. He analyzed the current required to excite individual motor axons and found that neurons were recruited in order of increasing action-potential amplitude. In subsequent experiments, Henneman and colleagues (1965) found that motor neurons innervating hind limb muscles in cats all exhibited a fixed recruitment order. This observation is known as the Size Principle, indicating that motor neurons are recruited in order of increasing size (Henneman and Olson, 1965; Henneman et al., 1965). The Size Principle implies that low levels of synaptic current selectively activates motor neurons with small innervation numbers, which produce less

force. As the required force increases, so must the net synaptic current in order to recruit motor units with greater force-generating capabilities. This physical principle provides a physiologically feasible method for activating motor units in a controlled order that does not have to be specified by descending signals.

Discharge rate characteristics within a motor nucleus in response to various synaptic inputs remain a matter of debate. Multiple investigators report a direct relation between recruitment threshold and maximal discharge rate; later recruited motor units achieve greater peak discharge rates and earlier recruited units reach a plateau in discharge rates despite an increase in synaptic input (Gydikov and Kosarov, 1972; Monster and Chan, 1977; Van Cutsem et al., 1997; Moritz et al., 2005). The saturation of discharge rate may come from intrinsic cellular factors, such as the progressive loss of driving potential at excitatory synapses on the dendrites or a gradual reduction in membrane resistance, but is unlikely due to extrinsic changes in excitatory drive (Fuglevand et al., 2015). Other studies, however, report an 'onion skin' phenomenon (De Luca et al., 1982; Kline and De Luca, 2015) in which low-threshold motor units always discharge action potentials at greater rates than high-threshold motor units. Some differences between the two sets of observations can be reconciled by considering the different measurement techniques used to record motor unit activity and the tasks that were performed.

1.3 Properties of Motor Units

Similar to the physiological characteristics of motor neurons, the contractile properties of motor units within a given muscle exhibit a range of values. Commonly measured characteristics include twitch force, twitch contraction time, and recruitment threshold. Twitch force is quantified as the transient force output elicited by a single action potential (Stein et al., 1972) and primarily depends on the innervation number of the motor unit (Kanda et al., 1992). Twitch

contraction time is the time from force onset until peak twitch force and depends on the rate of release of Ca^{+2} from the sarcoplasmic reticulum (Lee et al., 1991). Recruitment threshold corresponds to the muscle force at which a neuron begins discharging action potentials repetitively (Burke, 1967; Stein et al., 1972; Desmedt and Godaux, 1977b; Duchateau and Enoka 2011).

Twitch contraction time and twitch force may be experimentally determined using spike-triggered averaging (Stein et al., 1972). Spike-triggered averaging is a two-step process. First, the waveform of an individual motor unit action potential triggers an averaging algorithm. Next, the averaging algorithm extracts the force produced by a single motor unit from the net muscle force. In such an experiment, an individual performs a slow ramp contraction while investigators monitor the discharge of action potentials by a single motor unit. After averaging the force associated with several hundred action potentials, the resulting force profile is analyzed for the characteristics of interest.

The nervous system controls the force a motor unit produces by varying the rate at which it discharges action potentials (Bigland and Lippold, 1954; Duchateau and Enoka, 2011). When the synaptic currents barely exceed voltage threshold, a motor neuron will discharge action potential at rates between 5-15 pps with large standard deviations in the time between successive action potentials (interspike interval). As the synaptic currents increase, discharge rate increases up to a maximal value between 20-70 pps during ramp contractions (Person and Kudina, 1972; De Luca et al. 1982; Van Cutsem et al., 1997), but up to 120 pps during ballistic contractions (Desmedt and Godaux, 1977a). Furthermore, increases in discharge rate are accompanied by a decrease in the standard deviation of the interspike intervals and the temporal summation of twitch responses. The relation between discharge rate (or stimulus frequency) and motor unit

force is sigmoidal, as first reported for motor units in the triceps surae muscle of cats (Kernell et al., 1981), indicating a crucial non-linearity in the input-output characteristics of motor units.

A sigmoidal relation between stimulus frequency and force has also been found for human motor units. Macefield et al. (1996) stimulated individual motor axons in human toe extensors at different frequencies. The investigators used low-voltage pulses at varying frequencies (1-100 Hz) to activate individual motor axons and recorded the evoked forces. Similar to the findings on experimental animals, there was a sigmoidal relation between stimulus frequency and motor unit force. Stimulus frequencies between 5-15 Hz produced the steepest rise in motor unit force with little increase in force above 30 Hz.

1.4 Techniques used to measure motor unit properties

Various techniques are available to study the mechanical and electrical properties of motor units. Intramuscular, subcutaneous, and grid electrodes measure the potential differences between two or more bipolar recording sites. It is possible to record motor neuron output at the neuromuscular junction because the signal is highly preserved from the spinal motor neurons to muscle fibers (Heckman and Enoka, 2012). Adrian and Bronk (1929) were the first to record motor unit action potentials in humans. They did this using bipolar needle electrodes inserted into the triceps brachii muscle. Subsequently, Bigland and Lippold (1954) used a fine wire electrode that was inserted into the belly of the adductor pollicis and abductor digiti minimi muscles. Gydikov and colleagues (1967) modified the fine wire electrode by changing the location of the recording sites and inserted it under the skin, but not into the muscle (subcutaneous electrode). Subcutaneous electrodes detect the activity of superficial motor units, in contrast to intramuscular electrodes, but can be displaced more easily to improve the signal-to-noise ratio.

Although the intramuscular and subcutaneous electrodes can detect the discharge times of action potentials for single motor units, the signal is typically too noisy to identify more than two concurrently active motor units. Beginning with the work of Gydikov et al. (1967), it is now possible to record the activity of many concurrently active motor units with electrodes that contain multiple recording sites (Merletti et al., 2001; Merletti et al., 2009). Such electrodes are known as high-density electrodes and can be placed on the skin over a muscle (surface electrode) or inserted into a muscle (intramuscular electrode) (Negro et al., 2016a). High-density surface electrodes are also known as grid or array electrodes. The signals recorded with high-density electrodes can be analyzed with various algorithms to identify the action potentials associated with different motor units. One such decomposition algorithm uses a semi-automated convolution kernel compensation framework and a blind-source separation algorithm to quantify the times at which the identified motor units discharge action potentials (Holobar and Zazula, 2004; Negro et al., 2016a). Concurrent recordings from up to 20 motor units have been decomposed during a low-force isometric contraction (Farina et al., 2015; Negro et al., 2016a). Nonetheless, grid electrodes can only detect the activity of superficial motor units (Negro et al., 2016b) and some results from high-density recordings contrast (De Luca et al., 1996; Adam and De Luca, 2005) with those obtained using intramuscular electrodes (Carpentier et al., 2001; Erim and De Luca, 1996; Mottram et al., 2005).

1.5 Computational models of motor unit activity

The role of computational models in motor unit physiology is vital, given the inability to study dynamic physiology of motor unit populations in vivo. In 1993, Fuglevand and colleagues published a seminal computational model that captures the relations between motor unit discharge characteristics, surface EMG recordings, and muscle force. The model predicts the

recruitment and discharge times of 120 motor units in response to varying amounts of excitatory drive and derives the net force produced by the activated motor units. The Fuglevand model has three main components: a motor neuron model, motor unit force model, and a model of surface EMG to predict the force output in the first dorsal interosseus. The model was used to examine various hypotheses about the influence of the recruitment and discharge characteristics of motor units and the experimentally observed relations between EMG amplitude and net muscle force. When applying a broad range of recruitment forces (motor units recruited up to 57% MVC force), the simulated EMG-force relation was relatively linear and displayed signal-dependent noise characteristic of experimentally derived EMG-force relations (Heckman and Enoka, 2012).

In the motor neuron model, the level of excitation required to reach the recruitment threshold of individual motor neurons within a pool was based on experimental findings (Kernell and Monster 1981; Gustafsson and Pinter 1984) and resulted in many neurons exhibiting a low threshold current to discharge action potentials and relatively few requiring a high threshold current. Furthermore, the innervation number of these 120 motor units varied exponentially according to equation (2) above. The discharge rate of each neuron was related to its recruitment threshold and a gain that was characterized as a sigmoidal relation between excitatory drive and discharge rate.

The isometric force model linked the motor neuron discharges to motor unit force. As experimental results indicated, motor unit force was expressed as an exponential function in which many motor units produce low forces and few produce high forces (Van Cutsem et al., 1997). An increase in excitatory drive to the population of motor neurons increases the rate at which individual motor neurons discharge action potentials and recruits additional motor neurons. Lastly, the action potentials discharged by a motor neuron were transformed to motor

unit force by modeling each unit as a second-order system with nearly critical dampening (Milner- Brown et al., 1973). The Fuglevand model, therefore, is able to derive the force produced by an entire motor pool in response to given excitatory input.

The surface EMG component of the Fuglevand model is based on the discharge times of the activated motor units. Surface EMG is modeled as the temporal summation of motor unit action potentials. It was necessary to include parameters to model motor unit territory size, location, and propagation velocity of action potentials along muscle fibers that influence the EMG output. Motor unit territories were simulated as random (x,y) Cartesian coordinates with the origin in the middle of the muscle cross section and no fibers laying outside of the cross sectional area of the muscle. As a result, motor unit territories were interdigitated within the muscle. A uniform fiber density was assumed for each motor unit. Each muscle fiber action potential was represented as a dipole and the entire motor unit's action potential was the sum of the constituent dipoles. Furthermore, the conduction velocity of the muscle fiber action potential was estimated from an inverse relation with the motor unit twitch contraction time and ranged from 2.5 to 5 m/s. Because the distance from the recording electrode will influence the amplitude of the signal, the muscle was divided into many isopotential layers where any fiber within a given layer caused a similar potential, but the timing would depend on the conduction velocity of the muscle fiber. The muscle fiber action potentials within each layer were summed creating an element potential, and the output signal was the temporal sum of element potentials. Lastly, the signal was high-pass filtered at 5 Hz to represent the A-C coupling of bioamplifiers (Fuglevand et al., 1993).

Subsequent computational models have extended the Fuglevand model. A computational model by Keenan and colleagues (2005), for example, used the Fuglevand model to examine the

phenomenon of EMG cancellation (Day and Hulliger, 2001). Because motor unit action potentials comprise waveforms with positive and negative phases, some of the information is lost (canceled) when overlapping motor unit action potentials are summed. Keenan et al. (2006) simulated bipolar surface EMG recordings and compared the difference in signal amplitude in EMG when it was summed before and after rectification. Results indicated that EMG amplitude cancellation may reach 62% at maximal contraction intensities (Keenan et al., 2005). Results from this study demonstrate limitations in interpreting surface EMG as an index of muscle activation as well as explain the non-linearity in the EMG-force relation.

In adapting the Fuglevand model to characterize the adjustments in motor unit recruitment and rate coding during fatiguing contractions, Dideriksen and colleagues (2010) added time-varying parameters for twitch force, recruitment, discharge rate, and discharge variability. Key features of the expanded model included a metabolite model, which encodes the build up of metabolites seen in long-duration contractions. The accumulation of metabolites was used as feedback into a proportional-integral-derivative (PID) control algorithm, which adjusted the excitatory drive to match the target force. Metabolite build up impairs the ability of motor neurons to discharge action potentials, requiring the control algorithm to increase the excitatory drive delivered to the muscle to maintain the target force (Dideriksen et al., 2010). The output of this model replicated a number of experimental findings, including time to task failure for a force-matching task with an isometric contraction, the changes in motor unit discharge rates during such a task, and the skewness and kurtosis of interspike interval durations. The findings provided a much more comprehensive analysis of the adjustments in motor unit activity during fatiguing contractions than can be achieved during experimental studies.

Computational models are crucial to physiological research because they allow for

reverse engineering of the physiological results and the comparison with experimental data. These models allow us to extrapolate the recordings from relatively few motor units to the behavior of the entire motor pool. Critically, computational models can identify key gaps in knowledge that require experimental investigation.

2. Common modulation of motor unit discharge rate

Coordinating the large number of motor neurons in a motor nucleus is a demanding task for the nervous system. A common input signal may simplify the challenge. In the first motor unit study on humans, Adrian and Bronk (1929) speculated that a common presynaptic signal could synchronize motor unit discharges and control force output. Since then, others argue that a common input does not cause synchronization of motor unit discharge *times* (Kline and De Luca, 2015). However, a low-frequency common input to motor neurons may cause fluctuations in the discharge *rates* of all the units in a pool (De Luca and Erim, 1994; Negro et al., 2009). Central to this debate is the lack of a clear definition of common input (Boonstra et al., 2016). Furthering the understanding of the physiology and mathematical structure of a common signal will provide critical information for future rehabilitation interventions including human-computer interfaces.

Following early speculation of a common presynaptic input to motor neurons (Adrian and Bronk, 1929), the topic was not explicitly tested for almost 50 years. Since the 1970s, most studies have quantified common input as the degree of correlation or coherence in discharge times between two motor units. In a key early study, Sears and Stagg (1976) compared the discharge times for pairs of motor units in intercostal muscles of anaesthetized cats by recording pre- and post-stimulus time histograms. They hypothesized that the joint occurrence of excitatory post-synaptic potentials in pairs of motor neurons can be attributed to input from "common presynaptic fibers." Pre- and post-stimulus time histograms were constructed using the discharge

time of one neuron as a ‘stimulus’ and the discharge time of another neuron as the ‘response’. The histograms of paired discharges revealed narrow peaks at a time lag of zero, indicating an instantaneous correlation (Sears and Stagg, 1976).

A limitation of this work is the comparison of the discharge times of motor units with similar recruitment thresholds. To broaden the comparison, De Luca and colleagues (1982) used cross-correlation analysis between motor unit discharge rates in the deltoid and in the first dorsal interosseus muscles of humans. Within a given muscle, cross-correlations of discharge rates were greatest at a time lag of zero indicating synchronization of the discharge *rates*. This is a critical distinction because a common signal to all motor units would modulate their discharge *rates* based on physiological properties, such as afterhyperpolarization duration, and not necessarily their discharge *times* (De Luca et al., 1982). Subsequently, De Luca and Erim (1994) speculated that a low-frequency (< 4 Hz) common drive to motor unit discharges could “relieve the CNS from the burden of monitoring and regulating each motor unit separately”. Cross-correlation analysis was also used by Bremner et al. (1991) to examine trains of motor unit discharge times in pairs of motor units in finger muscles, and again a narrow peak with a zero lag was found, suggesting synchronization due to common synaptic inputs. Farmer et al. (1993) found synchronization in the frequency domain by calculating coherence between the discharges of action potentials in pairs of motor units, and again found synchronization in the frequency domain of intrinsic hand muscles (Farmer et al., 1993).

The practicality of a common input signal was limited until methods were developed to quantify it. In order to quantify the strength of the common input signal, Nordstrom and colleagues (1992) defined common input strength (CIS) as the “frequency of synchronous action potentials in the motor unit pair in excess of those expected due to chance” (Nordstrom et al.,

1992). In this framework, a narrow region of a cross correlation histogram was chosen based on the peak cross correlation time. Within this region, the number of synchronous discharges was divided by the average number of discharges at all other times, which created an index of common input strength (Nordstrom et al., 1992). This work was a critical step in quantifying the common input signal, but its reliance on pairs of motor units limits its ability to quantify the common input to a motor nucleus.

A common input could cause low-frequency oscillations of discharge times for the entire motor nucleus, but many early studies were limited by studying the activity of pairs of motor units. The pairwise correlations used in early investigations to assess common input have resulted in a low-to-moderate quantification of the common input to motor neurons (Nordstrom et al., 1992; Farina and Negro, 2015). Farina and colleagues (2009-present) have developed a more rigorous analytical model that quantifies the common input to a pool of motor neurons. In this model, the discharge times of each unit are summed at each instant to create a *cumulative spike train*. The modulation of the discharge times of the cumulative discharge train of action potentials is assumed to be due to *only* the common input signal (Farina et al., 2014; Farina and Negro, 2015). Studies utilizing grid electrodes, which allow for the concurrent tracking of 5-20 motor units, indicate that much of the variability in discharge times of the cumulative spike train can be attributed to a common input signal (Negro et al., 2009; Farina et al., 2014; Negro et al., 2016b). Furthermore, pairwise correlations in motor unit discharge times from the same recordings have high variability (Negro and Farina, 2012), which explains why some studies find low-to-moderate correlation values. Furthermore, a common input signal would affect the entire population of motor units; hence, inferring its existence from pairs of units is inappropriate (Farina and Negro, 2015; Negro et al., 2016ab).

The recent advances in recording motor unit techniques allow for novel investigation of the common input to motor nuclei (Merletti et al., 2009). Farina and colleagues provide a promising step to quantify the proportion of common input to motor pools by defining it as:

$$V_i(t) = \mu + \alpha_i s^c(t) + \eta_i(t), \quad (3)$$

where $V_i(t)$ represents the synaptic current to the i-th motor neuron, μ denotes a constant offset, $s^c(t)$ corresponds to a time-varying input that is common to all motor neurons, α_i, indicates a scaling factor, and $\eta_i(t)$ characterizes independent white noise. The combination of $\mu + \alpha_i s^c(t)$ represents the common input received by all motor units. The scaling factor governs how the i-th motor unit responds to a given synaptic input.

According to this hypothesis, each motor neuron receives three inputs: a common signal, common synaptic noise, and independent synaptic noise. Due to the non-linear input-output properties of motor neurons, the response of a pool of motor neurons receiving a shared common input and independent synaptic noise will preferentially contain the common input signal while the independent noise is cancelled out (Farina et al., 2014; Farina and Negro, 2015). In such a model, independent synaptic noise is filtered by the motor neurons, and the signal sent to the muscle corresponds to the effective neural drive (Farina et al., 2014). In theoretical derivations and computational simulations, the common input strength is quantified as the square root of the ratio of coherence between the input signal provided to the pool of neurons and the cumulative discharge train (Negro et al., 2016). This biophysical model was validated with experimental data from abductor digiti minimi, vastus medialis, and tibialis anterior muscles, and revealed that the much of the signal sent to motor neurons within a muscle could be attributed to a common input (Negro et al., 2009; Farina and Negro, 2012; Farina and Negro, 2015; Negro et al., 2016).

The common modulation of motor unit discharge rates or the times of the cumulative spike train is related to the force produced by the muscle (Negro et al., 2009; Farina and Negro, 2015; Negro et al., 2016b). When subjects attempt to maintain a steady submaximal force, for example, most of the variance in the force can be explained by the oscillations of motor unit discharge rates (Negro et al., 2009). When tracking a sufficient number of motor units, over 70% of the variance in force fluctuations is explained by changes in the common input signal. In this way, the pool of motor neurons acts as an effective linear filter of the independent noise resulting from noisy ion channels or random synaptic fluctuations (Katz and Miledi, 1970). High-density surface EMG recordings from tibialis anterior at three target forces (20, 50, and 75% maximal voluntary contraction) revealed an increase in the proportion of common synaptic input to motor neurons with an increase in target force (Castronovo et al., 2015). Critically, pairwise correlations of motor units with differing recruitment thresholds from the same set of data did not display a high coherence. Consistent with the common input signal being the *only* signal important in modulating the cumulative discharge train, Negro and colleagues (2016) conclude that motor neurons perform fast averaging of the synaptic inputs and the independent synaptic noise does not influence the accuracy of the output force (Negro et al., 2016). While these studies provide a promising step in quantify common input strength, it risks tautology (Boonstra et al., 2016) as, by definition, the only signal reaching the muscles is a common signal with an additive noise term. It is difficult to use this framework to explain differences between individuals as increased force fluctuations would be the result of the common input signal.

The practicality of a common input signal has been the subject of debate. Some groups argue that only the effective neural drive is important in force control (De Luca and Erim, 1994; Negro et al., 2009; Farina and Negro, 2015), and that the nervous system could not control motor

neurons without a common signal (Negro et al., 2016). Moreover, synergistic muscles, such as those that comprise quadriceps femoris, share most of their synaptic input (Laine et al., 2015). Alternatively, some groups argue that common input provides no explanation for motor neuron synchronization and would not simply force control (Kline and De Luca, 2015).

Boonstra et al. (2016) suggest that the field needs to agree on a uniform definition of common input that includes the physiological properties of motor pools. They propose the following biophysical model to describe the discharge characteristics of a pool of neurons:

$$C\frac{dV_i}{dt} = -g_i(V_i-E_i) + v_i(t) + \alpha\Sigma_j c_{ij}F(t,t_i) + \eta_i(t) \quad (4)$$

where V_i is the membrane potential for the i-th motor neuron with conductance *g*, the total synaptic current is represented by $v_i(t)$, E represents the Nernst potential, C corresponds to a coupling matrix, F indicates a low-pass filter function for the dendritic filtering of motor neurons, c_{ij} represents the influence of presynaptic neurons (j) on postsynaptic motor neurons (i), α denotes a scaling factor for the total sum of all synaptic currents from the dendrites into the soma, and $\eta_i(t)$ represents the individual noise that each neuron receives. This biophysical model includes key physiological properties of the motor neurons that would modulate the discharge rates. If the summed inward synaptic current exceeds the leak current, the membrane will depolarize and discharge an action potential.

There are limitations to studying a higher dimensional common input to pools of neurons using second-order statistics. Pairwise correlations (Sears and Stagg, 1976; De Luca et al.,1982, 2016) and principal component analysis (Farina et al., 2009-2016) cannot reveal the specific higher dimensional structure of a common signal. Novel research on the statistical structure of discharge characteristics in neural circuits in the brain reveals a more complex structure that

cannot be expressed with second-order statistics. Macke and colleagues have developed several statistical models that characterize discharge characteristics in neural networks. One such model that appears superior to previous generalized linear models is a Poisson linear dynamical systems (PLDS) model (Macke et al., 2011; Buesing et al., 2012; Archer et al., 2014). The PLDS model effectively replicates the interconnectivity of neurons in the primary visual cortex of cats and macaque monkeys. This group investigated the mathematical structure of the underlying common input to neurons and developed the following model: the discharge times [y(t)] of n-neurons [i = 1…N] is parameterized as a Poisson point process achieved by using the discharge rate, λ, as the time-varying intensity of the process.

$$\lambda_i(t) = e^{z(t)} \tag{5}$$

$$z(t) = Cx(t) + D\, y(t-1) + \mu \tag{6}$$

where x(t) is a d-dimensional vector (with d < n) that represents the latent common input. C denotes a d x n matrix that encodes the effects of the latent input on each individual neuron. This matrix models the relevant physiological properties, such as input conductance and afterhyperpolarization duration. D corresponds to an n x n matrix that models the effects of coupling between neurons and μ is the logarithm of the average discharge time.

$$x(t) = A\, x(t-1) + u\, S(t) + e(t) \tag{7}$$

where A is a d x d matrix that indicates how the latent state progresses through the trial, uS(t) encodes a time-varying component such as force level of stimulus intensity, and e(t) is a zero-mean Gaussian noise vector that models synaptic fluctuations (Macke et al., 2011; Buesing et al., 2012; Archer et al., 2014).

Macke and colleagues validated this novel method of neuron connectivity using animal

models (Archer et al., 2014). A 96-electrode array was placed over the motor cortex of a behaving monkey and the discharge characteristics of cortical neurons was recorded during a reaching task. Using a Poisson linear dynamical system (PLDS) model and a 5-dimensional latent state, they were able to effectively capture the underlying inputs. All trials revealed a zero peak in the correlation between the real data and the PLDS model.

This linear dynamical systems model may be adapted to motor neurons by eliminating the D y(t-1) term and utilizing uS(t) to encode the effects of the target force on the discharge rate of the neurons. With the development of high-density electrodes, the shared variability in discharge rates is dominated by a central peak with zero lag, which indicates the level of synchrony in discharge rates. Such a correlation is natural for a dynamical system and allows for modeling of physiological parameters (Boonstra et al., 2016). The method required to solve and optimize an underdetermined set of equations is referred to as Expectation Maximization (EM) algorithms. Critically, this framework explicitly delineates the common input signal as well as the signal-to-noise ratio, and could provide an explanation for individual differences in the strength of the common input signal.

Few actions of daily living require the activation of only one muscle, and it may be possible to control synergist muscles with the same control signal. Laine et al. (2015) quantified the common input to synergist quadriceps muscles by finding the pooled coherence of detected motor units. Similar to previous findings, there was a peak with virtually no lag indicating that synergistic muscles may share a common signal. This is critical in the control of movement on a larger scale. A knee-extension task involves all the quadriceps muscles as well as synergist muscles, so it is feasible that the control of a multiple muscles is accomplished with a common signal. Moreover, the proximity of the motor neurons innervating synergistic muscles within the

spinal cord facilitates the distribution of such a control signal (Demireva et al., 2011).

Coordinating the discharge rates of motor pools is an important control problem to understand and has direct physiological relevance. Farina and colleagues have found that variations in the common control signal are directly related to the low-frequency force oscillations when an individual is asked to produce a steady force during an isometric contraction (Negro et al., 2009; Farina and Negro, 2015; Negro et al., 2016b). The amplitude of these force oscillations during steady contractions is predictive of the time to complete a test of manual dexterity (Marmon et al., 2011a, Almuklass et al., 2016a). It follows that the common modulation of discharge rates may be crucial for performing activities of daily living.

3. Coordination and variability in manual dexterity and walking

The NIH Toolbox is a validated set of tests that quantify neurological health and function across the lifespan in four domains: motor, cognitive, emotional, and sensation (Gershon et al., 2010; Reuben et al., 2013). Motor function is quantified with tests of dexterity, strength, balance, locomotion, and endurance. Manual dexterity is essential for accomplishing activities of daily living, such as eating, writing, and interacting with an increasingly digital environment. The NIH Toolbox quantifies manual dexterity as time to complete a 9-hole pegboard test (Gershon et al., 2010). Walking is also integral to maintaining a high quality of life and independence, and is quantified with the 4-m walk test (locomotion) and the 2-min walk test (endurance). Both dexterity and walking ability decline with healthy aging as well as in disease or injury states. The ability to coordinate motor pools and the larger scale coordination of limbs is central in the performance of these tasks as well as maintaining a high quality of life.

3.1 The relation between dexterity, force steadiness, and common input

The NIH Toolbox defines dexterity as "the coordination of small muscle movements which occur in body parts, such as the ability to coordinate fingers to manipulate objects quickly and accurately." Such actions require the coordination of the motor units responsible for the requisite muscle contractions. The primary measure of dexterity in the NIH Toolbox is the time to complete a 9-hole pegboard test (Gershon et al., 2010). A more sensitive measure is the Lafayette grooved pegboard test, which requires the insertion of 25 key-shaped pegs into randomly oriented key shaped holes (Wang et al., 2003). Performance on the Lafayette grooved pegboard test improves from age 3 yrs until approximately 30 yrs, after which it gradually declines with a sharp drop after 75 yrs (Ruff and Parker, 1993; Wang et al., 2011). Moreover, a longitudinal study of 128 elderly women revealed that pegboard test performance explained 51% of the variance in the women's residential living situation (i.e., nursing home, retirement home, or living in the community) (Ostwald et al., 1989), which underscores the importance of dexterity tests as a measure of health status. Lawrence et al. (2015) used principal component analysis (PCA) to decompose the results of 6 tests of manual dexterity to identify subdomains of dexterity. Older adults who were healthy (n = 66) or had osteoarthritis (n = 33) performed each of the tests. Three identified latent domains explained 90% of the covariance in the tests of dexterity (Lawrence et al., 2015). Consistent with multiple-regression studies on hand function, the latent domains were made up of indices of muscle strength (Marmon et al., 2011), force steadiness (Marmon et al., 2011; Almuklass et al., 2016), and pegboard performance (Ruff and Parker, 1993; Wang et al., 2003), indicating these are key markers of health and function.

Manual dexterity and the ability to maintain a steady, submaximal force during an isometric contraction are closely linked (Marmon et al., 2011a; Almuklass et al., 2016). Force steadiness is defined as the oscillations about a submaximal target force during an isometric

contraction, and is quantified as either the standard deviation or the coefficient of variation of these oscillations with respect to the mean force. Multiple-regression models indicate that an index of force steadiness is a key predictor of pegboard performance for young and old adults (Marmon et al., 2011, Almuklass et al., 2016). Galganski and colleagues (1993) found that young adults have superior force steadiness (lower fluctuations) compared with older adults, at least for the first dorsal interosseus muscle. Force steadiness is directly correlated with grooved pegboard times in old adults, which indicates force steadiness is crucial in the ability to finely manipulate objects (Marmon et al., 2011a). In contrast, young adults who exhibit superior force steadiness perform more slowly on the pegboard test, which may indicate a decision-making strategy of placing greater emphasis on accuracy than speed (Almuklass et al., 2016).

There is a direct link between indices of force steadiness and of the common input signal to the motor pool (Negro et al., 2009; Farina and Negro, 2015). Negro and colleagues showed that the force fluctuations during a steady contraction are primarily determined by a common input signal to the motor pool (Negro et al, 2009; Farina and Negro, 2015). Due to the association between force steadiness and dexterity, it is likely that changes in the common input signal to motor neurons may influence dexterity. In a seminal demonstration of the importance of common modulation of motor unit discharge in force production, Negro et al. (2016a) decomposed (Holobar and Zazula, 2007) the discharge times of ~200 motor units using kernel decomposition of recordings obtained with high-density grid electrodes. The discharge times of the motor units were combined into a cumulative spike train and smoothed with a 400-ms Hanning window. A principal component analysis performed on the cumulative spike train found that the first principal component explained 70% of the force fluctuations during a steady isometric contraction (Negro et al., 2009). As a result, force steadiness may be analyzed as a

proxy for the fluctuations within the common input signal. Furthermore, the relation between dexterity and force steadiness suggests that increases in the common input signal may contribute to declines in dexterity.

Multiple sclerosis (MS) is a neurological disorder that degrades the myelin sheath surrounding the axons of neurons, resulting in impairments in both sensory and motor signal transduction. As a result, 77% of individuals with MS experience problems with manual dexterity (Johansson et al., 2007). Recent work in our lab demonstrated that 78% of the variance in grooved pegboard times for persons with MS could be explained by the time it took to select a peg from the well during the test. This peg-manipulation phase requires tactile discrimination and the ability to exert a steady, low-level force. Given the effects of the disease and the declines in dexterity, it is likely that individuals with MS exhibit greater variability in common synaptic input to motor neurons, however this hypothesis has yet to be tested.

Electrical stimulation can be exploited to probe the source of force fluctuations during isometric force tasks. Jones and colleagues (2002) investigated how the integration of synaptic inputs by motor neurons contributes to the modulation of force steadiness. To do so, they compared the standard deviation of the force fluctuations at a range of target forces during voluntary contractions and those evoked by neuromuscular electrical stimulation (NMES) (Jones et al., 2002). When participants voluntarily matched a force target, the standard deviation for force increased with force level. In contrast, the standard deviation for force remained relatively constant across target forces when the contractions were evoked by eliciting action potential in intramuscular axons with NMES. This demonstrates two key findings; first, force fluctuations remain similar regardless of stimulation intensity when elicited over the muscle due to different distances the current must travel resulting in asynchronous action potentials. Second, a large

portion of force fluctuations observed during voluntary contractions may be attributable to the synaptic inputs received by motor neurons.

The application of NMES over muscles creates a current field that primarily elicits action potentials in intramuscular axons causing muscular contractions. The specific intramuscular axons engaged by electrical stimulation vary based on the intensity of the applied current as well as the pulse duration and frequency of the stimulus trains (Amiridis et al., 2015; Chipchase et al., 2011; Collins, 2007). NMES is often applied under a relatively low current (< 100 mA), with frequency ranges of 40-80 Hz, and pulse durations of 0.2 to 0.5 ms (Colson et al., 2009; Jones et al., 2002; Vanderthommen and Duchateau, 2007). Longer duration pulses— such as 1 ms— likely engage a broader range of sensory fibers in addition to motor fibers, which could result in key differences in force output when only evoked by wide-pulse NMES. The differences in the coefficient of variation for force during contractions evoked by NMES compared with voluntary contractions provides insight into the relative role of common synaptic input. The magnitude of this change may differ between age groups or in certain disease states such a Multiple Sclerosis.

3.2 Motor variability in walking

The decline in walking performance observed with healthy aging and with injury or disease may be the result of changes in the common input signal sent from descending centers to the motor unit pool or in the coordination of the musculoskeletal multi-joint system (Clark et al., 2010). There are many degrees of freedom available to the neuromuscular system to control motor tasks, such as walking (Bernstein, 1967). The classic problem of excessive degrees of freedom concerns how the central nervous selects a particular solution to accomplish a desired movement task.

Muscle synergies are quantified using latent variable analysis to discover underlying patterns in EMG activity (Cappellini et al., 2006; Clark et al., 2010). Clark and colleagues (2010) used non- negative matrix factorization and principal component analysis to decompose the EMG signals during walking from 8 leg muscles of healthy controls and individuals post-stroke. Results indicated fewer factors were needed to explain 90% of the covariance in all EMG signals during a stride in the stroke patients, indicating the use of fewer synergies by these individuals. Furthermore, functional measures of walking performance, such as preferred walking speed, were inversely correlated with the number of observed synergies for individuals (Clark et al., 2010).

A degree of variability is likely beneficial in biological systems to prevent rigidity and injury (Hamill et al., 2012). Individuals with greater motor variability demonstrate faster learning (Wu et al., 2014) and more stability in response to perturbations (Latash et al., 2007); however, too much variability is associated with low accuracy and greater end-point variability (Christou, 2013). Future work should focus on finding the functional relevance of muscle synergies in clinical populations. Studies such as these would not only provide more information in how the nervous system controls movement, but also broaden the clinical scope of variability analyses. If musculoskeletal disorders are associated with disrupted muscle synergies or joint kinematics, it could be possible to treat these conditions by establishing the activation patterns observed in healthy adults.

Conclusion

Successful performance of voluntary actions requires the nervous system to send appropriately scaled motor commands to control the discharge characteristics of motor nuclei that produce the requisite limb kinematics. The nervous system controls the discharge rates of

motor nuclei through a common input signal to motor neurons, which produce variable kinematic outputs. The common input modulates motor unit discharge rates based on their physiological properties, and is responsible for the much of the variance in force during steady submaximal contractions. Relatively simple measurements of force steadiness can explain much of the variance in tasks that involve many degrees of freedom.

Some theories suggest there may be an optimal amount of variability in movement to ensure that the end goal is achieved, but allow for responses to perturbations. Perhaps declines in motor performance with healthy aging or a result of an injury or disease could be due to limited variability in movement patterns. While more work is required to verify this concept, it appears that motor neurons are controlled with a common input signal and the total motor output may be controlled through synergies formed to provide an optimal degree of flexibility and stability.

Chapter II

CONTROL OF FORCE DURING RAPID VISUOMOTOR FORCE-MATCHING TASKS CAN BE DESCRIBED BY DISCRETE TIME PID CONTROL ALGORITHMS

Abstract

To enable precise movements, the nervous system adjusts the neural commands to the muscles to minimize movement error. We hypothesized that the variability in force trajectories during rapid force-matching tasks can be explained by discrete time proportional, integral, derivative (PID) control algorithms with varying parameters. To this end, we analyzed the pinch force trajectories of 24 subjects performing two rapid force-matching tasks with visual feedback. Both tasks involved isometric contractions to a target force of 10% maximal voluntary contraction (MVC). One task involved a single action (pinch) and the other required a double action (concurrent pinch and wrist extension). 50,000 force trajectories were simulated with a computational neuromuscular model whose input was determined by PID controller with different PID gains and frequencies at which the controller adjusted muscle commands. The goal was to find the best match between each experimental force trajectory and all simulated trajectories. It was possible to identify one realization of the PID controller that matched the experimental force produced during each task for most subjects (average index of similarity: 0.87 ± 0.12; 1 = perfect similarity). The similarities for both tasks were significantly greater than what would be expected by chance (single action: $p = 0.01$; double action: $p = 0.04$). Furthermore, the identified control frequencies in the simulated PID controller with greatest similarities decreased as task difficulty increased (single-action: 4.0 ± 1.8 Hz; double-action: 3.1 ± 1.3 Hz). Overall, the results indicate that discrete time PID controllers are realistic models for the neural control of force in rapid force-matching tasks involving isometric contractions.

Introduction

The nervous system enables accurate movements by sending appropriately scaled motor commands to the relevant muscles. To determine the magnitude and timing of these commands, an estimate of the current state of the limbs involved in the task is formed through integration of sensory information and prior experience (Diedrichsen et al. 2010). From this estimate, the difference between the planned movement and the current state (error signal) can be derived to determine the appropriate changes to the motor command required to continue or complete the task (Bays and Wolpert 2007). These voluntary adjustments in the activation signal occur intermittently (Loram et al. 2014) and, in the case of solution redundancy, the set of muscle commands that minimizes the overall effort is selected (O'Sullivan et al. 2009). Exactly how the nervous system determines appropriate adjustments in the motor commands based on the dynamics of the error is uncertain.

An attractive experimental setup for studying this control process is rapid force-matching tasks. In such tasks, the subject receives real-time visual feedback to gauge force errors, thereby making the perceived error highly reliable. Assuming that the level of muscle coactivation is low, which is usually the case in such tasks (Maluf et al. 2005; Rudroff et al. 2010), the target force can only be achieved by one muscle activation pattern with little or no redundancy. This implies that no training is required to learn how to perform the task in the way that minimizes the total effort. The performance in rapid force-matching tasks with visual feedback, therefore, likely reflects the ability of the central nervous system to adjust the motor commands based on the error with minimal bias from differences in the ability to estimate limb state or accommodate cost functions across subjects.

Despite of the simplicity of visually guided force-matching tasks, there is remarkable variability in how such tasks are executed across subjects. One commonly studied feature of these tasks is the ability to maintain a constant force during an isometric contraction. This ability, however, varies substantially even within uniform groups of subjects (Moritz et al. 2005; Tracy et al. 2005; Sosnoff et al. 2006; Almuklass et al. 2016). Because force variability is determined by the common synaptic input to the motor neuron population (Negro et al. 2009; Dideriksen et al. 2012), differences in the coefficient of variation for force directly reflect variations in the ability of the nervous system to maintain stable motor commands. Therefore, any model of the control process must be sufficiently flexible to account for the variability between subjects during force-matching isometric contractions.

We have previously shown that control of force in visuomotor tasks involving isometric contractions can be emulated in a computational model using a discrete time proportional-integral-derivative (PID) control algorithm (Dideriksen et al. 2010; Dideriksen et al. 2012). This algorithm samples the instantaneous difference between the simulated muscle force and the target force (force error) at a fixed frequency in order to scale the output (supraspinal neural drive) to minimize the force error. With this approach, the neural drive to the muscle is represented as a linear combination of the error itself (proportional term), the integrated error, and the first derivative of the error. The gains of each of these three terms (PID gains) determine the characteristics of the simulated force. For example, high gains of the proportional or integral terms imply rapid responses at the expense of overshooting the target and the risk of high steady state variability, whereas high derivative gain minimizes the time it takes for the output to settle to a stable level (Ang et al. 2005). We have shown previously that appropriate selection of PID gains and frequency at which the force error is sampled enable accurate simulations of the

average differences in force variability observed at different target forces (i.e., signal-dependent noise (Jones et al. 2002)) (Dideriksen et al. 2012). It remains unclear, however, if PID control can capture the variability observed in force trajectories across individual subjects.

The goal of the current study was to evaluate the capacity of PID control algorithms with different model parameters to account for the variability observed in the characteristics of experimental force trajectories of different subjects. We reanalyzed experimental force trajectories during two types of force-matching tasks recorded in a previous study (Almuklass et al. 2016) and examined the degree to which they could be replicated by simulations relying on PID controllers. With this approach, we were able to investigate if it is possible to identify one set of model parameters that could provide a simulated force trajectory similar to that of an observed experimental trial. Furthermore, the level of similarity was compared with that expected due to chance. A statistically significant difference between the average similarity index for the PID simulations and the observed experimental recordings with the mean of the probability distribution of similarity indices due to chance would suggest that a PID controller is a realistic representation of force control during rapid force-matching isometric contractions

Methods

The methods used to obtain the experimental measurements included in the current study have been reported in detail elsewhere (Almuklass et al. 2016) and are only briefly described in the following section. In contrast, more information is provided on the analytical approach used to characterize the experimental findings.

Experiment

Thirty healthy young adults (24.2 ± 4.0 yrs) with no history of neurological disease or injury to the upper extremity participated in a protocol that was approved by the Institutional Review Board at the University of Colorado Boulder (Protocol # 14-0356).

The force-matching tasks required the subjects to perform isometric contractions and produce a force that matched a target displayed in real-time on a monitor. The target forces were 5% and 10% of the maximal voluntary contraction (MVC). The target was located at the center of the monitor. In the current study, we analyzed the trials with targets of 10% MVC force to capture the common motor neuron input (output of the PID control algorithm; see *Simulations* for details) rather than the random, independent variability in the motor unit discharge rates (Dideriksen et al. 2012). The subjects performed two types of force-matching tasks: a single-action task and a double-action task. The single-action task required the subject to generate a wrist extension force, index finger abduction force, or pinch force that was shown as a circle on a horizontal axis and move it to a target location. The double-action task was similar, but required the subject to perform two of these tasks concurrently. The second target force during the double-action task was displayed o a vertical axis and the task was to move the circle to the intersection of the two axes (see Figure 1 in (Almuklass et al. 2016)).

In the current study, we analyzed pinch forces during the single- and double-action tasks. The double-action task involved the pinch force with concurrent wrist extension, which has high predictive ability for the variance in the time it takes to complete a test of manual dexterity (Almuklass et al. 2016). Due to the anatomical and functional links between grip actions and wrist movement (Werremeyer and Cole 1997; Ambike et al. 2013), it was assumed that it would be more challenging to match the pinch force in the double-action task. After a brief introduction to the tasks, the participants were instructed to reach the displayed target as quickly

as possible after hearing a "Go" signal from one of the investigators and to keep the force at the target for the next 10 s as steady as possible. Subsequently, the task was repeated twice, but at a self-selected steady pace. The first trial was analyzed in the current study because the PID control algorithm requires an explicit target force at all times to calculate the instantaneous force error (see *Simulations* for details). In the second and third trials, the 10% MVC force cannot be assumed to have been the explicit target force during the first few seconds (before 10% MVC was reached). For example, the subjects may have envisioned a steadily increasing ramp force from 0% to 10% MVC rather than a step increase to the target force.

The force signals were low-pass filtered at 50 Hz (V75-48 High Performance Bandpass Filter, Coulbourn Instruments, White Hall, PA, USA) and sampled at 2 kHz with an analog- to-digital converter (Power 1401, Cambridge Electronic Design, Cambridge, UK). The data were obtained with Spike2 data acquisition software (Version 5.20, Cambridge Electronic Design, UK) and stored offline for analysis in MATLAB 2014b (Mathworks, MA, USA).

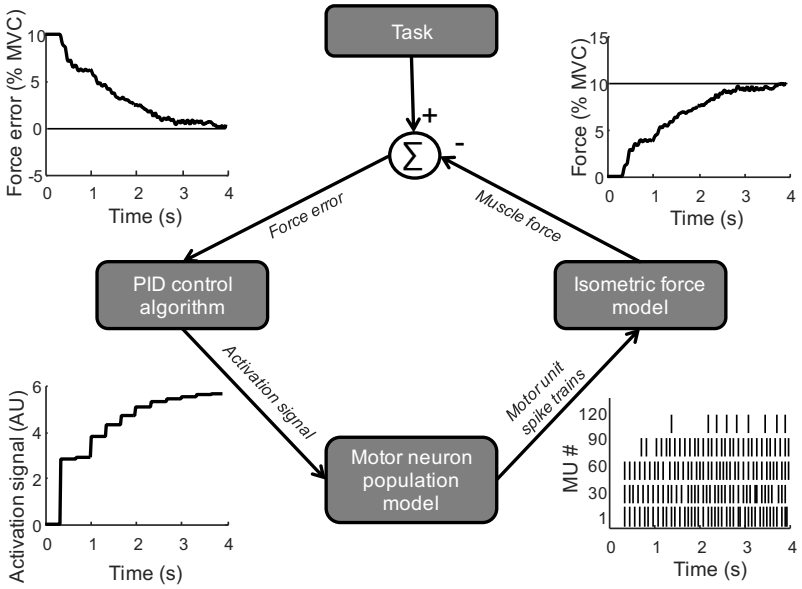

Figure 1 Model structure. The task was to maintain a steady force at 10% MVC. The force error was calculated as the difference between the instantaneous force and the target force, which was provided by visual input during the experiment. The force error provided an input signal to the PID control algorithm,

which estimated the activation signal (representing the supraspinal drive) that was required to minimize the force error (given the gains of the proportional, derivative, and integral error) and match the target force. The activation signal was sent to the model of the motor neuron population to generate motor unit spike trains that were transformed into muscle force.

Simulations

The approach adopted a previously published computational model that established the recruitment and rate coding characteristics in a population of motor neurons, and the isometric force generated from the motor neuron activation (Fuglevand et al. 1993; Barry et al. 2007). The motor neuron population in the model comprised 180 motor units. The sizes of these motor units followed an exponential distribution in which most were small (low-threshold, low-amplitude, slow contracting) and few were large (high-threshold, high-amplitude, fast contracting). In addition, a PID control algorithm was implemented to emulate the supraspinal control of force during a visually guided, force-matching task involving an isometric contraction, as previously described (Dideriksen et al. 2010). The "Task" component of the model (Figure 1) indicates the desired target of 10% MVC force. The difference between the target force and the instantaneous simulated force (force error) provided the input to the PID control algorithm, as indicated by Eq. 1.

$$A(t + D_{VM}) = K_p \cdot FE(t) + K_i \cdot \int_{\tau=0}^{t} FE(\tau)d\tau + K_d \cdot \frac{dFE(t)}{dt} \quad (1)$$

where A denotes the activation signal (input to the *Motor neuron population model*; Fig. 1), FE the force error, and K_p, K_i, and K_d the gains of the proportional, integral, and derivative terms, respectively. D_{VM} represents the visuomotor delay, which corresponds to the delay between a visual stimulus and subsequent reaction and was set to 135 ms (Carlton 1981). The algorithm was implemented as an intermittent controller, indicating that the value A was adjusted with a discrete time interval (t), which was varied in the range 167-667 ms depending on controller frequency (see details below). The activation signal to the motor neurons was constant within

the intervals *t* (simulation frequency was 1 kHz). Random Gaussian noise was added to the input received by individual motor neurons to achieve realistic discharge rate variability (Dideriksen et al. 2010). The values assigned to the three gains determined the characteristics of the relation between force error and activation signal. The activation signal determined the motor unit spike trains (*Motor neuron population model*; Fig. 1), from which the muscle force was simulated (*Isometric force model*; Fig. 1). The model was implemented in MATLAB 2014b (Mathworks, MA, USA).

The approach involved a series of 8-s simulations with the target force set at 10% MVC. Across the simulations, the values of the three gains (K_p, K_i, and K_d) were varied systematically. In each simulation, the gain of the three terms was assigned one of 10 evenly spaced values within predefined ranges (K_p: 0-55; K_i: 5-65; K_d: 0-25) that were determined in pilot simulations. Simulations with PID gains at the limits of the selected ranges yielded either an inability to reach the target force in less than 8 s (low values of K_i) or large force fluctuations (coefficient of variation for force > 15%; high values for all three gains). The frequency at which the controller sampled the error and adjusted the activation signal to the motor neurons was varied between 1.5 Hz and 6 Hz (Slifkin et al. 2000; Sosnoff and Newell 2006; Loram et al. 2014) in intervals of 0.5 Hz. All combinations of these gain values were simulated (1,000 iterations) for each controller frequency. Each combination was repeated five times to accommodate variability in the simulated force due to the stochastic elements in the model (Dideriksen et al. 2010). A total of 50,000 simulations were performed.

The resolution for each of the four trajectory measures was estimated for all simulations conducted at the same controller frequency (n = 5,000). The resolution characterized the distribution of the simulated trajectory measures across the range of experimentally observed

values for that measure. If, for example, the simulated values for one trajectory measure were distributed evenly in this range with small differences between consecutive values, the resolution would be high. Conversely, if there were large gaps between trajectory measures obtained in simulations with different model parameters, the resolution would be low. A low resolution could imply that PID controllers are fundamentally unable to simulate all values of that trajectory measure, or that too few combinations of different values of the model parameters were tested. To this end, the values for each simulated trajectory measure were ordered according to size and values outside the experimentally observed range were excluded. These values were differentiated to obtain the difference between the size-ordered values (nearest, non-identical value) of each measure. All zero-values (indicating simulations with the same value for the parameter) were removed, because large numbers of simulations with the same value of the measure would bias the average difference towards lower values and present a risk of overestimating the resolution. Finally, the average value was obtained. With this approach, one value per simulated controller frequency was obtained for each of the four trajectory measures, indicating the degree to which the simulated measures covered the experimentally observed range for that measure.

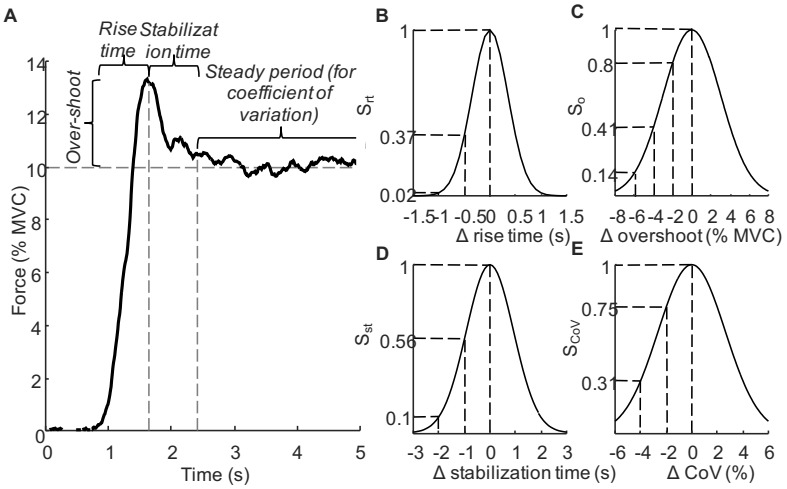

Figure 2. Parameterization of force. A. The following parameters were calculated from the force trace: initial force error, rise time, stabilization time, and coefficient of variation (CoV) for force once the target force was achieved (see text for definition of parameters). B-E. The distributions of the four parameters across the 5,000 simulations (black lines) relative to the values for the 24 subjects (grey vertical lines). The rise time in most simulations were 300-400 ms, but were >500 ms in 989 simulations and >1,000 ms in 263 simulations.

Data analysis

Four trajectory measures were extracted from the experimental and simulated forces, as illustrated in Figure 2A. 1) Rise time – the duration between the time at which the force exceeded 0.5% MVC force and the first turn in the force trajectory. Turns were identified as the instant when the sign of the first derivative of the smoothed force (moving average filter, 250 ms Hamming window) changed from positive to negative. 2) Overshoot – difference between the force at the first turn and the target force, which meant that a turn in the force below the target force was denoted as a negative value. 3) Stabilization time – the duration from the end of the rise time until the force became steady based on a standard-deviation criterion. The standard deviation of force was estimated with moving 1-s windows (overlapping by 999 ms). The criterion was defined as the mean plus three times the standard deviation during the preceding 3 s. The first point in time after force onset at which the standard deviation (estimated in the moving 1-s window) was below the criterion was defined as the end of the stabilization period

and the beginning of the steady force trajectory. 4) The coefficient of variation (CoV) for force – calculated from the end of the stabilization period until the task was terminated.

The values for these four trajectory measures in the experimental force trajectories were verified by visual inspection and unusual adjustments were noted. It was evident from the force trajectories that 6 of the initial 30 participants failed to perform the double-action task as instructed. For example, some subjects maintained the pinch force steadily either several percentages of MVC force below or above the target for up to 5 s before making any adjustments. We assumed these subjects did not understand the instructions for the rapid force-matching task and the data from these subjects for both tasks were not included in the current study.

The simulated forces were compared with the experimental recordings, and the simulated force (equivalent to one set of PID-gains) most similar to the force trajectory for each subject was identified. This was accomplished with the Gaussian functions shown in Figure 2B-E. The similarity (S_m) of each trajectory measure (rise time, overshoot, stabilization time, CoV for force) depended on the difference between the experimental and simulated value for that measure (Δm). In this way, the similarity was assigned the value of 1 when the difference was 0 and declined with an increase in the difference between the simulated and experimental forces. The standard deviation of the Gaussian function for each trajectory measure (σ_m) was set to the standard deviation of the experimentally obtained values for that measure across both tasks and across the 24 subjects. This implied that if one trajectory measure derived from one experimental force trajectory deviated by one standard deviation from the value of that measure in a given simulation, the similarity for that measure, S_m, would be 0.59. The simulated values were the

median of the values obtained from the five simulations performed with the same PID-gains and the same controller frequency.

The similarity for each of the four trajectory measures (m) was determined from the match between the forces simulated with each combination of PID gains and controller frequency (*F*) and the value derived from the force for each subject:

$$S_m(K_p, K_i, K_d, F) = e^{-\frac{(\Delta m(K_p, K_i, K_d, F))^2}{2\sigma_m{}^2}} \quad (2)$$

The similarity index (*SI*) quantified the strength of the association between the simulated and experimental force trajectories across the four trajectory measures for each subject:

$$SI(K_p, K_i, K_d, F) = S_r(K_p, K_i, K_d, F) \cdot S_o(K_p, K_i, K_d, F) \cdot S_s(K_p, K_i, K_d, F) \cdot S_{CoV}(K_p, K_i, K_d, F) \quad (3)$$

where *r* denotes rise time, *o* overshoot, *s* stabilization time, and *CoV* the coefficient of variation for force. The greatest value for SI across all simulated forces indicated the extent to which the force control used by each subject during each task could be characterized by a PID-like feedback controller as well as the most likely model parameters. The result was a distribution of SI values (one per subject) for each task.

The hypothesis was evaluated by comparing the probability distribution of similarity indices with those that could be obtained by chance. The experimental data comprised 48 combinations of the four trajectory measures (one per force trajectory), which determined the SI values. In principle, however, different realistic values of the four trajectory measures can be combined in infinitely many ways. It can be assumed that some of these combinations can be replicated well by simulations with SI values near 1, whereas others cannot be simulated as precisely. A distribution of SI values obtained by combining trajectory measures in all possible ways would represent the SI values that can be expected to be obtained by chance. Such a "chance distribution" indicates the ability of the PID control algorithm to simulate any force trajectory by

appropriate tuning of the model parameters. If, for example, this distribution primarily contained SI values near 1, it would indicate that this algorithm is sufficiently flexible to simulate most combinations of the four trajectory measures with high accuracy. In order for the SI values obtained from the two tasks to be statistically significant, they had to be greater than the chance distribution. To approximate the chance distribution, the trajectory measures obtained from all experimental trials were randomly combined to generate new sets of these measures; for example, one set of measures compiling the rise time from the single action task of subject #1, the overshoot from the double action task of subject #8, and so on. Importantly, this procedure ensured that the chance distribution comprised random combinations of trajectory measures with realistic values. The result was 48 new force trajectories for which the greatest SI value for each trajectory was calculated (Eq. 3). This process was repeated 10 times with different random combinations to provide a total of 480 SI values. These represented the chance distribution of SI values that characterized the ability of the PID controller to simulate any random force trace. Wilcoxon signed rank test was used to analyze the difference between the experimentally obtained SI values and the chance distribution as well as the difference in the identified model parameters (PID-gains and controller frequency) for each subject across the two pinch tasks. The difference in SI across the two tasks for each subject was compared using a paired t-test. Linear regression analysis was applied to the SI values and each of the four trajectory measures (rise time, rectified overshoot, stabilization time, and CoV for force) to investigate if the absence of matches between experimental and simulated forces was related to particular characteristics of the force trajectories. The distributions of the four S_m (Eq. 2) at the setting with highest SI (Eq. 3) were compared across all subjects for each task using Kruskal-Wallis test. Statistical significance was set at $p < 0.05$.

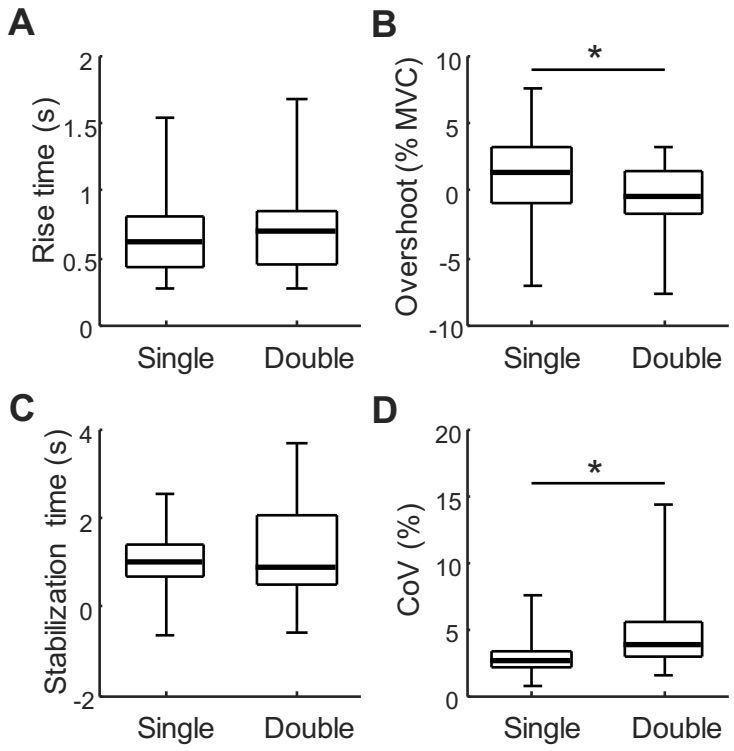

Figure 3. Calculation of the similarity between simulated and experimental forces. Gaussian functions were used to determine the similarity (S) for each parameter (r, rise time; fe, force error; S, stabilization time; CoV, coefficient of variation for force) based on the difference (Δ) between the simulated and experimental forces.

Results

Figure 3 summarizes the experimental values for the four trajectory measures from the 24 subjects in both tasks (single and double actions). Across all subjects there was considerable variability in the trajectory measures for the two tasks. The force overshoot was significantly greater ($p = 0.04$) and the CoV for force in the steady period was significantly less ($p = 0.01$) in the single-action task compared with the double-action task. The range of the trajectory measures across all simulations encompassed the entire range of experimentally observed values with one exception. In the single-action task, one subject presented a CoV for force of 0.8 %, whereas the lowest simulated CoV was 1.4%. Across all simulated control frequencies, the average resolutions of the four parameters were relatively high. Specifically, the average

differences between the nearest, non-identical values of each trajectory measure were: rise time = 1.9 ± 0.2 ms; overshoot = 0.007 ± 0.001 % MVC; stabilization time = 2.4 ± 0.4 ms; CoV for force = 0.003 ± 0.002 %. This indicates that the average difference between two consecutive (nearest, non-identical value) simulated rise times, for example, was approximately 2 ms within the range of experimentally recorded rise times (range: 0.15-1.58 s). These results demonstrate that PID controllers can be tuned to simulate practically all realistic values of each for the four trajectory measures individually; however, this does not imply that all possible combinations of the trajectory measures can be simulated to create any force trajectory. Furthermore, the low magnitude of the resolutions indicates that the analysis is robust enough to show an inability of the PID controller to simulate the experimental force trajectories only if such an inability actually exists (i.e., avoid false-negative results).

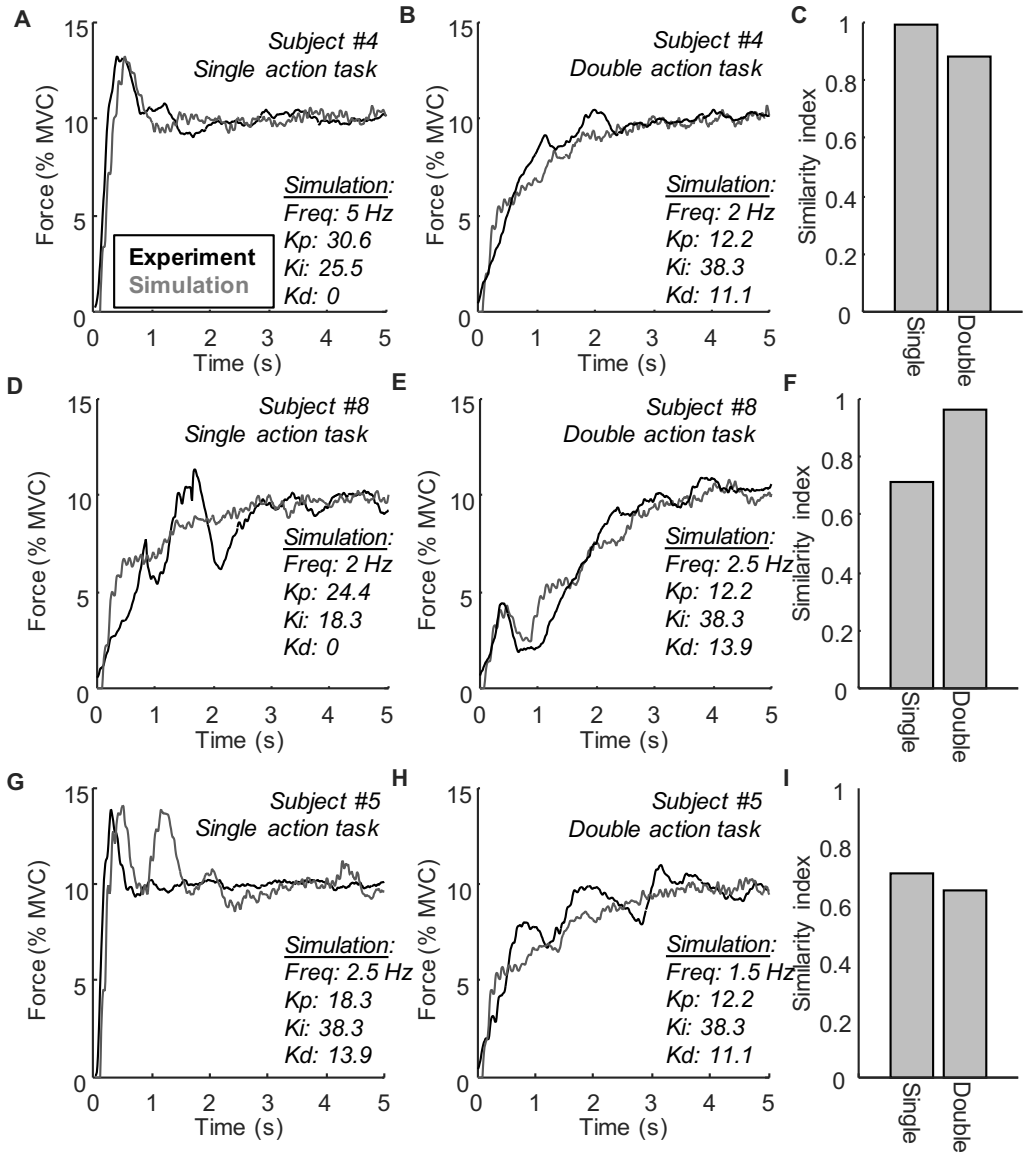

Figure 4. Examples of experimental (A, D, G, J) and most similar simulated forces (B, E, H, K) for four representative subjects. The similarity index for each subject is indicated in the right column (C, F, I, L).

Figure 4 depicts the experimental force trajectory for three representative subjects along with the simulated forces with greatest SI values. This example demonstrates that control of the experimental forces varied substantially across the two tasks and across subjects, which was also indicated in the average results for all subjects (Fig. 3). Furthermore, the figure illustrates the ability of the PID controller to simulate a wide range of forces; some of which were quite similar to the experimental trajectories. Specifically, the SI values for the best set of simulations for

subject #4 (Fig. 4C) were ≥ 0.89, indicating that the forces produced in both tasks by this subject were highly similar to forces simulated using PID control. In comparison, the forces of subject #5 were less well matched by any of the simulations (SI ≤ 0.70 for both tasks; Fig. 4I). Overall, the average values for the greatest SI across all subjects were 0.88 ± 0.12 and 0.86 ± 0.12 for the single- and double-action tasks, respectively (Fig. 5) (no significant difference between tasks; p = 0.69). According to Eq. 3, an SI of 0.86 could be achieved, for example, if the similarity (*S*; Eq. 2) for the four trajectory measures was 0.96. This result suggests that PID controllers with different model parameters were able to replicate most experimental force trajectories. In comparison, the average SI of the chance distribution was 0.79 ± 0.19 (Fig. 5), which was significantly lower than the SI values from the single action task (p = 0.009) and the double action task (p = 0.039). Across 16 subjects, the difference in the greatest SI value across the two tasks was < 0.1 (average difference: 0.11 ± 0.12), indicating that most subjects used PID-like control in both tasks.

There was no relation between the SI values and overshoot ($r^2 = 0.01$), stabilization time ($r^2 = -0.02$), or CoV for force ($r^2 = 0.06$), but SI was inversely related to rise time ($r^2 = 0.25$; p = 0.0002). This implies that trials with forces compatible with PID control (i.e., high SI values) tended to be those where the first turn in force was reached most rapidly (i.e., short rise time). Across all subjects, there was no significant difference in the similarities between each of the four trajectory measures (S< Eq. 2) in the experimental and the simulated force trajectories with greatest SI. The median S_m for all trajectory measures was >0.96, which indicates that failure to achieve SI = 1 was not due to a consistent difference between simulated and experimental forces in one of the four measures.

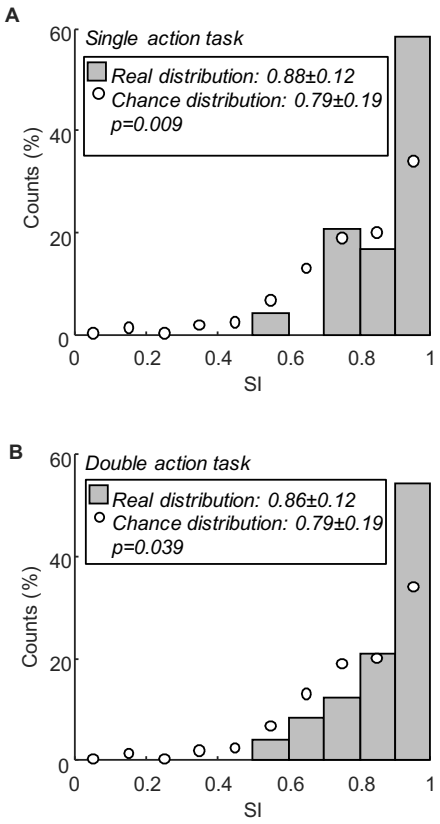

Figure 5. Histograms representing the distribution of values of the similarity index (SI) across all subjects in the single (A) and double (B) action tasks (grey bars). The circles represents the values of SI of the reference distributions. These distributions were obtained by randomly combining four parameters from each trial. In this way, 24 new artificial force traces were created, representing the ability of the PID control algorithm to simulate force traces with any characteristics. For each task, 10 sets of these artificial forces were created. The circles and error-bars represent the mean and standard deviation of the histograms for the 10 sets.

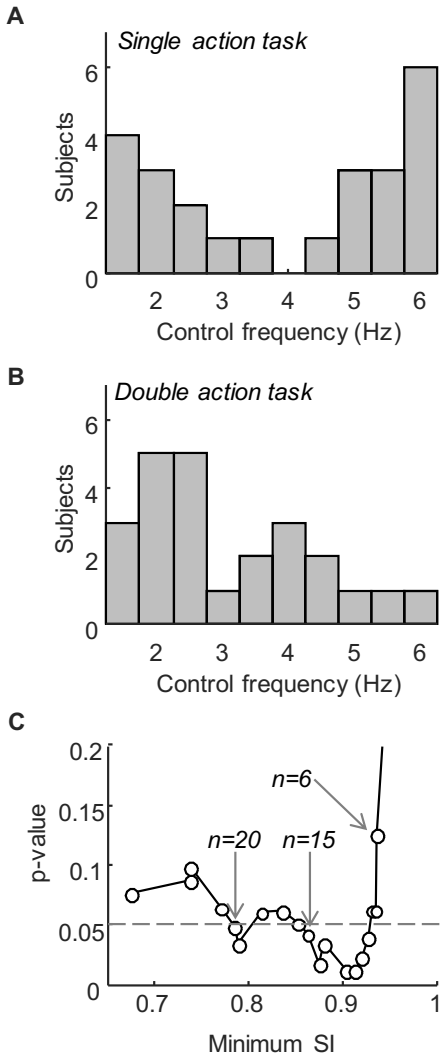

Figure 6. The best control frequency corresponds to the simulated frequency at which the PID-control algorithm sampled the force error and adjusted the activation signal to produce the greatest SI values across all subjects in the single (A) and double (B) action tasks. Panel C shows the p-value (Wilcoxon signed rank test) indicating the conditions in which a statistically significant difference between the best control frequencies for the two tasks was found. The p-value is calculated for a series of subgroups of subjects determined by the SI value, each indicated by a circle. The left-most circle indicates the p-value when considering all subjects. In the next subgroup (circle at SI = 0.73), the subject with the lowest SI value was excluded (n = 23) and so forth for the next subgroups (n=22, 21, 20…). In this way, the value on the x-axis represents the lowest average SI value in the subgroup and a decreasing number of subjects (indicated by n) were included in the analysis when the lower limit for SI value was increased. Note that the y-axis is truncated, and that the p-value for subgroups with less than 6 subjects (SI > 0.94) was >0.2.

The distributions of the frequencies at which the PID controller produced the greatest SI value in each task for each subject are depicted in Figure 6. The average control frequency for all subjects (grey bars) was 4.0 ± 1.8 Hz for the single-action task and 3.1 ± 1.3 Hz for the double-

action task; however, the difference in control frequency across the two tasks was not statistically significant ($p = 0.077$). Because low SI values suggest partial or complete failure of the PID model to replicate the experimental force, the estimated control frequency of subjects with low SI values may not reflect the actual frequency at which that subject adjusted the activation signal to the muscles. For this reason, the estimated control frequencies from subjects with high values of SI are likely to be more reliable than for those with lower SI values. Based on this rationale, the statistical test was repeated excluding subjects with low average SI values from the population. Once the four subjects with the lowest values of SI was excluded ($SI \leq 0.77$), the difference in control frequency across the two tasks was statistically significant (should we include the p value here?) (Fig. 6C). When the best control frequency identified for one of the two tasks was imposed on the other task, the peak SI decreased by an average of 0.14 ± 0.12. This comparison indicates that there were substantial differences in the degree to which the experimental data could be replicated by simulations depending on the simulated control frequency. Furthermore, the comparison underscores the observation that control frequencies tended to be lower during the double-action task.

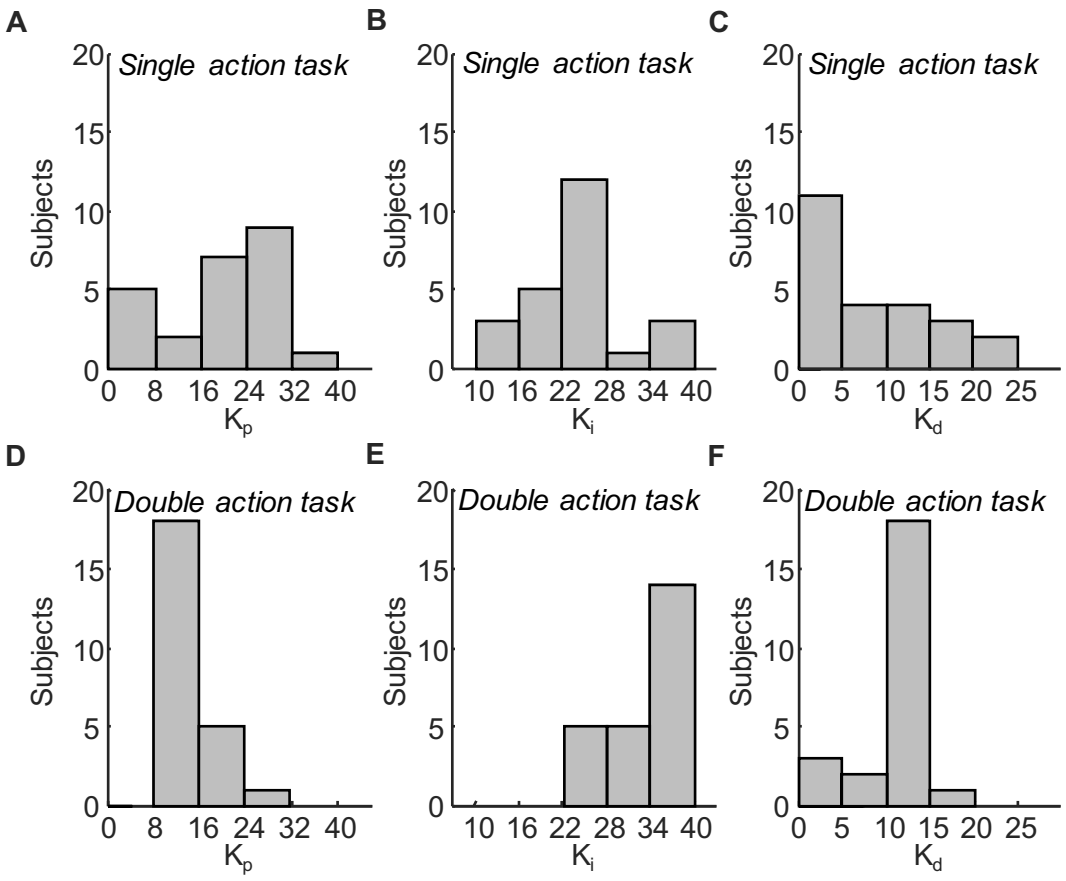

Figure 7. The distributions of PID-gains across all subjects in the single (A, B, C) and double (D, E, F) action tasks.

Figure 7 shows the distribution of PID gains for the simulations with greatest SI value in each task for each subject. The average gains for the single- and double-action tasks, respectively, were: $K_p = 19.6 \pm 10.0$ and 14.0 ± 3.4 ($p = 0.03$); $K_i = 23.9 \pm 7.5$ and 34.2 ± 5.5 ($p = 0.002$); and $K_d = 7.6 \pm 7.5$ and 10.6 ± 3.7 ($p = 0.15$). This comparison indicates that subjects tended to change the control strategy, not only in terms of control frequency (Fig. 6), but also in terms of PID gains across the two tasks. According to general control theory, decreasing K_p minimizes force overshoot and steady-state variability (CoV for force), at the expense of longer rise times. Conversely, increasing K_i increases the overshoot. The observed decrease in the overshoot during the double-action task in combination with an increase in the CoV for force (Fig. 3) likely

reflects these changes in the gains. As indicated by the smaller standard deviations of the gains in the double action task, the control strategies adopted in the single-action tasks across all subjects were more diverse than those for the double-action tasks.

A possible limitation of the analysis underlying these results, however, is that it focuses only on the single set of model parameters (PID gains and control frequency) yielding the greatest SI values. However, it is possible that another set of model parameters would provide SI values nearly as great in both tasks, making it unnecessary for the subjects to change the motor strategy (i.e., model parameters) across the two tasks, as Figure 7 seems to indicate. To address this possibility, the single set of model parameters providing the greatest average SI values across the two tasks were identified for each subject. It was found that this set of parameters involved an average decrease in SI of 0.30 ± 0.19 with respect to the greatest values for each task across subjects. This indicates that the force trajectories observed across the two tasks for each subject could not be explained by a single set of model parameters for the PID control algorithm.

Discussion

The goal of the study was to examine the sensorimotor control used by individuals when rapidly matching pinch forces at 10 % MVC using visual feedback of force error. The approach evaluated the capacity of PID-control algorithms with different model parameters to match experimental force trajectories produced by subjects during single- and double-action isometric contractions. There was substantial variability in the characteristics of the force trajectories (Fig. 3) across the 24 subjects and the two experimental tasks (Almuklass et al. 2016). The results, however, indicated that PID control algorithms with different PID gains and control frequencies

(model parameters) were able to capture this variability to a greater degree than expected due to chance (Fig. 5).

The applied control strategies as identified by the model parameters providing the greatest SI values varied substantially across subjects and across tasks (Fig. 6 and 7). One consistent task-related difference was that the frequency of the PID control decreased when the subject was asked to perform an additional force-matching task (double-action task) during the pinch task (single-action task) (Fig. 6). An intuitive interpretation of this finding is that the nervous system increased the interval between adjustments in the activation signal to generate pinch force in order to accommodate the additional computational demands related to performing another concurrent task. Similarly, other studies have demonstrated that the control frequency decreases when the complexity of the task is increased (Loram et al. 2009; Loram et al. 2014). For example, van de Kamp et al. (2013) showed that the refractory duration (the period between adjustments in the activation signal) was 250 ms for zero-order systems (equivalent to 4 Hz), but 550 ms for second-order systems (equivalent to approximately 2 Hz). This suggests that the nervous system requires more time to plan the appropriate response when the complexity of the task increases.

These results suggest that the PID-control architecture represents an appropriate mathematical description of the neural control of pinch force during force-matching tasks involving isometric contractions. Further validation of this hypothesis, however, is made difficult by the highly adaptable nature of human motor control. For example, an alternative experimental design could be to analyze and compare multiple repetitions of the same task under the assumption that the same model parameters are used across the trials. However, such comparisons are difficult because humans can adapt the strategy in new simple motor tasks rapidly in order to optimize the

outcome (Burge et al. 2008). Furthermore, repeated training of the same task enables the development of some level of feed-forward control for the task (Körding and Wolpert 2004) that would confound the identification of the characteristics of the feedback processing. For example, it is likely that multiple repetitions of the force-matching task would enable the subject to reach a contraction level near the target force rapidly without using visual feedback. As a result, the characteristics of the rising phase of the force trajectory should not be used to identify model parameters for a PID controller. Consequently, failure to identify identical PID model parameters across multiple repetitions of the same task cannot falsify the hypothesis and invalidate the PID control architecture as a descriptor of the underlying neural processes. Instead, the current study investigated the performance of two different tasks (one trial per task), and evaluated the degree to which the force trajectories could be replicated by simulations across both tasks.

Although the experimental force trajectories from most trials were compatible with PID control, a subset of the trials exhibited a lower degree of similarity with PID control (Fig. 5). Several reasons may explain these exceptions. One possible explanation is that these subjects relied on a fundamentally different control strategy. An alternative explanation, however, is that a low SI value was attributable to an inconsistent use of PID-like control. For example, it is possible that the subjects adjusted the model parameters between different phases of the task (e.g., rising phase and stable period; Fig. 2), which could make it impossible to identify one set of PID gains representative for the entire task and result in a low SI value. Furthermore, it is likely that adjusting gains during the task is potentially a more effective strategy, such as to minimize the overshoot and obtain a low CoV for force (Ang et al. 2005). Trials with low SI values, however,

tended to have lower rise times and did not stabilize faster or reach a more stable CoV for force compared to trials with high SI values.

Although the results indicate that the PID control algorithm is capable of replicating experimental force trajectories, it remains an open question if it also reflects actual underlying neural processes for motor control. However, there are at least four reasons why the approach seems reasonable. First, proportional, integral, and derivative error terms are evident in other motor control systems. For example, muscle spindles, whose output contributes to proprioception and elicits changes in the synaptic input to motor neurons (Proske and Gandevia 2009), encode changes in muscle length (proportional) and the lengthening velocity (derivative) (Mileusnic et al. 2006). Furthermore, muscle spindle sensitivity is adjusted by gamma motor neuron activity (Mileusnic et al. 2006), which usually co-varies with the level of alpha motor neuron activation (Bessou et al. 1990). The output of muscle spindles, therefore, reflects the error between the intended and the actual muscle length, similar to the output of a PID controller. Furthermore, by integrating the information provided by muscle spindles with other sensory systems, neural pathways can estimate spatial location with respect to the starting point (McNaughton et al. 2006). It seems plausible that a similar integration of the visually perceived force error can occur during force-matching tasks to represent the integral term of the controller.

Second, the PID control algorithm was implemented as an intermittent controller, sampling the force error at a regular interval and adjusting the activation signal once per sample (also known as serial ballistic control). Intermittency in human motor control was first proposed by Craik (1947) and has since been established as a theoretically plausible model (Neilson et al. 1988; Gawthrop et al. 2011; Gawthrop et al. 2014) that explains a range of experimentally observed motor behaviors (Miall et al. 1986; Miall et al. 1993; Loram et al. 2011; Loram et al. 2014).

Importantly, the intermittent control model applies only to voluntary adjustments in the activation signal, whereas feed-forward commands and spinal and supraspinal reflexes generating involuntary adjustments operate as continuous control systems (Loram et al. 2014). The tracking tasks analyzed in this study, however, are unlikely to involve substantial reflexive control, which suggests that intermittent control based on visual input is a plausible control strategy for the computational model.

Third, the PID-control algorithm represents pure feedback control, whereas human sensorimotor control typically depends on both intermittent feedback as well as continuous feed-forward processes (Diedrichsen et al. 2010; Loram et al. 2014). For example, visually guided reaching does not require vision of the hand during the movement, which reflects the ability of the nervous system to predict the sensory consequence of the motor command issued to the muscles (Goodale et al. 1986). Consequently, reaching movements can be performed using only feed-forward control. The ability to execute such actions, however, requires at least some experience with the task (Wolpert et al. 2011), which is not difficult for the reaching movements included in activities of daily living. In contrast, the rapid force-matching task used in the current study was unfamiliar to the subjects and it seems reasonable to assume that the subjects did not have sufficient experience to build the internal forward models required to predict the sensory output the recorded trial. Instead, it is more likely that they relied primarily on visual feedback during the task to alter the force trajectory.

Fourth, a potential difference between the simulated and the actual control process is that the PID algorithm reflects control of one functional unit (in the model, one muscle), whereas pinch force reflects the interplay between several muscles. Synergistic muscles, however, receive large amounts of common synaptic input in the bandwidth of force control (De Luca and Erim 2002;

Laine et al. 2015), indicating that they are largely controlled as one functional unit by the central nervous system. To summarize, these considerations support the notion that an intermittent PID control algorithm with a single output is a realistic model for the neural control for force-matching tasks involving isometric contractions.

It is feasible that a relatively simple control system, such as the PID algorithm, is desirable as it enables rapid changes in motor commands. As indicated by the results, the subjects tended to change the motor strategy across the two tasks (Figs. 6 and 7). In the more general case, a motor control system needs to be flexible to compensate for acute changes in the transfer function from activation signal to muscle force, such as during fatiguing contractions, changes in loading conditions, or the emergence of a new task requirement. A linear system with four model parameters (PID gains and control frequency) appears simple enough to produce robust adaptations, but remains sufficiently flexible to enable simulations across a wide range of force profiles (Fig. 4). In addition, computational models successfully simulate the cerebellar control of posture using PID controllers (Peterka 2002; Peterka and Loughlin 2004) or extended control algorithms relying on the same basic principle (Jo and Massaquoi 2004; Welch and Ting 2008). Similar to posture, grip forces are coordinated primarily by the cerebellum (Manto et al. 2012), which supports the notion that the PID control algorithm may not only successfully emulate the motor output, but also characterizes the actual control processes in the nervous system during fine motor control of hand and arm muscles.

Irrespective of the validity of a PID controller to represent the neural processes underlying force control in the force-matching task, this approach is useful in understanding the variability of the control process across subjects and tasks. Specifically, the approach presented in this study can be used to decompose any isometric force task into three PID gains and the control frequency.

This enables comparison of the control strategies used across different tasks, including tasks with time-varying target forces, where simple measures such as the root mean square error would not be comparable. In similar ways, much has been learned from the application of techniques such as Bayesian estimation theory as a computational model for sensory integration in motor control (Scott 2012) and muscle synergy analysis for supraspinal control of muscle groups (Tresch and Jarc 2009), even though these approaches may not directly reflect actual neural processes.

Conclusion

The current study compared force trajectories of young, healthy subjects performing two force-matching tasks with simulated forces in which a discrete time PID control algorithm manipulated the activation signal based on the force error. Overall, the results indicated that this algorithm generated force trajectories similar to those observed experimentally during the two pinch tasks, and that different model parameters explained the large differences observed in the force trajectories across the subjects and tasks. In conclusion, the results demonstrate that a discrete time PID control algorithm can describe mathematically the control of the activation signal sent to muscles during rapid force-matching tasks involving isometric contractions.

Chapter III

A LATENT LOW-DIMENSIONAL COMMON INPUT DRIVES A POOL OF MOTOR NEURONS: A PROBABILISTIC LATENT STATE-SPACE MODEL

Abstract

Motor neurons appear to be activated with a common input signal that modulates the discharge activity of all neurons in the motor nucleus. It has proven difficult for neurophysiologists to quantify the variability in a common input signal, but characterization of this signal may improve our understanding of how the activation signal varies across motor tasks. Contemporary methods of quantifying the common input to motor neurons relies on compiling discrete action potentials into continuous signals, assuming the motor pool acts as a linear filter, and requiring signals to be of sufficient duration. We introduce a space-state model in which the discharge activity of motor neurons is modeled as inhomogeneous Poisson processes and propose a method to quantify a latent trajectory that represents the common input received by motor neurons. The approach also approximates the synaptic noise in the common input signal. The model is validated with four datasets: a simulation of 120 motor units, a pair of integrate-and-fire neurons with a Renshaw cell providing inhibitory feedback, the discharge activity of 10 integrate-and-fire neurons, and the discharge times of concurrently active motor units during an isometric voluntary contraction. The simulations revealed that a latent state-space model can quantify the trajectory and variability of the common input signal across all four conditions. When compared with the cumulative spike train method, the state-space approach was more sensitive and was less influenced by the duration of the signal. The state-space approach appears capable of detecting rather modest changes in common input signals across conditions.

New and noteworthy: We propose a state-space model that explicitly delineates a common input signal sent to motor neurons and the physiological noise inherent in synaptic signal transmission. This is the first application of a deterministic state-space model to represent the discharge characteristics of motor units during voluntary contractions.

Introduction

When Adrian and Bronk (1929) first recorded motor unit action potentials in humans, they hypothesized that a common presynaptic signal could underlie the control of motor neuron discharge characteristics. Initial attempts to characterize the common input signal focused on quantifying the correlated activity between pairs of motor units (Sears and Stagg, 1976). However, the magnitude of the pairwise correlations has generally been found to be weak and variable (Bremner et al., 1991; De Luca et al., 1982, 1994; Farmer et al., 1993; Nordstrom et al., 1992), suggesting that such comparisons cannot be used to quantify common input (Farina and Negro, 2015). An alternative approach is to record the discharge times of ≥5 concurrently active motor units and to assume that the motor unit pool acts as a linear filter of the independent synaptic noise delivered to motor neurons, which produces an output that corresponds to the neural drive to the muscle (Farina et al., 2014; Farina and Negro 2015; Negro et al., 2009; Negro et al., 2016a). As an extension of this approach, Boonstra and colleagues (2016) proposed an explicit biophysical model to represent the effect of the common synaptic input onto the motor neurons. Each neuron was represented as an integrate-and-fire neuron that filtered the weighted synaptic inputs to allow more realistic connection topology and enable a structural definition of common input.

However, these approaches have mathematical and methodological limitations. One principal objection is that action potentials are discrete events and should be represented as point processes rather than continuous-time stochastic processes (Buesing et al., 2012; Macke et al., 2011). The computation of second-order statistics, such as coherence (e.g., Sears and Stagg, 1976; De Luca et al., 1982, 1994) or principal component analysis (Negro et al., 2009), is not adapted to point processes (Kuhn et al., 2003). Additionally, contemporary approaches rely on the motor unit

pool acting as a linear filter of the synaptic input, whereas some properties of the motor pool, such as persistent inward currents, make the motor unit pool highly nonlinear (Powers and Heckman, 2017). Moreover, failure to account for distinct sources of input to the motor neuron pool (Boonstra et al, 2016) means that the same second-order statistics could be produced by quite different physiological mechanisms.

In contrast, state-space models explicitly describe the interactions between neurons and the influence of common input. Such probabilistic models are uniquely characterized by a few parameters that can be estimated from the discharge times of activated neurons. The models are able to decode neuronal connectivity, the common input, and their associated statistical significances. These models have been used successfully to analyze spike trains of neuronal data recorded in the central nervous system (Dempster et al., 1977; Ahmadian et al., 2010; Trucollo, 2010, Paninski et al., 2010; Pnevmatikakis et al., 2016). Moreover, current approaches require a sufficiently long signal to create a cumulative spike train that is amenable to frequency analysis. A state-space model, in contrast, can be used to examine relatively brief isometric contractions. The current study analyzes, for the first time, the activity within an entire motor unit population with a state-space model. The proposed model expresses the common modulatory input as an unobserved (latent) state vector that varies in time to generate a net muscle force that matches a target force. The latent common input is perturbed by random synaptic noise. The temporal variation exhibited by the latent state, which encodes the synaptic input common to the motor neuron pool, can be interpreted as an abstract trajectory.

State-space models seek to explain the activity of many outputs through an n-dimensional vector referred to as the latent state of the system. The latent state changes over time with an abstract magnitude, where the absolute value at any one time need not be physiologically meaningful, but

the trajectory of the latent state provides insight on the overall dynamics of the common input received by the motor neurons. Additionally, the variance in the latent-state trajectory may approximate the synaptic noise that is common to all motor units. More generally, the common input estimated by the state-space model could be used to assess the influence of other confounding factors, such as adjustments during fatiguing contractions or age-related differences.

The key idea of the current study is to represent the discharge activity of each motor neuron using an individual Poisson process (Berg et al., 2008; Perkel et al., 1967; Person, 1974; Person and Kudina, 1971; Powers et al., 2005; Townsend et al., 2006); the parameters of the proposed model are relatively insensitive to the distribution characteristics of the motor unit interspike intervals. The rate (intensity) of the Poisson process is modulated by the latent common input, and the activity of the other neurons in the pool. The discharge times of each motor unit are represented as a Poisson point process that can be sampled at a high rate and evaluated with fast algorithms that have already been developed (Macke et al., 2011; Buesing et al., 2012). The parameters of the model and the common input can be estimated from the discharge times of the motor neurons (Mangio et al., 2011; Smith and Brown, 2003).

The dimensionality of the latent common input can also be estimated using a goodness-of-fit criterion (Macke et al., 2011). Once the parameters have been estimated, the model allows for explicit quantification of the trajectory of the common input signal and— separately—a synaptic noise term. Macke and colleagues (Macke et al., 2011) note that dynamical state-space models provide a good fit for discharge times for two reasons: first, they can accommodate data for many neurons at fine time scales, which reduces the likelihood that shared variability is coincidental. Second, this class of models naturally captures the almost instantaneous (time lag

~ 0) peak in cross correlation of motor unit discharge rates (De Luca et al., 1982, 1994) through a latent state trajectory (Macke et al., 2011).

The purpose of the current study was to estimate the synaptic input and its associated variance that is common to a pool of motor neurons. The model was derived from state-space models that have been used to decode the influence of sensory pathways on activity exhibited by cortical neurons (Macke et al, 2011) and spinal cord neurons (Buesing et al., 2012). The approach is validated with four different datasets: the replication of experimentally observed motor unit discharge characteristics; the discharge times for a pair of integrate-and-fire neurons with a Renshaw cell providing negative feedback; the discharge activity of ten integrate-and-fire neurons, which is compared with the contemporary approach to assess common input; and quantification of the common input to motor neurons derived from an experimental recording of motor unit discharge rates.

Methods

The mathematical model comprises a low-dimensional common input to a pool of motor neurons to represent a common input signal and a synaptic noise term explicitly. This work advances previous models of motor unit recruitment (Fuglevand et al., 1993; Dideriksen et al., 2010; Moritz et al., 2005) and is based on work performed on the statistical structure of neuronal discharge times in the motor cortex (Macke et al., 2011) and sensory pathways (Archer et al., 2014). Although some previous models of motor unit recruitment model the presynaptic input to a motor unit pool (Williams and Baker, 2009; Watanabe et al., 2013), most do not (Fuglevand et al., 1993; Moritz et al., 2005). The present work provides a model based on a dynamical system, which can be fit to experimental recordings of motor units for the purpose of quantifying the common input to the motor neuron pool.

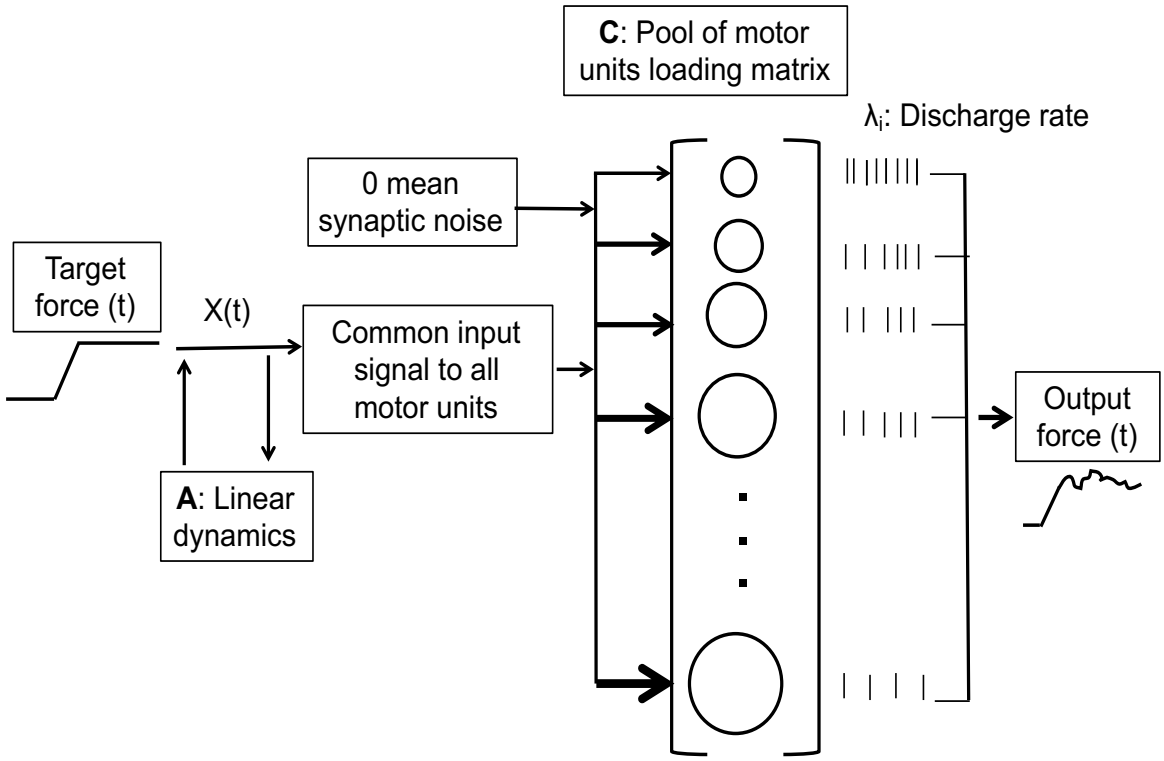

Figure 1. The state-space model represents the processes that are engaged to enable a population of motor units to produce a force that matches a desired target force. The trajectory of the latent state, X(t), must evolve to provide sufficient activation to the pool of motor neurons for them to discharge action potentials. The changes in the latent state over time are captured by the matrix, A, which represents a linear approximation of the latent-state dynamics. All neurons receive two inputs, a common input (the latent state) that excites the motor neurons and zero mean Gaussian synaptic noise. The physiological properties of each neuron are modeled with the C matrix, which encodes the effects of the input signal on discharge rate. The output is instantaneous discharge rates of each motor neuron, which evolve as the latent state changes. The forces generated by the activated motor units are summed to create the net muscle force.

An overview of the proposed model is shown in Figure 1. This model utilizes the discharge rate $\lambda_i(t)$ to represent the nonlinearity between an input current and the discharge times of a neuron *i*. The discharge times $y_i(t)$ of each motor unit (i = 1…n) are parameterized as a Poisson point process where the time-varying intensity (discharge rate), $\lambda_i(t)$, of the ith motor neuron takes the following form,

$$\lambda_i(t) = \exp\big(z_i(t)\big). \tag{1}$$

The exponential relation ensures the rates are positive and explicitly encodes the influence of a latent, low-dimensional common input through the n-dimensional vector $\mathbf{z}(t)= [z_1(t),..,z_n(t)]$ in the following linear model:

$$\mathbf{z}(t) = \mathbf{C}\,\mathbf{x}(t) + \mathbf{D}\,\mathbf{s}(t) + \boldsymbol{\mu}, \tag{2}$$

where $\mathbf{x}(t)$ is a d-dimensional vector that represents the unobserved common input; $\mathbf{C}$ is a $n \times d$ matrix that encodes the physiological effects of the latent common input on the motor discharge rates; $\mathbf{D}$ is an $n \times n$ matrix that models the coupling between the n motor units; $\mathbf{s}$ may be defined to model the interconnectivity of motor neurons; and $\boldsymbol{\mu}$ is the logarithm of the average discharge rate, which provides a baseline discharge rate. Additionally, s(t) may be conditioned by the previous discharge activity of the motor units (Buesing et al., 2012; Macke et al., 2011; 2015), which allows for feedback to be modeled from a motor neuron to itself as well as the other neurons in the network. For example, an inhibitory input between neurons could be modeled with a value between 0 and 1 on the corresponding entry in s(t) between the neurons, whereas an excitatory input would be modeled with an entry greater than 1. With this approach, s(t) allows for modulation of discharge rate by excitatory and inhibitory inputs.

The common input is expected to vary as a function of time and target force. The dynamics of the common input is described as follows:

$$\mathbf{x}(t) = \mathbf{A}\,\mathbf{x}(t-1) + \mathbf{b}f(t) + \boldsymbol{\varepsilon}(t) \tag{3}$$

where $\mathbf{A}$ is an $n \times n$ matrix that provides a linear approximation to the dynamics of the n motor units; the n-dimensional vector $\mathbf{b}$ weights the influence of the force target, $f(t)$, on each coordinate of $\mathbf{x}(t)$; and the Gaussian vector $\boldsymbol{\varepsilon}(t)$ zero mean Gaussian noise vector that models the synaptic noise inherent in signal transmission, such as the opening and closing of ion channels (Katz & Miledi, 1970).

In this model, $\boldsymbol{x}(t)$ represents the low-dimensional approximation to the latent state that activates a pool of motor neurons, which is often described as the common input. Following Macke et al. (2011), we assume the common input evolves according to linear Gaussian dynamics, which depends on the intended target force $\boldsymbol{bf}(t)$ according to the following probability distributions,

$$\begin{aligned} \mathbf{x}_1 &\sim \mathcal{N}(\mathbf{x}_o, \mathbf{Q}_o), \\ \mathbf{x}_t|\mathbf{x}_{t-1} &\sim \mathcal{N}(\mathbf{A}\mathbf{x}_{t-1} + \mathbf{b}\mathrm{f}_t, \mathbf{Q}), \end{aligned} \tag{4}$$

where $\mathbf{x}_0$ and $\mathbf{Q}_0$ represent the initial state and covariance matrix of the latent input $\mathbf{x}_t$, respectively. $\mathbf{Q}$ is a covariance matrix of the latent state $\mathbf{x}_t$, and represents the physiological random fluctuations in the common input signal. We further assume that $\mathbf{Q}$ remains constant over time.

Motor unit model

The first experiment demonstrated the ability of the model to recover the parameters of a synthetic dataset generated by modeling ramp contractions of a pool of 120 motor units in the first dorsal interosseus muscle (Feinstein et al., 1955). The model was based on the original Fuglevand model (Fuglevand et al., 1993). Simulations were performed 10 times at each target force (from 5- 30% MVC). Each trial involved an excitatory drive function that comprised a linear 1-s ramp from 0 N to the target force (percentage of maximal voluntary contraction [MVC]) that was maintained for 4 s. Each motor neuron received a common input signal and a noise signal inversely proportional to the difference between its recruitment threshold force and the target force. The recruitment threshold excitation (RTE) for the i^{th} motor unit was set to:

$$\mathrm{RTE(i)} = e^{a*i} \tag{5}$$

where 'a' establishes an exponential range of threshold values based on the upper limit of motor unit recruitment: $a = (\ln 60)/120$, where 60 refers to 60% MVC force and represents the upper

limit of motor unit recruitment (Dideriksen et al., 2010; Moritz et al., 2005) and $n = 120$ denotes the number of motor units in the model. Motor units were recruited during the ramp contraction once the level of excitation exceeded RTE. The resulting discharge rate was determined by the evolution of the latent state and the physiological parameters of the motor unit pool. In these simulations, the common input was approximated with a one-dimensional latent input that activates the pool of motor neurons to reach the target force in 1 s and maintain it for 4 s.

The matrix $\mathbf{C}$ was modeled as a $1\times n$ matrix where n represented the number of active units. Each row of $\mathbf{C}$ represented the response of a motor neuron to the latent input. The 120 units were assigned to respond to the latent input so the minimal discharge rate for the first recruited motor unit was between 6-8 pps. The column in $\mathbf{C}$ was derived to represent the range of physiological parameters within a motor pool that would influence discharge rate, such as the 5-fold range in afterhyperpolarization duration and 10-fold range in input conductance (Heckman and Enoka, 2012). The magnitude of each row was estimated to produce realistic discharge rates and thereby demonstrate the feasibility of the algorithm. The following linear function determined the values of $\mathbf{C}$,

$$C_i = 2 + 0.0054 * i, \tag{6}$$

The evolution of the latent state during the 5-s simulations was modeled by equation (3). After the target force was reached (1-s ramp), the force term, $\mathbf{b}f(t)$, was held constant. The synaptic noise $\boldsymbol{\varepsilon}(t)$ received by each motor neuron was modeled by a zero-mean white Gaussian noise, and was added to the signal using awgn in MATLAB. This noise was proportional to the difference between RTE for the i^{th} unit and the current level of excitation. The plateau in

discharge rate (saturation) observed in low-threshold motor units (Bigland and Lippold, 1954; Fuglevand et al., 2015; Monster and Chan, 1977; Moritz et al., 2005, Barry et al., 2007), captured by the vector **b** in equation (3), was modeled using a hyperbolic tangent function,

$$b_i = \frac{1}{2}\left(\tanh\left(\mathrm{ARTE}(i)\right) + 1\right), \quad (7)$$

where ARTE was the difference between RTE for the i^{th} motor unit and the force (% MVC) at any time *t*, which represented the current level of excitation being received by the motor neurons. Based on this relation, the difference between the level of excitation and the recruitment threshold force influenced motor unit discharge rate through **b**. The discharge rate $\lambda_i(t)$ of each neuron *i* was updated every 10 ms according to the following equation

$$\exp([\mathbf{C}(\mathbf{A}\mathbf{x}(t) + \mathbf{b}f(t) + \boldsymbol{\varepsilon})]_i). \quad (8)$$

Force model

The force produced by each motor unit in response to an action potential was modeled as a critically damped second-order system (Fuglevand et al., 1993; Milner-Brown et al., 1973). As defined in the Fuglevand model, the twitch force, $f_i(t)$, for the i^{th} motor unit was determined as:

$$f_i(t) = \frac{P_i * t}{T_i} * e^{1-(\frac{t}{Ti})} \quad (9)$$

where **P** represents the twitch force and **T** denotes the twitch contraction time for each of the n motor units. Peak twitch force for the 120 motor units was assigned with an exponential function that established a 100-fold range of twitch forces (Fuglevand et al., 1993):

$$P(i) = e^{b*i} = e^{\frac{\ln(100)}{120}*i}. \quad (10)$$

The twitch contraction times varied with peak twitch force so that units with the greatest peak twitch forces also had the fastest twitch contraction times (Fuglevand et al., 1993). Twitch contraction times were scaled to exhibit a 3-fold range:

(11)

$$T(i) = 90 * (\frac{1}{Pi})^{1/4.2}.$$

The nonlinearity between stimulus frequency and motor unit force (Fuglevand et al., 1993; Kernell, 1981; Milner-Brown et al., 1973) was modeled with a sigmoid gain that augmented force for brief adjacent interspike intervals. Specifically, the normalized discharge rate for the i^{th} unit with an interspike interval (ISI) at time t, (T_i/ISI_t) summed twitch forces with the following gain:

$$S(\frac{T_i}{ISI}) = 1 - e^{-2(\frac{Ti}{ISI})^3} \quad (12)$$

Normalized discharge rate was defined as the contraction time for the i^{th} motor unit divided by the interspike interval between t and t-1. The gain was defined with a piecewise function for each unit at time t. The sigmoidal gain was expressed as the ratio of the gain divided by the instantaneous normalized discharge rate for rates ≥ 0.4. At normalized discharge rates below 0.4, motor unit forces were not scaled with a gain. Overall, the gain was defined by

$$Gain = \begin{cases} \frac{S(\frac{Ti}{ISI})}{\frac{\mathrm{Ti}}{\mathrm{ISI}}} \; if \; \frac{T_i}{ISI} \geq 0.4 \\ 0 \; otherwise \end{cases} \quad (13)$$

The net force produced by the motor unit pool was calculated as the instantaneous sum of the i^{th} motor unit force at time j updated at a rate of 10 Hz:

$$\sum_{i=1}^{k} f_{i,j} = f(t - t_{i,j}) \quad (14)$$

The force model was developed in MATLAB (MathWorks, Natick, MA, Version 2015a) and run 10 times at 4 target forces: 5, 10, 20, and 30 % MVC. The outputs of the model were instantaneous discharge rates for the pool of motor units. Random realizations of an inhomogeneous Poisson process were generated using the intensity, $\lambda_i(t)$, (using the MATLAB function exprnd). The variables of interest were the average discharge rates for the motor units

during the steady portion of the contraction, the variability in discharge times (interspike intervals), the mean force and its variability, and the spectral content of the force signal.

Integrate-and-fire neuron models

The model was used to simulate the discharge times of action potentials for a pair of integrate-and-fire neurons with a Renshaw cell providing negative feedback from one neuron to the other one (Kirkwood et al., 1981; Windhorst, 1989). The purpose of the simulation was to demonstrate that the state-space model is able to quantify neural pathways with inhibitory and excitatory feedback loops. Additionally, the simulation provided an intuitive understanding of the characteristics of a latent-state trajectory in that there was a change in the magnitude of the latent state when the neurons discharged action potentials. Both neurons were simulated with a capacitance of 1 nF, a resistance of 40 mΩ, a resting membrane potential of -65 mV, and a voltage threshold of -55 mV. A sinusoidal input current (1 nA) was delivered to both neurons at 3 Hz. A recurrent collateral from neuron A projected to a Renshaw cell (C), which synapsed onto neuron B and elicited an inhibitory post-synaptic potential of 1 mV decaying to 0 mV over 10 ms after each action potential discharged by neuron B. The currents received on the soma of the neurons were integrated using Euler's method updating every 1 ms. Figure 2 provides an overview of the model for a pair of integrate-and-fire neurons.

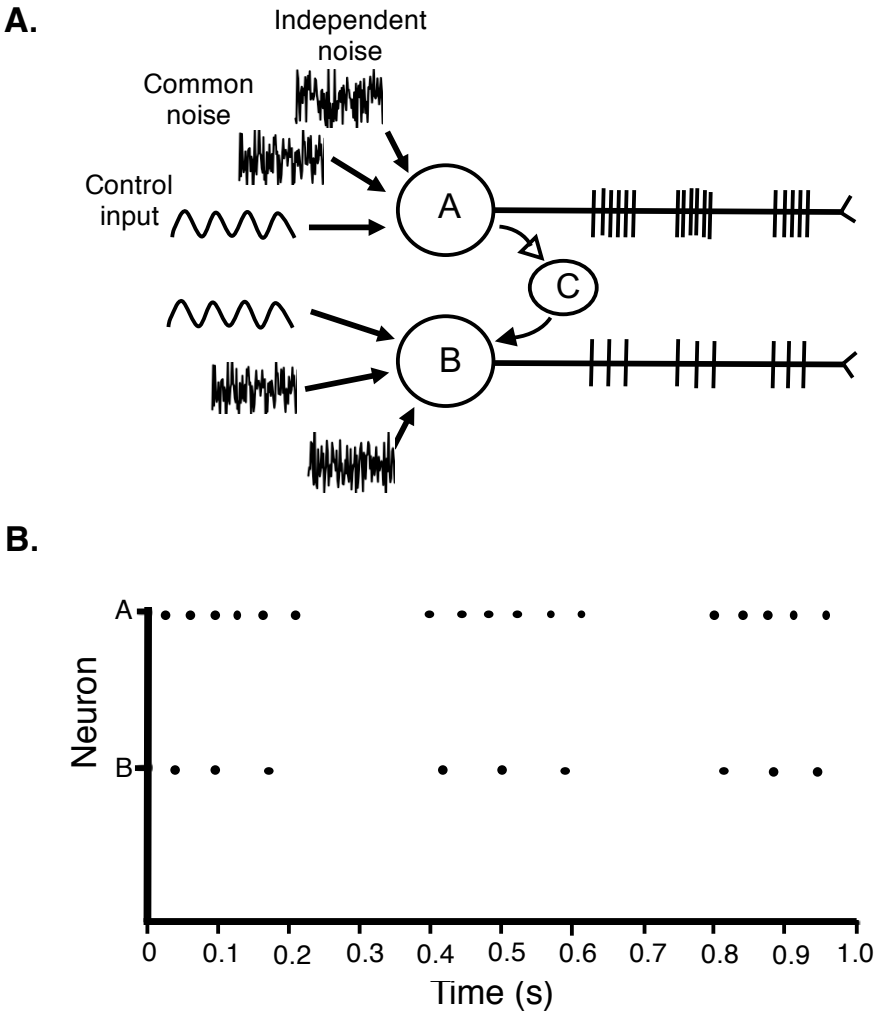

Figure 2. Schematic for a pair of motor neurons with a collateral from neuron A projecting to a Renshaw cell (C) that then elicited inhibitory postsynaptic potentials in the second motor neuron (B). The solid arrow projecting to neuron B indicates an inhibitory projection. A. Schematic overview of the leaky integrate-and-fire neurons (A and B) with an interposed Renshaw. Motor neurons (A and B) received three inputs: control signal, common noise, and independent noise. B: Raster plot of the discharge times for action potentials from motor neurons A and B.

Each neuron received three inputs concurrently: a sinusoidal common input, zero mean Gaussian common noise, and zero mean Gaussian independent noise. When the potential difference across the membrane reached voltage threshold (-55 mV), the neuron discharged an action potential with an overshoot that reached +10 mV, followed by an afterhyperpolarization phase where the potential difference dropped to -70 mV and rose to -65 mV linearly over the course of

50 ms. The discharge times of the two motor neurons (A and B) were summed at each instant to form a cumulative spike train (CST), which was subsequently low-pass filtered (6^{th} order Butterworth filter, cutoff frequency 10 Hz) (Castronovo et al., 2016; Farina et al., 2014; Negro et al., 2016a). The filtered CST represents one method to represent the common input to the motor neurons. The coherence between the filtered CST and the input current was calculated with Welch's periodogram method in MATLAB using the function mscohere with a 90% overlap and a 0.25s Hanning window. Additionally, the latent vector, $\mathbf{x}(t)$, and its corresponding covariance matrix were optimally estimated using an Expectation Maximization (EM) algorithm (Buesing et al., 2012; Macke et al., 2011; Demptster et al., 1977). The integrate-and-fire neurons were simulated for two durations (1 s and 10 s) to demonstrate the capacity of a state-space model to estimate common input for relatively brief signals for which frequency analysis is less robust.

A set of 10 integrate-and-fire neurons were simulated for two input frequencies (3 Hz and 4 Hz) and three current amplitudes (0.1, 0.5, and 1 nA). The neurons were simulated with a range of input resistances linearly spaced from 35-80 mΩ and capacitance from 0.9-1.8 nF. All neurons received two inputs: the control input (either 3 or 4 Hz) and a common noise using the awgn function in MATLAB with a signal-to-noise ratio of 25. All simulations were performed for 10 s. Cumulative spike trains (CSTs) were constructed (Castronovo et al., 2016; Farina et al., 2014; Negro et al., 2016a) and low-pass filtered. The spectral content of the CST was calculated with a Fast Fourier transform (fft in MATLAB). Additionally, the discharge times from the 10 integrate-and-fire neurons were used to estimate the parameters of the state-space model using PLDSexample (Macke et al., 2015). The number of neurons included in the simulations was set at 10 to match the number of concurrently active motor units that can be discriminated from high-density surface EMG recordings during submaximal voluntary contractions.

The code for these simulations is available at github.com/dfeeney31 within the neural models repository.

Experimental procedures

The IRB at the University of Colorado Boulder approved this study (approval number: 16-0782). A single subject performed isometric contractions at 10% MVC force with the elbow flexor muscles. High-density grid electrodes (64 mm, 4 mm interelectrode distance) (Bioelettronica, Torino, Italy) were placed over the long head of the biceps brachii muscle. The EMG signals from the grid electrodes were recorded at 2048 Hz and decomposed using a semi-automated convolution kernel algorithm implemented in MATLAB (Holobar and Zazula, 2004; Negro et al., 2016b). The discharge times for seven motor units were identified during the trial. The motor unit discharge times were arranged into an nxT binary discharge matrix with each row representing a motor unit at T time samples during the last 20 s of the isometric contraction. The matrix of motor unit discharge times was down sampled to bin widths of 10 ms for purposes of estimating the parameters of the state-space model. The parameters of the state-space model (specifically $\boldsymbol{x}(t)$ and Q) were estimated using an EM algorithm (Buesing et al., 2012; Macke et al., 2011). Coherence was calculated between the trajectory of single dimensional latent state and the net elbow flexor force. The trajectory and variance of the latent state estimate of the common input received by the motor neurons were estimated during the last 20 seconds of the contraction. Welch's averaged modified periodogram was used to calculate the coherence between the input current (or the force signal) and the trajectory of the latent state using the function 'mscohere' in MATLAB with a 90% overlapping window and a Hanning window of 0.5 s as suggested in Castronovo, 2016. The 95% confidence intervals of the coherence were determined using the function cmtm in MATLAB.

Estimating model parameters

An open-source expectation maximization (EM) algorithm (PLDSExampleWithExternalInput from the pop_spike_dyn directory on Atlassian BitBucket, authors: Macke, Buesing, and Gao) was used to estimate the parameters of the proposed state-space model for the simulations and experimental data. A Poisson subspace identification method was used for all estimations, which has been shown to be the most accurate for neural data and is described in detail by Buesing and colleagues (2012). Briefly, the input to the algorithm was a matrix of the motor unit discharge times that were used to estimate the trajectory of the latent state and to quantify the variability in its trajectory (Buesing et al., 2012; Macke et al., 2015). The parameters of the model were initialized using a Poisson subspace initialization (Buesing et al., 2012). Subsequently, a Ho-Kalman filter state space identification algorithm (Ho and Kalman, 1966) was used to estimate the parameters of the state-space model iteratively. The maximal log likelihood of the posterior distribution of the latent vector (x(t)) was used to determine the goodness-of-fit of the model. The EM algorithm iteratively refined the initial estimation until a local maximum of the log-likelihood function had been reached. The EM algorithm was stopped when either a maximum number of iterations (100) was reached or when the relative error in log-likelihood became smaller than 10^{-3}.

In principle, the estimation of the latent space model can be performed for a latent-space vector of varying complexity by changing the dimension of that vector. To prevent over-fitting, however, the dimensionality of the latent state was chosen to be the lowest dimension after which the log-likelihood no longer increased (Macke et al., 2011). Additionally, any dimension for which the estimated variance was numerically negligible was removed. Consequently, the dimension of the latent space was the lowest dimension that resulted in the maximum of the

estimated log-likelihood, while keeping the variance of all coordinates greater than a threshold chosen to be 10^{-4}.

State-space models assume the variance in the input signal is constant (stationary) during a particular task. However, non-stationary input to motor neurons, such as during long-lasting isometric contractions, can be examined by dividing the recording into segments in which the estimated parameters are relatively stationary. With this approach, it is possible to estimate how the latent input changes during long-lasting isometric contractions.

Results

The results comprise predicted discharge rates of the motor neuron pool and the force fluctuations during a ramp-and-hold contraction. The discharge characteristics and force fluctuations of the model were compared with experimental findings for the first dorsal interosseus muscle.

Table 1: Motor unit discharge characteristics obtained from the state-space model activating 120 simulated motor units. Minimal discharge rates were calculated by setting the target force equal to the recruitment threshold of each motor unit. Subsequently, the force was set to 100% MVC and the maximal discharge rates for each motor unit was determined. Recruitment threshold was calculated by solving equation (5), RTEi = ea*i where a = ln(60)/120 for each motor unit.

Motor Unit #	Min DR	Max DR	Recruitment threshold (% MVC)
10	7.5	13.2	1.4
20	7.8	14.5	2
30	8.3	15.4	2.8
40	9	16.8	3.9
50	9.8	17.5	5.5
60	10.8	18.3	7.7

70	12	20.1	10.9
80	13.3	21.2	15.3
90	14.8	23.2	21.6
100	16.5	24.5	30.3
110	16.8	26.9	42.7
120	17.3	30.2	60

Motor neuron discharge characteristics

Table 1 lists the recruitment thresholds and the minimal and maximal discharge rates for every 10^{th} motor unit in the simulated pool of units. As specified by equation (2), minimal and maximal discharge rates increased with recruitment threshold force. Minimal discharge rates ranged from 7.5 to 17.3 pps and maximal discharge rates ranged from 13.2 to 30.2 pps. The data are similar to minimal (7 - 12 pps) and maximal (30 pps) discharge rates reported by Moritz et al. (2005) during steady isometric contractions with the first dorsal interosseus muscle. Coefficient of variation for the interspike interval for motor units ranged from 12.4 to 19.8% during the last 2 s of each contraction, which is slightly less than the 15 to 35% reported by Moritz et al (2005).

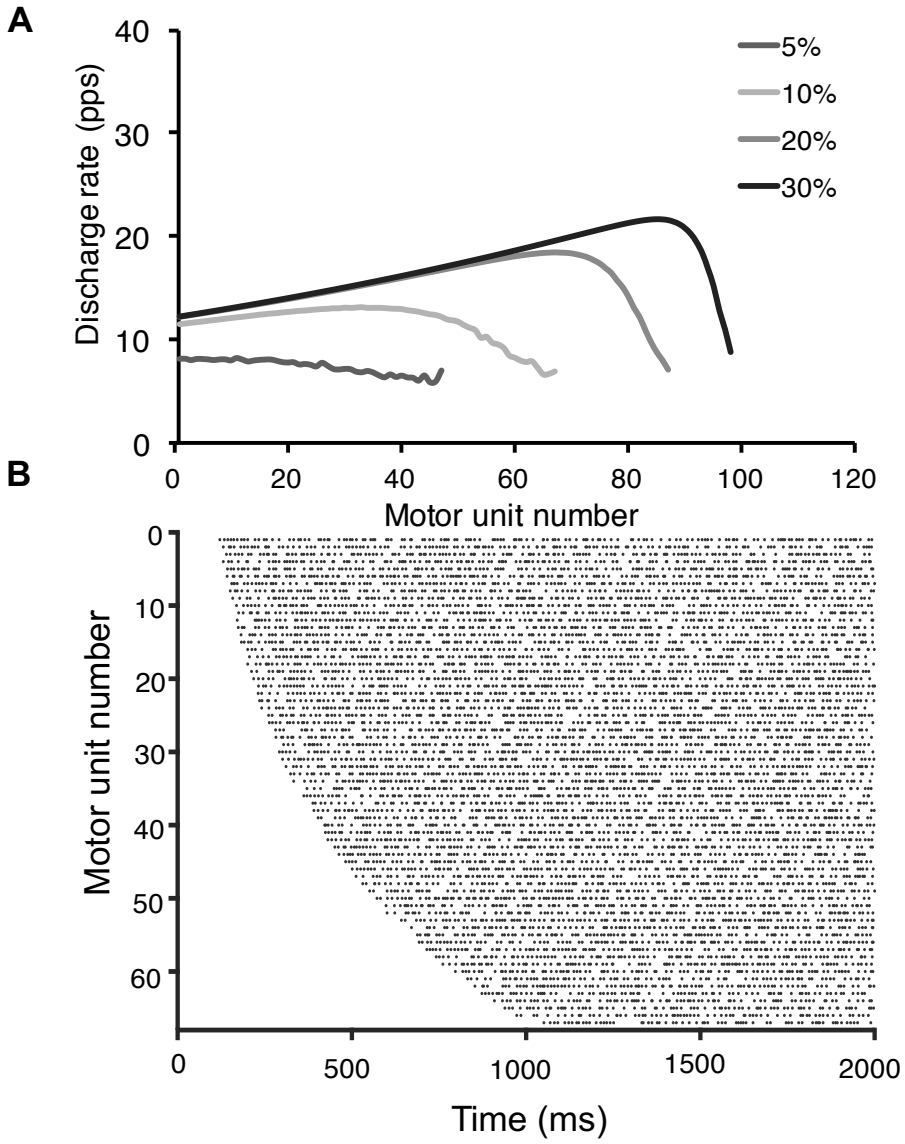

Figure 3. A: The number of motor units recruited and their discharge rates during simulated isometric contractions to match four target forces (5, 10, 20, and 30% MVC). Average discharge rate was calculated from the last 2 s of each simulated contraction. B: Raster plot of the motor unit discharge times for the 67 motor units that were recruited during the first two seconds of a simulated 5-s contraction to a target force of 10% MVC. The task comprised a 1-s ramp and then a 4-s hold. The latent state activated the motor neurons to discharge action potentials as specified by the prescribed physiological properties. Each bin represents 10 ms.

Figure 3 depicts the number of motor units recruited and their discharge rates during simulated contractions to target forces of 5-30% MVC. Data are similar to those reported by Moritz et al. (2005). The hyperbolic tangent function also modeled the saturation of discharge rates seen

when low-threshold motor units are tracked during ramp contractions (Fuglevand et al., 2015; Moritz et al., 2005; Monster and Chan, 1977). At the 5% target force, for example, the first motor unit discharged action potentials at a rate of 8.5 pps and the 47th motor unit at 7.3 pps. At the 30% target force, the first motor unit had reached its peak discharge rate of 13.2 pps and the 47th motor unit discharged action potentials at 16.4 pps. These discharge rates compare well with those for Moritz et al. (2005) where an early recruited unit (motor unit 2 in table 1 of Moritz et al. 2005) exhibited an initial discharge rate of 6.8 pps and a peak discharge rate of 13.8 pps. Similarly, the motor unit recruited at 9.2% MVC force (motor unit 14 in table 1 of Moritz et al. 2005) displayed an initial discharge rate of 6.8 pps and a peak discharge rate of 19.2 pps.

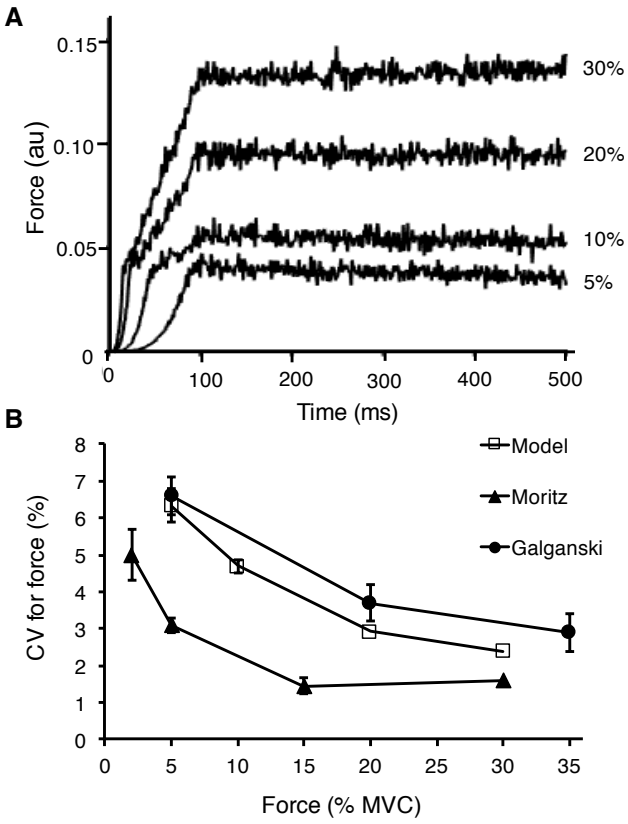

Figure 4. Simulated muscle forces during isometric contractions at four target forces. A. Forces produced by the state-space model. The force fluctuations were quantified as the coefficient of variation for force during the last 2 s of each contraction. B. Comparison of the simulated results obtained in the current study with experimental findings for the first dorsal interosseus muscle (Galganski et al., 1992; Moritz et al., 2005). Error bars represent the standard deviation.

Force model

The discharge times of motor neurons were converted to motor unit forces as described in equation (15). The simulated muscle force at each target force is shown in Figure 4A. The coefficient of variation of force during the hold phase (2-4 s) was greatest (5.9 ± 0.5%) for the simulated contraction at 5% MVC and least (2.1 ± 0.2%) for the simulated contraction at 30% MVC. The simulated values are compared in Figure 4B with experimental measurements for first dorsal interosseus (Galganski et al., 1993; Moritz et al., 2005). Due to the low-pass filtering characteristics of muscle (Partridge, 1965), 99% of the power in the force signal was in the low frequency (0-10 Hz) spectrum, which contains most of the spectral content important in force production during human movement (De Luca and Erim, 1994; Farina and Negro, 2015).

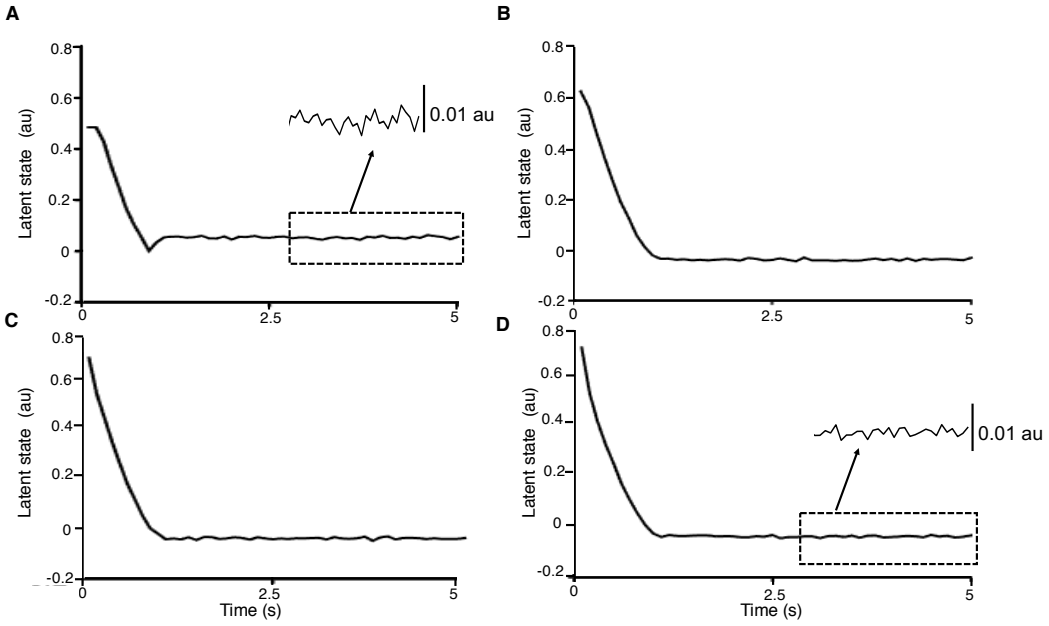

Figure 5. Estimated trajectory of the latent input from the state-space model at 5% (A), 10% (B), 20% (C), and 30% (D) MVC.

Estimated parameters of the state-space model

After the instantaneous discharge rates of motor neurons were converted into discharge times (see methods for explanation), the parameters of the state-space model at each target force were estimated using the EM algorithm described in the Methods section. The discharge times of all motor neurons were arranged into a nxTmatrix, where n is the number of active neurons during the trial and T is the number of time samples, using a resolution of 10 ms. Figure 6A-D shows the estimated latent-state trajectory in a single dimension during the 5-s trials at the four target forces (5, 10, 20, and 30% MVC). Both the ramp and steady portion of the trials were identified using the EM algorithm. Additionally, the variance in the single dimension of latent-state trajectory decreased with target force (0.0024 at 5% MVC) compared with 0.0010 at 30% MVC). This decline in variance for the common input is consistent with the results reported by Castronovo and colleagues (2015) wherein the proportion of common input (relative to synaptic noise) was demonstrated to increase with net excitatory input.

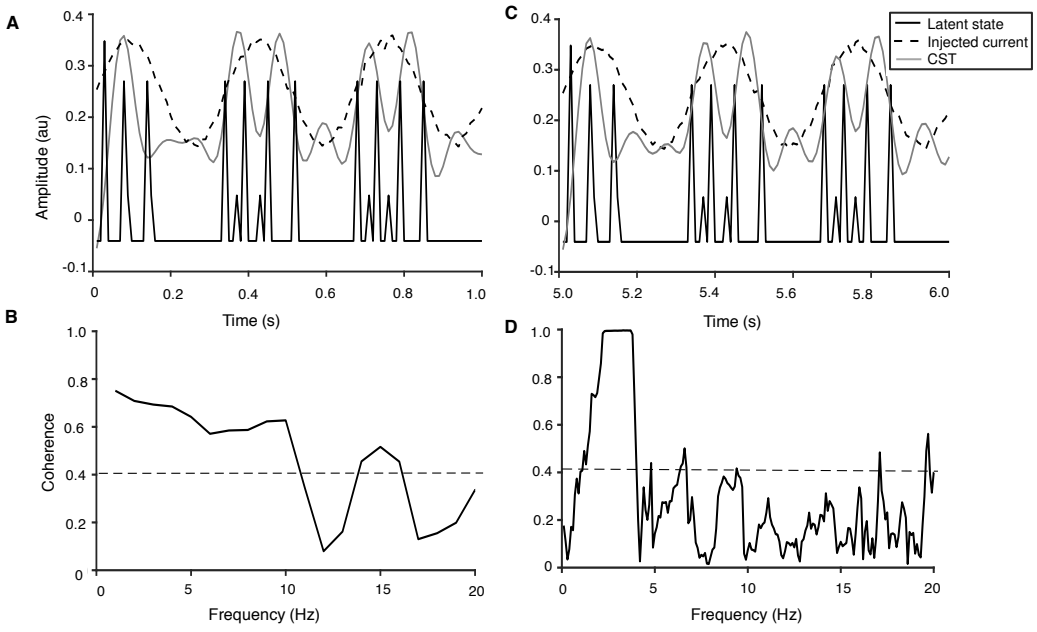

Figure 6. Estimation of the state-space model from a pair of integrate-and-fire neurons (Figure 2) simulated for 1 s (A and B) and 10 s (C and D). Both neurons discharged action potentials in response to a 0.1 nA sinusoidal current with an input frequency of 3 Hz as well as receiving independent and common Gaussian noise. Additionally, neuron B received an inhibitory current from neuron C (a Renshaw cell) in

response to input from neuron A, which reduced the discharge rate of neuron B. The trajectory of the single-dimension approximation of the latent state for the pair of neurons as solved with the EM algorithm is shown as a black solid line (Macke et al., 2011; Buesing et al., 2012), the injected current with common noise superimposed is drawn as a dashed line, and the low-pass filtered (10 Hz) cumulative spike train (CST) is indicated as a grey line. There was a strong temporal relation between peaks in the injected current and changes in the latent state for both simulations (1 s and 10 s), whereas the association between injected current and modulation of CST was only observed for the longer simulation (C). There was moderate coherence (0.58) between the injected current and latent state at ~ 2.5 Hz (data not shown). B and D. The coherence between the low-pass filtered CST and the input current. The coherence was moderate for all low frequency (<10 Hz) values due to the inhibitory input from the Renshaw Cell (C) onto neuron B as well as the brief length of the trial. However, coherence between the two signals was much stronger for the 10-s simulation (D).

Integrate-and-fire neurons

The discharge of action potentials by the integrate-and-fire neurons was simulated for 1 s when they were provided with three currents: common input, common noise, and independent noise (Figure 2A). The discharge times of the two motor neurons are displayed in Figure 2B. Motor neuron A discharged action potentials at 13 pps and, due to the negative feedback from the Renshaw cell (C), the second motor neuron (B) discharged action potentials at 9 pps, which represented a 30% decline in its discharge rate. The space-state vector was estimated from the discharge times of the two motor neurons with an EM algorithm (see Methods). Critically, the latent-state trajectory aligned with the peaks in injected current to the pair of integrate-and-fire neurons (Figure 6A), which demonstrates the feasibility of this model to identify the space-state parameters for groups of neurons with negative feedback from Renshaw cells. In contrast, the CST approach was unable to detect any difference in coherence below 10 Hz between the common input signal (at 3 Hz) and the low-pass filtered CST when the simulation only lasted 1 s (Figure 6B).

When the duration of the simulation was increased to 10 s (Figure 6C and D), however, the CST approach could decode the common input current more clearly and there was strong coherence between the common input signal and low-pass filtered CST at 2-4 Hz. In contrast, signal

duration did not influence the association between the injected current and the state-space trajectory.

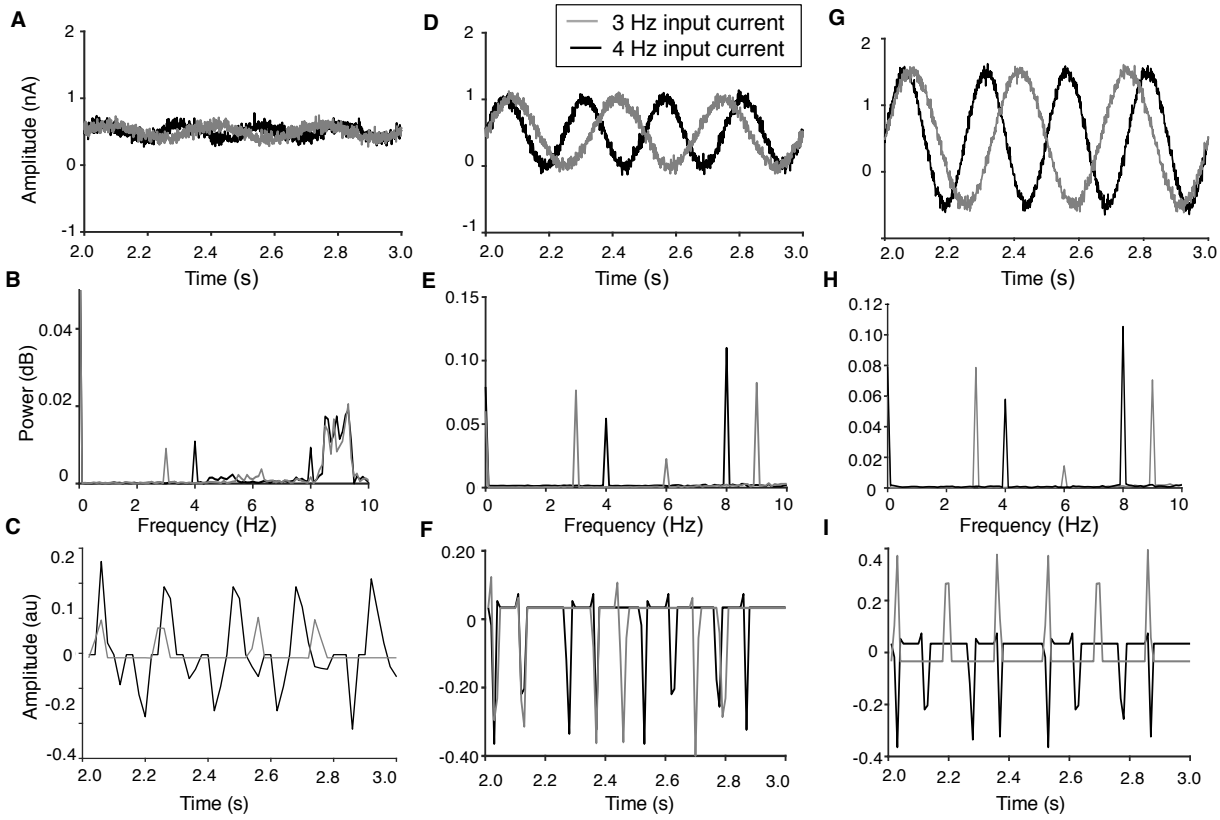

Figure 7. Ten integrate-and-fire neurons were simulated when receiving input currents at two frequencies and three amplitudes for 10 s. A, D, G. The common input current at 3 Hz (grey) and 4 Hz (black) with superimposed Gaussian noise (awgn with a signal to noise ratio of 25 in MATLAB) used to activate the 10 neurons. B, E, H. Spectral content of the low-pass filtered CST derived with the fft function in MATLAB. C, F, I. Estimation of the latent-state trajectory from the discharge activity of the 10 integrate-and-fire neurons at the two frequencies and three input-current amplitudes.

The discharge activity of 10 integrate-and-fire neurons was simulated for 10 s with input currents at two frequencies (3 and 4 Hz) and three amplitudes (0.1, 0.5, and 1 nA) (Figure 14A, D, and G). The spectral content of the CSTs for the 10 neurons was compared to the input current with a Fast Fourier Transform (fft) in MATLAB (Figure 7B, E, and H). The CST approach produced peaks at the two input frequencies (3 and 4 Hz), but the spectral power at these frequencies increased with input current amplitude (Figure 7H), as previously demonstrated by Farina and colleagues (Farina et al., 2014; Negro et al., 2016a). However, the smallest input current (Figure

7A) resulted in the CST approach detecting higher frequency oscillations as the dominant input (Figure 7B). At the intermediate input currents (0.5), the CST method also detected spectral peaks at twice the input frequency (Figures 7E) with the largest peaks at the input frequency for an input current of 1.0 nA (Figure 7H). In contrast, the state-space model estimated a trajectory of the latent state with a higher frequency content at 4 Hz compared with 3 Hz for all three current amplitudes (Figure 7C, F, and I), which indicates greater sensitivity for the state-space model to the details of the input currents.

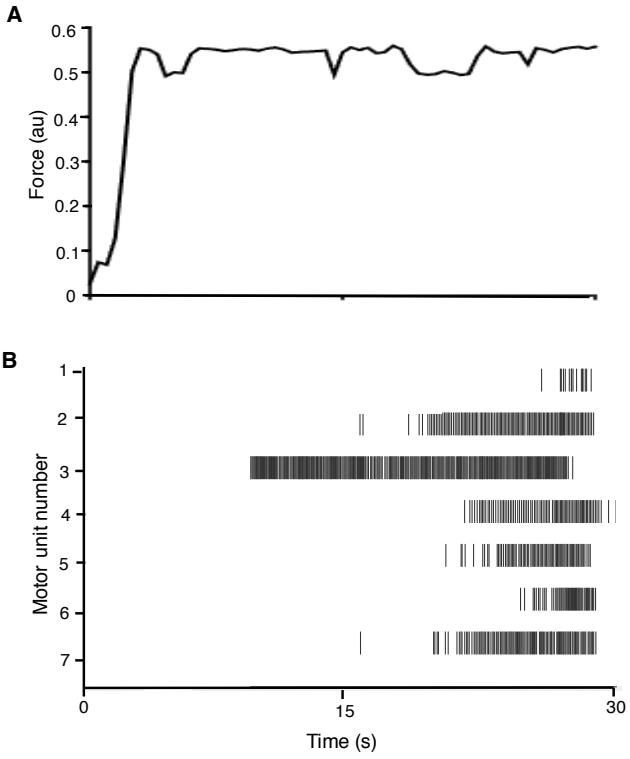

Figure 8. A. The force exerted by a subject during a ramp-and-hold task to a target force of 10% MVC with the elbow flexors. B. Raster of discharge times for seven motor units in the long head of biceps brachii. The motor unit activity was decomposed from high-density surface EMG recordings by a semi-automated blind source kernel compensation algorithm (Holobar and Zazula, 2004; Negro et al., 2016b) during the hold phase of the task. The motor unit discharge times are shown from the last 20 s of the 30-s contraction.

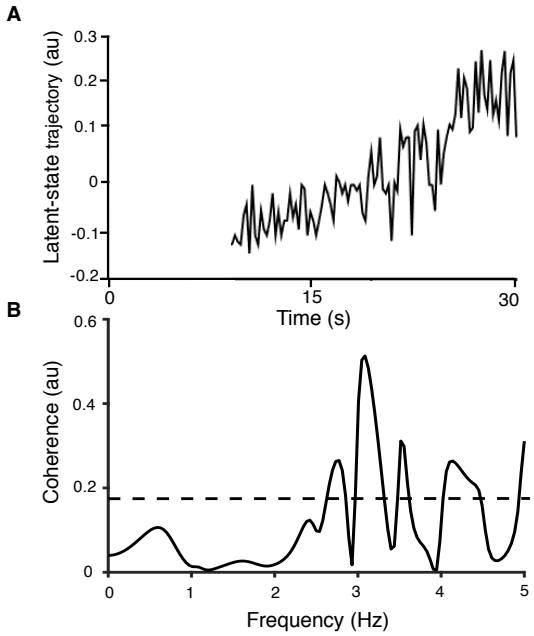

Figure 9. A. Estimation of the single dimension latent-state trajectory from the EM algorithm during the hold phase of the ramp-and-hold task (Buesing et al., 2012; Macke et al., 2011). The latent-state trajectory began after the participant had reached a relatively stable force due to the difficulty in discriminating motor unit discharge times (which are necessary to estimate the model parameters) during the ramp phase. B. Coherence between force during the hold phase and the estimated latent-state trajectory, which reached a peak of 0.53 at ~3 Hz.

Experimental results

The experimental recordings comprised the discharge times of seven motor units in the long head of biceps brachii (Figure 8B) during the last 20 s of an isometric voluntary contraction with the elbow flexors (Figure 8A). The coefficient of variation of force during the hold phase of the task was 2.4%. The algorithm estimated that a one-dimensional latent-space variable resulted in the sparsest model capable of maximizing the log-likelihood of the posterior distribution of the latent state. The coherence between the estimated one-dimensional latent state and the force output was computed, and it reached its maximum (0.54) at 3 Hz. Figure 9 shows the graph of the latent state $x(t)$ during the last 20-s of the 30-s ramp-and-hold trial. Furthermore, the variability in the latent state was estimated to be 0.0032, which could be used as an index of the noise associated with the common input signal. Interestingly, the magnitude of $x(t)$ gradually

increased throughout the contraction, which is consistent with the hypothesis that a gradual increase in neural drive is needed to sustain an isometric contraction, as confirmed by the recruitment of a motor unit (number 1 in figure 8B) relatively late in the task. The finding that a one-dimensional latent state provided the optimal estimate of the common input to the 7 motor units is also consistent with the concept that a single common input signal is critical for force generation during voluntary contractions (Farina et al., 2014; Farina and Negro, 2015; Negro et al., 2009).

Discussion

The goal of the study was to demonstrate that a state-space model is able to estimate the synaptic input and its associated variance that is common to a pool of motor units. The study involved four different datasets, each chosen to evaluate the adequacy of the model to capture a physiologically relevant feature of a pool of motor neurons. First, a pool of motor units was modeled as a Poisson linear dynamical system excited by a one-dimensional common input. This dataset created realistic motor unit discharge times and force characteristics observed during experimental studies. Second, the discharge characteristics of a pair of leaky integrate-and-fire neurons connected to an inhibitory interneuron was examined. This model captured the influence of the interposed Renshaw cell on the discharge rate of the receiving motor neuron and provides an intuitive understanding of how a state-space trajectory may activate such a pathway. Moreover, the state-space trajectory was not influenced by the duration of the simulation. Third, the spectral content of the CSTs for 10 integrate-and-fire neurons at two input current frequencies yielded similar high-frequency spectral content values for the lowest input current (0.1 nA). In contrast, the latent state-space model produced a state-space trajectory for the 10 neurons that differed for the two frequencies of input current at all amplitudes of input current.

Lastly, the common input observed in experimentally recorded discharge times of motor units in biceps brachii during a submaximal isometric contraction can be represented by a one-dimensional latent state.

State-space models have been used successfully to model unobserved neural activity that modulates neurons in cortical circuits (Cunningham and Yu, 2014; Macke et al. 2015). These models combine a description of the coherent dynamics of an unobserved latent state, which is interpreted as the common input to the motor neuron pool in the current study, with the random nature of neural discharge activity (modeled as a Poisson process). The ability to quantify the common input distributed to motor neurons has been a matter of debate since the seminal work of Sears and Stagg (1976). Contemporary methods of quantifying neural drive have resulted in a renewed interest in the area (Farina and Negro, 2012; Farina et al., 2017).

A key feature of current approaches to assess common input is the combination of the discharge times of many motor units into a cumulative spike train (Farina et al., 2014; Farina and Negro, 2015) and examination of the coherence between fluctuations in the cumulative spike train and force during steady isometric contractions. The approach relies on approximating the motor unit pool as a linear filter excited by a common input and independent noise sources. As a result, the neural drive to the muscle comprises the common input signal and the common noise. This methodology has advanced the approach used to quantify the neural drive to muscle (Farina et al., 2014; Farina and Negro, 2015), and the astounding ability to provide intuitive control of human-machine interfaces during reaching movements (Farina and Negro, 2012; Farina et al., 2017).

Negro and colleagues (2016a) have proposed a method that quantifies the proportion of common input driving a pool of motor neurons (Negro et al., 2016a), but the approach cannot distinguish between a common input signal and synaptic noise. Other contemporary techniques also rely on assumptions that are mathematically convenient but difficult to justify in terms of physiology, such as the linearity of the motor unit pool, the approximation of the neural discharges by continuous signals, and Gaussian distributions of noise sources. Although the cumulative spike train method (Farina and Negro, 2015; Farina et al., 2014; Negro et al., 2016a) provides a reasonable estimate of the common input to motor neurons, a latent state-space model appears capable of detecting smaller differences in input current. Moreover, the frequency analysis used in the CST approach is sensitive to the duration of the signal, whereas the state-space approach is more versatile. As such, a state-space model provides a more sensitive method for approximating the common input—and separately—the synaptic noise (both shared and independent) received by a pool of motor neurons.

The EM algorithm provided reproducible estimates of the common input that activated the neurons in all simulations and during the experimental measurement of motor unit activity during a voluntary contraction. The time series of the latent state exhibited moderate coherence (0.53 at 3 Hz) with the applied force in the functional bandwidth of force production (De Luca and Erim, 1994; Negro et al., 2016a), lending support to the concept that the fluctuations in the common input to motor neurons are directly observed in the force output (Castronovo et al., 2015; Farina et al., 2014; Farina and Negro, 2015). The moderate coherence between the estimated latent state and the net force is remarkable because the discharge times from only seven motor units were observed during the experiment; it has been demonstrated that the ability

to characterize the neural drive to muscle improves with an increase in the number of identified motor units (Farina et al., 2014; Farina and Negro, 2015).

Although previous studies have demonstrated a link between force fluctuations during submaximal isometric contractions and oscillations in the neural drive to muscle (Castronovo et al., 2015; Negro et al., 2009), no study has differentiated between the control signal and the noise. In contrast, the covariance matrix, **Q**, in the state-space approach can be used to estimate the noise in the common input. The covariance could be used to examine the association between neural drive and force steadiness, even during long-lasting isometric contractions when the covariance in the input signal might change. This could be accomplished by separating the data (force and discharge times) into multiple segments in which the covariance is more stationary. Additionally, as suggested by Boonstra and colleagues (2016), the state-space model includes relevant physiological properties within the **C** matrix to encode the differential effects of the common input on motor units. The proposed model does not estimate specific physiological properties, but it does allow for entries in the **C** matrix to represent all key properties that influence the discharge of action potentials, such as input conductance and afterhyperpolarization duration (Gustaffson and Pinter, 1984; Heckman and Enoka, 2012; Henneman et al., 1965).

Although the state-space trajectory for the integrate-and-fire simulations contained frequency content that was greater than the injected current, its interpretation is intended to provide a qualitative approximation of the common input to the pool of motor neurons rather than quantify the frequency of the input. For example, the changes in the latent-state trajectory were more frequent for the 4-Hz current than the 3-Hz current (Figure 7C, F, and I). Moreover, the state-space trajectory for the experimental recordings of motor unit activity from a human subject did

not include an input current with high spectral content. The higher frequency oscillations seen in the integrate-and-fire simulations could be due to overfitting of the parameters due to the relatively stable statistical structure of the simulated discharge times. These higher frequency oscillations were absent in the state-space trajectory for the experimental recording and the 120 simulated units.

The results from the simulations using relatively few parameters compared well with experimental data. For example, the variance in the estimated latent input signal decreased with an increase in target force for the 120 motor units simulated as a Poisson linear dynamical system, which has been demonstrated experimentally (Castronovo et al., 2015). Specifically, the coherence between cumulative spike trains of motor units increased with greater target forces (up to 75%) and at the end of submaximal isometric contractions sustained until failure. These results suggest that the proportion of common input increases with net synaptic input. Additionally, the variability in force from the 120 motor units simulated as a Poisson linear dynamical system was within the experimentally reported range of values during steady isometric contractions for the first dorsal interosseus (Galganski et al., 1992; Moritz et al., 2005). The force variability of the simulated contractions—when expressed as the coefficient of variation for force—was greatest at low force outputs (5.9 ± 0.5 % at 5% MVC) and decreased at greater target forces (2.1 ± 0.2% at 30% MVC).

Moreover, the current study demonstrated that the discharge times for a motor neuron receiving inhibitory input, such as is provided by Renshaw cells (Pratt and Jordan, 1987), can be simulated with the state-space model. The parameters of the state-space model estimated from the discharge times of the pair of integrate-and-fire motor neurons with negative feedback were solved using the interconnectivity term within the model, and produced a moderate peak in

coherence (0.58) near the input frequency. Additionally, Figure 6 demonstrates how latent-state trajectory fluctuates when the injected current (control signal + common noise) is greatest. These results indicate that a state-space model can identify the input to a system of neurons with a negative feedback pathway.

Similar to the simulations, the estimated parameters from the motor unit activity during a voluntary contraction provided an intuitively accurate representation of the common input. The magnitude of the common input gradually increased over the course of the 20-s contraction. Experimental studies demonstrate the recruitment of additional motor units during the later stages of fatiguing contractions (Carpentier et al., 2001; Enoka et al., 1988; Person and Kudina, 1972), which was seen in the current study (Figure 8B, motor unit 1), and expressed in the model as an increase in the magnitude of the common input.

The current study proposes a method to analyze motor unit discharge times and quantify the trajectory and variance of the common input underlying the discharge activity of a pool of motor units. The physiologically plausible model represents the discharge times of motor neurons as a discrete process and does not require modeling neuron activity as a continuous time signal, or approximating the motor neuron pool with a linear filter. The feasibility of an EM algorithm to estimate a latent input was demonstrated with two computational simulations and the discharge times of 7 motor units during a ramp-and-hold voluntary contraction. Importantly, the coherence between the one-dimension latent input and the applied force showed a relatively high coherence in the critical bandwidth for force control. The current study demonstrates that a state-space model can be used to estimate an unobserved latent input signal that modulates the discharge times of the motor units even from relatively brief signals. Furthermore, the approach yields an independent estimate of the variance of the input, which may provide an index of the synaptic

noise within the input signal. The approach could be used to quantify changes in the common input and the variability in the synaptic inputs across a range of conditions.

Conclusion: A Poisson linear dynamical system can replicate the motor unit discharge times and muscle force characteristics observed experimentally during low-force steady contractions. The parameters of the model quantify a common input signal and the synaptic noise inherent in signal transmission to motor neurons. The approach can be used to quantify the common input received by pools of motor neurons, on a trial-by-trial basis, during brief and long-lasting voluntary isometric contractions.

Chapter IV

VARIANCE IN THE COMMON SYNAPTIC INPUT ACTIVATING MOTOR NEURONS MODULATES FORCE STEADINESS AND MANUAL DEXTERITY

ABSTRACT

We investigated the associations between grooved pegboard times, force steadiness (coefficient of variation for force), and variability in an estimate of the common synaptic input to motor neurons innervating the wrist extensor muscles during steady contractions performed by young and older adults. The discharge times of motor units were derived from recordings obtained with high-density surface electrodes while participants performed steady isometric contractions at 10% and 20% of maximal voluntary contraction (MVC) force. The steady contractions were performed with a pinch grip and wrist extension, both independently (single action) and concurrently (double action). The variance in common synaptic input to motor neurons was estimated with a state-space model. There was a statistically significant association between the coefficient of variation for force during the steady contractions and the estimated variance in common synaptic input in young ($r^2 = 0.31$) and older ($r^2 = 0.39$) adults, but not between either the mean or the coefficient of variation for interspike interval of single motor units with the coefficient of variation for force. Moreover, the estimated variance in common synaptic input during the double-action task with the wrist extensors at the 20% target was significantly associated with grooved pegboard time ($r^2 = 0.47$) for older adults, but not young adults. These findings indicate that longer pegboard times of older adults were associated with worse force steadiness and greater fluctuations in the estimated common synaptic input to motor neurons during steady contractions.

INTRODUCTION

Manual dexterity is defined as the ability to coordinate small movements of the hands and fingers quickly and accurately (Gershon et al., 2010). One measure of manual dexterity is the time it takes to complete the Lafayette grooved pegboard test (Wang et al., 2011), which increases with advancing age (Ruff and Parker, 1993; Wang et al., 2011). Some of the age-associated variance in pegboard times can be explained by the magnitude of the force fluctuations—force steadiness (Galganski et al., 1993)—during steady, submaximal isometric contractions with hand and arm muscles (Almuklass et al., 2016; Hamilton et al., 2017; Marmon et al., 2011a). For example, Marmon et al. (2011a) found that 36% of the variance in pegboard times for 75 adults (18-89 yrs) was explained by the coefficient of variation for force, a measure of force steadiness, during index finger abduction (partial $r = 0.57$) and grip strength (partial $r = -0.34$). Moreover, a 28% decrease in grooved pegboard times after older adults practiced the task on five occasions was accompanied by significant reductions in the coefficient of variation for force during isometric contractions with the index finger abductors (Marmon et al., 2011b).

To examine the influence of force steadiness on pegboard times in more detail, subsequent studies included double-action tasks in which subjects were required to match target forces with steady contractions while performing two actions concurrently, such as a pinch grip and wrist extension, as occurs during tests of manual dexterity (Ambike et al., 2013; Werremeyer et al. 1997; Yu et al., 2010). With this approach, Almuklass et al. (2016) found that selected features of these double-action tasks could explain 70% of the variance in the pegboard times of young adults (Almuklass et al., 2016). Moreover, the coefficient of variation for force was greater during double-action tasks than single-action tasks, despite similar target forces during both actions (Almuklass et al., 2016; Hamilton et al., 2017), which indicates a difference in the control strategy used for each task (Dideriksen et al., 2017).

The greater coefficients of variation for force often exhibited by older adults during steady contractions were initially attributed to differences in the discharge characteristics of motor units (Galganski et al., 1993; Moritz et al., 2005). Subsequent studies, however, demonstrated that the greater coefficients of variation for force of older adults could not be explained by differences in either the mean or the coefficient of variation for interspike interval (ISI) of single motor units during steady isometric contractions (Barry et al., 2007). Rather, age-associated differences in the coefficients of variation for force depend more on the cumulative activity of the recruited motor units. In a seminal study, Negro et al. (2009) showed that 74% of the variance in force during steady isometric contractions with a hand muscle could be explained by the first principal component of the instantaneous motor unit discharge rates, which was attributed to the common synaptic inputs received by the motor neurons (Farina et al., 2014; 2016, Negro et al., 2016a).

Given the associations between pegboard times and the coefficient of variation for force (Almuklass et al., 2016; Hamilton et al., 2017; Marmon et al., 2011a), and between low-frequency oscillations in force and common synaptic input to motor neurons (Farina and Negro, 2015; Negro et al., 2009), the purpose of our study was to examine the associations between pegboard times, force steadiness (coefficients of variation for force), and variability in an estimate of the common synaptic input to motor neurons during steady contractions in young and older adults. We hypothesized that (1) variability in common synaptic input would be positively correlated with the coefficient of variation for force during steady contractions for both groups of subjects, (2) the coefficient of variation for force and variability in common synaptic input would be greater during double-action than single-action tasks, and (3) the pegboard times of older adults, but not young adults, would be associated with greater coefficients of variation for force

and greater variability in common synaptic input during steady isometric contractions with hand and arm muscles.

METHODS

Thirteen young [25 (4) yrs] and 12 older adults [78 (5) yrs] with no history of neurological disease or injury to the upper extremity consented to participate in a protocol that was approved by the Institutional Review Board at the University of Colorado Boulder (Protocol # 16-0782). All participants were right handed with a mean Edinburgh Handedness of 0.9 (0.1) (Table 1).

Table 1. Subject characteristics. Data are presented as mean (SD).

	Young	Older
Men/women	5/8	7/5
Age (yrs)	25 (4)	78 (5)
Height (cm)	175 (8)	175 (7)
Mass (kg)	63 (13)	73 (7)
Handedness (1 = right)	0.8 (0.2)	0.9 (0.2)
Grooved pegboard test (s)	51 (5)	73 (19)
MVC force (N)		
Wrist extension	105 (27)	117 (46)
Pinch	42 (14)	32 (10)

Experimental protocol. Each subject participated in a single experimental session lasting approximately 60 min. The primary outcome variables were time to complete the grooved pegboard test, coefficient of variation for force during steady isometric contractions with the wrist extensors and thumb-index finger pinch at two target forces (10% and 20% maximal voluntary contraction force), and motor unit recordings from the wrist extensors during steady

isometric conditions. As in some of our recent studies (Almuklass et al., 2016; Hamilton et al., 2017), the coefficient of variation for force was measured for each task independently (single-action tasks) and when the two tasks were performed concurrently (double-action task). In addition, we measured the root mean square of the electromyographic (EMG) activity for the wrist extensors during the force-steadiness tasks.

Grooved pegboard test. The grooved pegboard test requires individuals to place key-shaped pegs into a 5x5 grid of key-shaped holes with varying orientations. Individuals used only their right hand and completed the grooved pegboard from left to right, top to bottom, and as quickly as possible. Each participant was familiarized with the test by inserting pegs into a single row immediately preceding the timed trial. Pegboard time corresponded to the duration from a verbal cue to being the test through to the insertion of the final peg.

Maximal voluntary contraction. The maximal voluntary contraction (MVC) force was measured for the wrist extension and pinch grip tasks. Each MVC required individuals to gradually increase force over 3 s and to maintain the maximal force for approximately 3 s. Vigorous verbal encouragement was provided during the task, which was repeated until the peak force for two trials was within 5% of each other. The average of those peak forces was deemed the MVC force. The force applied by the back of the hand during wrist extension was measured with a JR-3 force transducer (0.0056 V/N, Model 45E15A-U760-A; JR3, Woodland, CA), whereas the pinch force was quantified with a hand-held transducer (0.049 V/N, Model LLB130; Futek, Irvine, CA).

The force signals from both force transducers were low-pass filtered at 50 Hz (V75-48 High Performance Bandpass Filter, Coulbourn Instruments, White Hall, PA, USA) and sampled at 2 kHz with an analog-to-digital converter (Power 1401, Cambridge Electronic Design,

Cambridge, UK). The data were obtained with Spike2 data acquisition software (Version 5.20, Cambridge Electronic Design, UK) and stored offline for analysis in MATLAB 2017a (Mathworks, MA, USA).

Force steadiness tasks. The steadiness tasks required participants to match a target force displayed on a monitor approximately 1.5 m in front of them (Figure 1A and B). The single-action tasks comprised two trials at each target force (10 and 20% MVC) for wrist extension and pinch force, separately (Figure 1C). The double-action tasks comprised 2 trials at both 10 and 20% MVC during which both the pinch and wrist extension forces were matched to the same target force (10 or 20%) concurrently for 30 s (Figure 1D). The steadiness tasks were performed with low-gain visual feedback to minimize online corrections (Christou, 2013); the vertical axis of the monitor represented 100% MVC force, which created a visual angle of 0.75 degrees. All participants were familiarized with the steadiness tasks and then performed two 30-s trials of each task (two actions and two target forces). In each trial, subjects were asked to reach the target force displayed on the monitor and to maintain a steady force until told to stop.

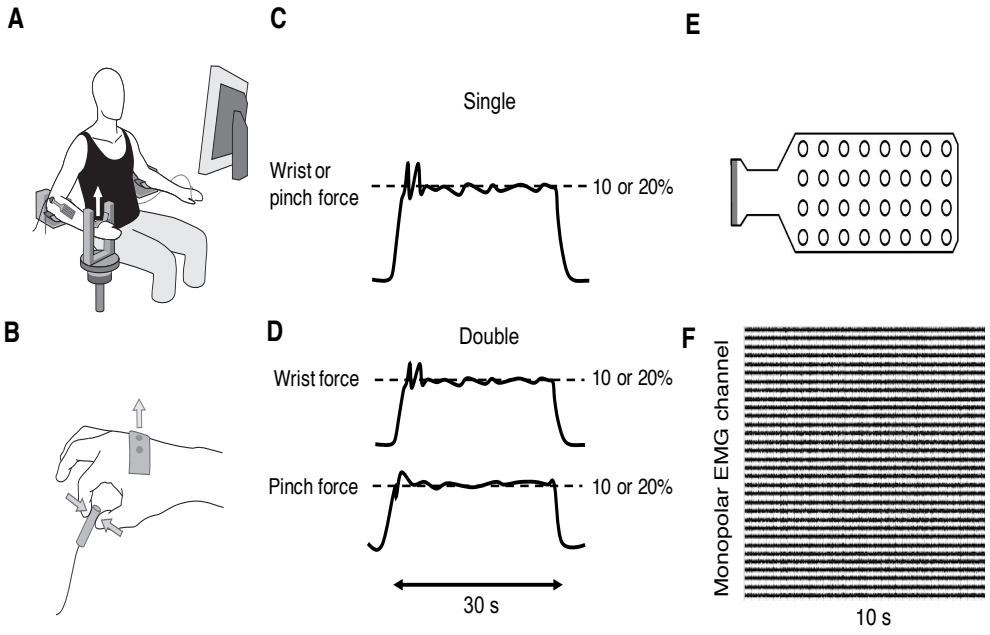

Figure 1. Experimental setup. A. Seated participant facing the monitor. B. Location of the transducers to measure the wrist extension and pinch forces. C. Force for the single-action task. D. Forces for the double-action task. E. The 4 x 8 grid electrode (OTB Bioelettronica) that was placed over the wrist extensor muscles. F. Monopolar EMG recordings from the grid electrode.

Prior to the steadiness tasks, the skin over the extensor digitorum communis was shaved, cleaned, and abraded with a 70% ethanol solution. Subsequently, high-density EMG (OT Bioelettronica, Torino, Italy) signals were recorded from extensor digitorum communis using a 4 x 8 grid electrode with 10 mm interelectrode spacing (Figure 1E). The electrode was attached directly over the extensor digitorum communis muscle as determined by palpation. The electrodes were placed lengthwise from proximal to distal and a reference electrode was fixed over the olecranon process. Monopolar signals (Figure 1F) were recorded at 2 kHz (3 dB bandwidth, 10-500 Hz, multi-channel amplifier OT Biolettronica, Torino, Italy).

Data analysis. The force signals were low-pass filtered (4^{th} order bidirectional Butterworth, cutoff 20 Hz) and representative data are shown in Figure 2. Force steadiness was quantified as the coefficient of variation for force during the steadiest 10 s of each 30-s trial (Figure 2A and B). Each force signal was visually inspected after a semi-automated analysis in which a 10-s

moving average started from the end of the trial and moved backward to find the 10-s region with the lowest coefficient of variation for force. The trial with the lower coefficient of variation for force was used for further analysis.

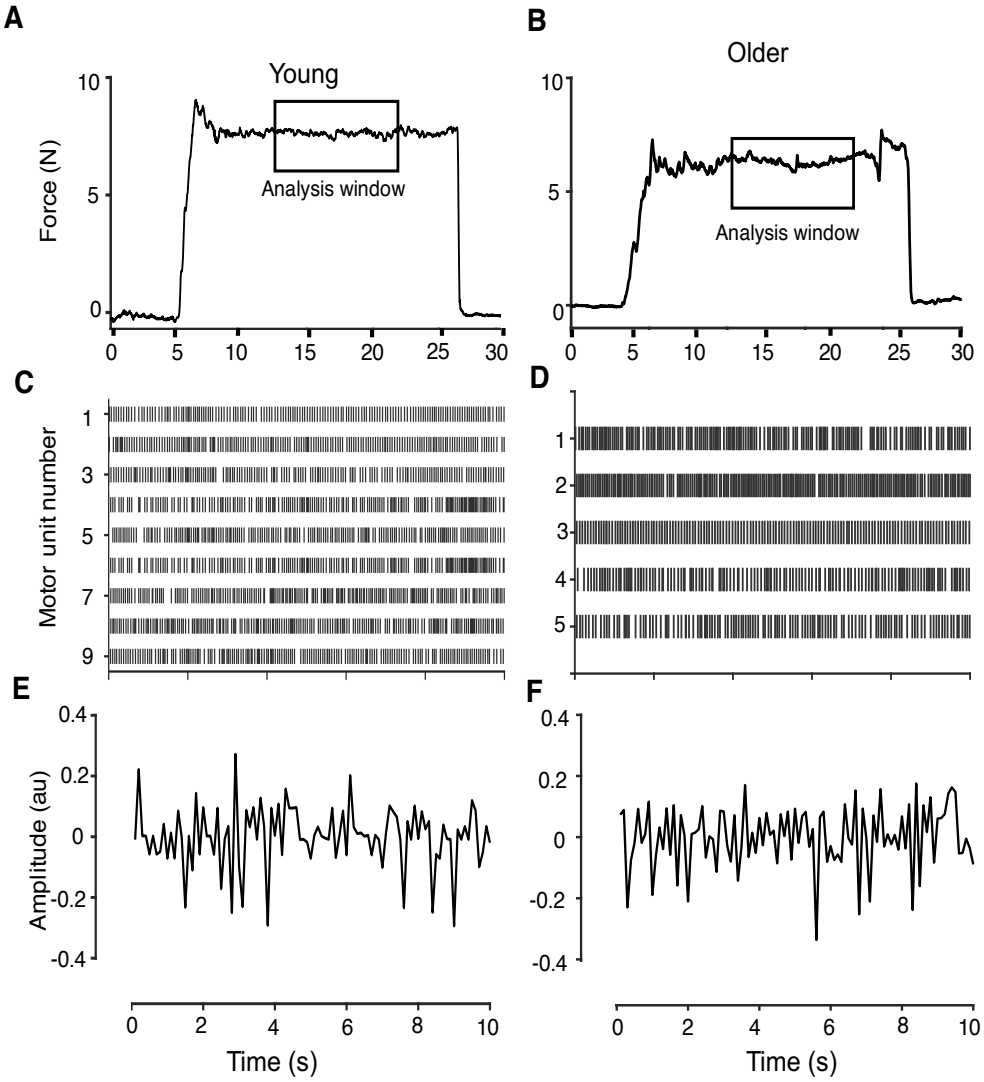

Figure 2. Representative force traces during the 30-s contraction for a young (A) and older (B) adult. The analysis windows indicate the steadiest 10 s of each trial. Raster plot of motor unit discharge times for the young (C) and older (D) adult during the 10-s window. Estimated state-space trajectory for the young (E) and older (F) adults during the 10-s window.

EMG amplitude (mV) was quantified as the root mean square of the rectified and averaged single differential signals from all adjacent pairs of recording sites on the high-density electrode.

In addition, the high-density EMG signals were decomposed into motor unit discharge times (Figure 2C and D) using a semi-automated convolution kernel algorithm (Holobar and Zazula, 2004; Negro et al., 2016b) from OT Bioelettronica. This algorithm has been validated previously (Del Veccio et al., 2017; Negro et al., 2016b) and was initially implemented using an SIL of 0.8. The motor unit discharge characteristics were then inspected and only motor units that met four criteria were included in the analysis: (1) a mean ISI between 20 and 200 ms; (2) coefficient of variation for ISI ≤50%; (3) a skewness for the ISI distribution of less than 2; and (4) an observable waveform in bipolar differential recordings.

The motor unit discharge times were used to fit the parameters of a state-space model (Feeney et al., 2017) to estimate the common synaptic input signal to motor neurons during the force steadiness tasks. In this model, discharge rate ($\boldsymbol{\gamma}$) of the ith recorded motor unit is parameterized as a Poisson process and is represented by equations 1 and 2:

$$\boldsymbol{\gamma}_i(\mathrm{t}) = \exp[\boldsymbol{z}(t)] \quad (1)$$

$$\boldsymbol{z}(t) = \boldsymbol{C}\boldsymbol{x}(t) + \boldsymbol{D}s(t) + \mu \quad (2)$$

X(t) represents the latent common input driving the pool of motor neurons, whereas **C** corresponds to the physiological parameters that encode how the discharge rate of each neuron will be influenced by **x**(t). **D**s(t) denotes the potential coupling between motor neurons, such as from persistent inward currents (Heckman et al., 2008; Johnson et al., 2017) or Renshaw cell inhibition (Kirkwood et al., 1981; Windhorst, 1989), and μ is the logarithm of the average discharge rate. The dynamics of the common input are modeled as follows:

$$\boldsymbol{x}(t) = \boldsymbol{A}x(t-1) + \boldsymbol{b}f(t) + \boldsymbol{E}(\boldsymbol{t}) \quad (3)$$

A is a linear approximation of the dynamics of the common input signal, **b**f(t) allows for modeling the influence of the target force (or other external factors) on discharge rate, and **E**(t) is

a Gaussian noise vector that models the synaptic noise in signal transmission within the neuromuscular system (Katz and Miledi, 1970). The parameters of the model evolve according to Poisson linear dynamics with the following distributions:

$$\boldsymbol{x_i} \sim \mathcal{N}(x_o, Q_o)$$
$$\mathbf{x}_t \mid \mathbf{x}_{t-1} \sim \mathcal{N}\ (\mathbf{A}\mathbf{x}_{t-1}\ \mathbf{b}\mathbf{f}_t, \mathrm{Q}) \tag{4}$$

Where x_O and Q_o represent the initial state and covariance matrix, which evolves over the trial. Q is an estimate of the physiological fluctuations in the common input signal. The estimate of the common input, **x**(t), may be visualized as the trajectory of a vector over the trial (Figure 2E and F), whereas the variability in the common synaptic input (Q) may be estimated. We assume Q remains constant during brief, steady, isometric contractions.

We used an existing open source Expectation-Maximization (EM) algorithm (Macke et al., 2011; Buesing et al., 2012) to estimate the parameters of the state-space model to quantify common input—and its variance—to the motor neurons. The motor unit discharge times were down-sampled to 10-ms bins and arranged into an *n* x *T* binary matrix where 1 represented the occurrence of an action potential. The EM algorithm was initialized with a Poisson subspace estimate of the single-dimension, state-space trajectory and iteratively refined until a local maximum of the log-likelihood function of the posterior distribution of trajectories had been reached. The EM algorithm was terminated when either a maximum number of iterations (100) was reached or when the relative error in log-likelihood became less than 10^{-3} (Feeney et al., 2017). The variance in the state-space trajectory represents the variability in synaptic input to motor neurons and is represented by model parameter Q.

Statistics. All data were tested for normality with a Shapiro-Wilk test. A 3-way ANOVA (age x force level x action) was used to compare the influence of age and task on force steadiness

and variability in common input. Within each age group, 2 x 2 repeated-measures ANOVAs examined the influence of action (single versus double) and target force (10% versus 20% MVC force) on the coefficient of variation for force and the estimate of variance in common input (Q). Paired t-tests with Bonferroni corrections were applied post-hoc to examine differences in the coefficient of variation for force and Q between actions and target forces. Effect size for ANOVA was estimated with partial eta squared and Cohen's *d* was used for post-hoc pairwise comparisons. To estimate the relation between variance in the common input with the coefficient of variation for force, a linear regression model was created across all tasks (two actions and two target forces) for both age groups.

To examine relations between grooved pegboard times with the coefficient of variation for force and variance in synaptic input, a backward stepwise multiple regression model was created for all subjects and, separately, for young and older adults. Subsequently, q-q plots were created to ensure normality of the residuals for each multiple-regression model. All statistics were performed in R version 3.4.1.

RESULTS

Force and high-density surface EMG signals were recorded during four force steadiness tasks for the wrist extensors and pinch grip: two target forces (10% and 20% MVC force) and two actions (single and double action). In addition to a single trial of the grooved pegboard test, each participant completed two trials of each steadiness task.

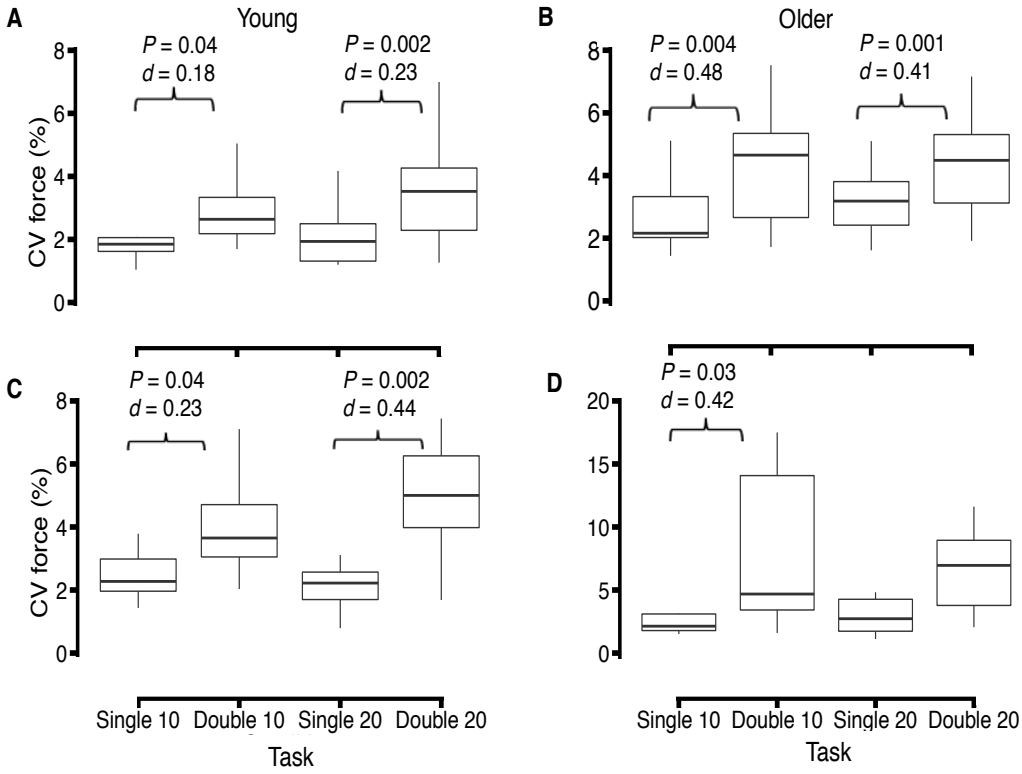

Figure 3. Coefficient of variation (CV) for force from the steadiest 10 s during the steadiness tasks in young (A and C) and older (B and D) adults during wrist extension (A and B) and pinch (C and D). Boxes display the median with hinges representing the 25% and 75% quartile and the whiskers extending to the minimum and maximum value. There was a significant effect of task (action and target force) on force steadiness for both groups of subjects during wrist extension and pinch. A pairwise t-test with a Bonferroni post-hoc correction was applied between all tasks and adjusted P-values ($P < 0.05$) and effect size (Cohen's d) is denoted.

Force steadiness. A 3-way (2 ages x 2 target forces x 2 actions) ANOVA for all subjects detected a main effect for action, which indicated that young and older adults were less steady (greater coefficients of variation for force) during the double-action tasks compared with the single-action tasks ($P = 0.0007$, $F = 12.4$, $\eta^2 = 0.19$). Similarly, a main effect for age indicated that older adults were less steady than young adults ($P = 0.03$, $F = 4.6$, $\eta^2 = 0.08$). There was no main effect for target force on force steadiness ($P = 0.91$, $F = 0.011$, $\eta^2 = 0.001$). All subjects completed each condition, so subsequent analyses were performed within each age group to optimize the statistical power with a repeated-measures design.

Within age groups, young adults exhibited a main effect for task (target force and type of action) on the coefficient of variation for force during both wrist extension ($P = 3.4 \times 10^{-4}$, $F = 7.9$, $\eta^2 = 0.19$) and pinch ($P = 2.5 \times 10^{-7}$, $F = 18.3$, $\eta^2 = 0.45$). Similarly, older adults displayed a main effect for task on the coefficient of variation for force for both wrist extension ($P = 0.013$, $F = 4.16$, $\eta^2 = 0.15$) and pinch ($P = 0.003$, $F = 5.9$, $\eta^2 = 0.21$). Post-hoc analyses indicated that the coefficient of variation for force exhibited by the young adults (Figure 3A and C) was greater during the double-action tasks than the single-action tasks at both target forces for wrist extension (10%: $P = 0.04$, Cohen's $d = 0.18$; 20%: $P = 0.002$, Cohen's $d = 0.23$) and pinch (10%: $P = 0.004$, Cohen's $d = 0.48$; 20%: $P = 0.001$, Cohen's $d = 0.41$). In older adults (Figure 3B and D), the coefficient of variation for force was greater during the double-action task compared with the single-action task for wrist extension at both target forces (10%: $P = 0.004$, Cohen's $d = 0.45$; 20%: $P = 0.002$, Cohen's $d = 0.44$) and for the pinch at the lower target force only ($P = 0.03$, Cohen's $d = 0.42$).

Table 2. Discharge characteristics of motor units in the wrist extensors for the two groups of participants during the four force steadiness tasks. Data are presented as mean (SD)

	Young				Older			
Action	Single		Double		Single		Double	
Number of motor units	141		134		149		156	
Target force	10%	20%	10%	20%	10%	20%	10%	20%
EMG amplitude (mV)	4.3 (1.5)	5.8 (1.7)*	4.6 (1.3)	6.8 (2.0)*	3.8 (1.3)	5.1 (1.6)*	5.0 (1.8)	6.4 (2.3)*†
Mean ISI (ms)	72.7 (8.2)	71.6 (9.3)	74.9 (11.2)	62.8 (11.1)	72.1 (9.0)	70.2 (11.6)	65.9 (12.6)	67.7 (19.9)
CV for ISI (%)	33.5 (6.0)	33.3 (7.9)	31.3 (4.8)	38.8 (7.6)	31.7 (5.4)	33.8 (7.6)	32.7 (9.7)	34.7 (5.0)

EMG and motor unit discharge characteristics. Root mean square EMG amplitude during the steady isometric contractions differed between target forces for young and older adults

(Table 2). A repeated-measures ANOVA revealed a main effect for target force on EMG amplitude for both young ($P = 6.2 \times 10^{-8}$, $F = 20.6$, $\eta^2 = 0.29$) and older adults ($P = 2.8 \times 10^{-7}$, $F = 18.7$, $\eta^2 = 0.25$). EMG amplitude was greater for the 20% target forces for single-action wrist extension and pinch ($P = 0.002$, Cohen's $d = 0.85$). Similarly, EMG amplitude was greater during double-action tasks at 20% compared with double-action tasks at 10% target force ($P = 0.001$, Cohen's $d = 1.1$).

In contrast to the differences in EMG amplitude for the two target forces, there were no statistically significant differences in discharge characteristics for the 275 motor units in young adults and 305 motor units in older adults recorded in the wrist extensors across actions and target forces (Table 2). We accepted an average of 5.5 ± 2.6 motor units in young and 6.2 ± 2.5 in older adults across the steadiness tasks. There were no significant effects for age on either mean ISI ($P = 0.31$) or coefficient of variation for ISI ($p = 0.13$) across actions and target forces. Additionally, there were no significant effects of action or target force on either mean ISI for young ($P = 0.54$) or older ($P = 0.49$) adults or the coefficient of variation for ISI for young ($P = 0.72$) or older adults ($P = 0.49$).

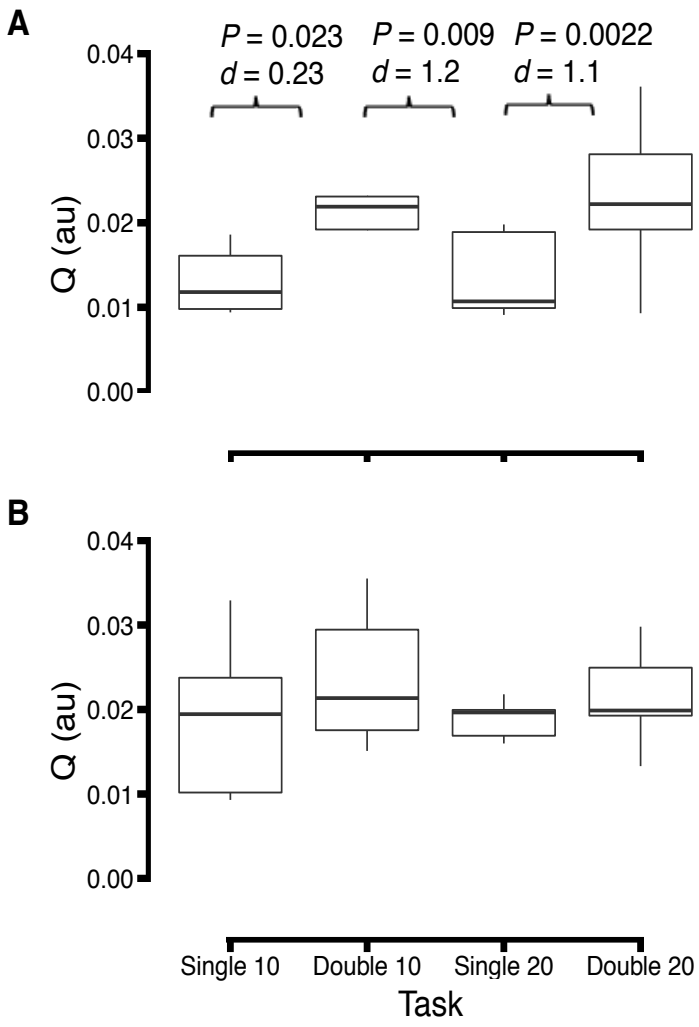

Figure 4. Estimated variability in the common synaptic input to motor neurons (Q). The estimate was derived from the discharge times of motor units in the wrist extensors during the force steadiness tasks in young (A) and older (B) adults. Boxes display the median with hinges representing the 25% and 75% quartile and the whiskers extending to the minimum and maximum value. There was a significant effect of task on Q for the wrist extensors in young adults ($P = 3.5 \times 10^{-4}$, $F = 7.9$, $\eta^2 = 0.25$), but not older adults. A pairwise t-test with a Bonferroni post-hoc correction was applied between all tasks and significant P-values (< 0.05) and effect sizes (Cohen's *d*) are indicated.

Variance in common input. A 3-way (age x force level x action) ANOVA indicated a main effect for action with young and older adults having greater values for the estimated variance in common synaptic input during double-action tasks than single-action tasks ($P = 0.002$, $F = 5.5$,

$\eta^2 = 0.15$) (Figure 4). In contrast, there was no significant main effect for age on Q ($P = 0.15$, $F = 1.7$, $\eta^2 = 0.02$) or target force ($P = 0.02$, $F = 0.11$, $\eta^2 = 0.01$).

Within age groups, there was a significant effect of task (type of action and target force) on Q in young adults ($P = 3.5 \times 10^{-4}$, F = 7.9, $\eta^2 = 0.25$). Q was greater in the double-action task than the single-action task for young adults (Figure 4A) at both target forces (10%: $P = 0.023$, Cohen's $d = 0.23$, 20%: $P = 0.0022$, Cohen's D = 1.1). Additionally, Q was greater during the 10% double-action task than the 20% single-action task for young adults ($P = 0.009$, Cohen's $d = 1.2$). There was no significant effect of task on Q for the older adults ($P = 0.32$, $F = 1.2$, $\eta^2 = 0.06$) (Figure 4B).

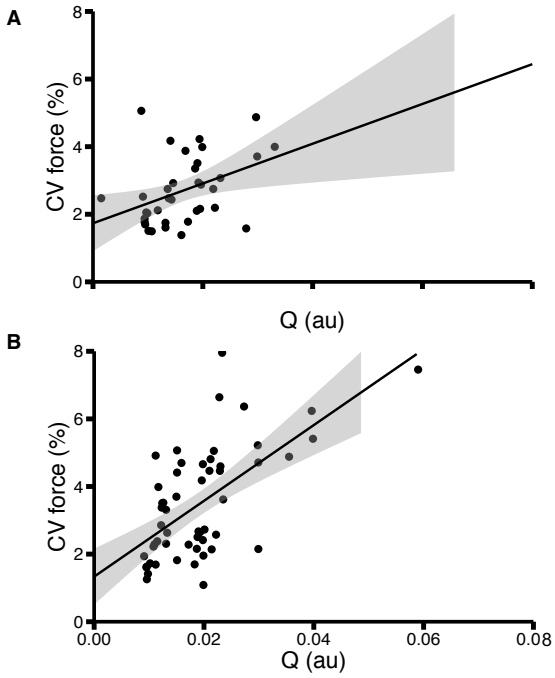

Figure 5. Relation between Q and the coefficient of variation (CV) for force in all tasks for young (A) and older (B) adults. Significant relations were found for young ($r^2 = 0.31$, $F = 16.1$, $P = 0.003$) and older ($r^2 = 0.39$, $F = 33.2$, $P = 4.5 \times 10^{-7}$) adults. The shaded area represents the standard error of the regression for each group.

There was a significant association between the estimated variance in common input and the coefficient of variation for force collapsed across type of action and target force for both young (Figure 5A) and older (Figure 5B) adults. A linear regression model revealed a significant correlation between Q and the coefficient of variation for force for young ($r^2 = 0.31$, $F = 16.1$, $P = 0.003$) and older adults ($r^2 = 0.39$, $F = 33.2$, $P = 4.5 \times 10^{-7}$). Each 0.01-unit increase in Q was associated with estimated increases of 1.1% and 1.3% in the coefficient of variation for force for young and older adults, respectively. There were no statistically significant relations between coefficient of variation for force and mean ISI ($r^2 = 0.006$, $P = 0.4$) or coefficient of variation for ISI ($r^2 = 0.008$, $P = 0.4$).

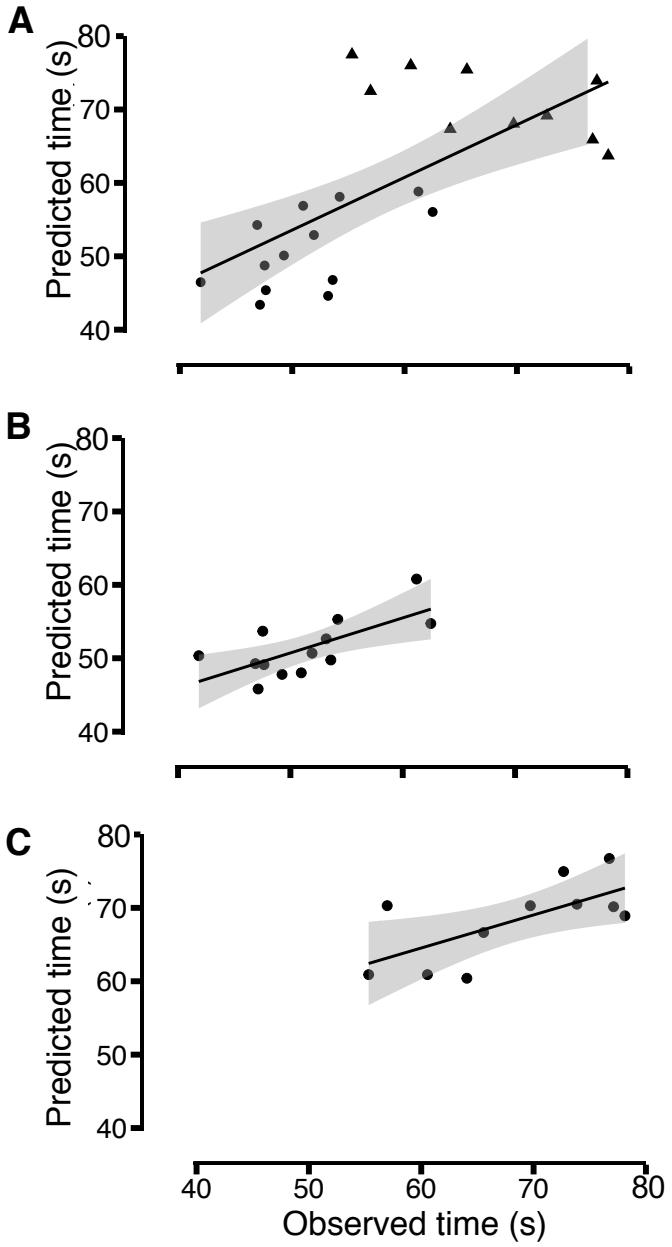

Figure 6. A. Multiple regression model for grooved pegboard time for both young (filled circles) and older (filled triangles) adults ($R^2 = 0.58$, F = 15.22, P = 6.5 x 10^{-5}). The explanatory variables were age (partial r = 0.67, estimate = 2.3) and the coefficient of variation for force during the double-action pinch at the 20% target (partial r = 0.55, estimate = 0.35). B. The regression model for the pegboard times of young adults ($r^2 = 0.47$, 10.06, P = 0.009). The single explanatory variable was the coefficient of variation for force during the single-action wrist extension task at the 10% target. C. The regression model for the pegboard times of older adults ($r^2 = 0.45$, F = 7.37, P = 0.02). The sole explanatory variable in this model was Q derived from motor unit discharge times during the double-action task at the 20% target. The grey areas represent the standard error for the regression models.

Associations with grooved pegboard test. Older adults took longer than young adults to complete the grooved pegboard test ($P = 3.5 \times 10^{-15}$, Cohen's $d = 1.2$, Table 2). To examine the relation between pegboard times, coefficient of variation for force, and estimated variance in the common input signal, we created multiple-regression models for both groups of subjects combined and the two groups separately (Figure 6A-C). A multiple-regression model for all subjects explained 58% of the variance in grooved pegboard times and comprised two explanatory variables: age (partial $r = 0.67$, intercept = 0.36) and the coefficient of variation for force at the 20% target during the double-action pinch task (partial $r = 0.55$, intercept = 2.3). Within this model, a one-year increase in age while holding all other variables constant predicted an increase of 0.36 s in grooved pegboard time. Additionally, a 1% increase in the coefficient of variation for force during the double-action pinch task at the 20% target, while holding age constant, was associated with a 2.3 s increase in grooved pegboard time. The regression model for young adults explained 47% of the variance in grooved pegboard performance with one variable: coefficient of variation for force during wrist extension at the 10% target ($r^2 = 0.47$, $F = 10.1$, $P = 0.009$). The regression model for older adults explained 45% of the variance in grooved pegboard time with one variable: Q during wrist extension at the 20% target ($r^2 = 0.45$, $F = 7.4$, $P = 0.02$).

DISCUSSION

We investigated the associations between grooved pegboard time, the coefficient of variation for force, and the estimated variability in common synaptic input to motor neurons during steady isometric contractions in young and older adults. The main findings were that the estimated variance in common synaptic input—Q in the state-space model—was significantly

related to the coefficient of variation for force during steady, submaximal contractions for both age groups, and that variability in the common input was directly correlated with grooved pegboard times for older adults. Moreover, despite a consistent and significant increase in EMG amplitude at the greater target force for both young and older adults, there were no statistically significant differences in either the mean or the coefficient of variation for motor unit ISI during the four steadiness tasks (two actions and two target forces). Nonetheless, the estimated variance in common synaptic input was greater during the double-action tasks, but only for the young adults.

Force steadiness tasks. Consistent with previous studies, the coefficient of variation for force was significantly greater for older adults (Galganski et al., 1993; Laidlaw et al., 2000; Tracy, 2007), and it was greater during the double-action tasks than the single-action tasks (Almuklass et al., 2016; Hamilton et al., 2017). Also, as found in other studies that used high-density electrodes to quantify EMG activity (Vila-Cha et al., 2010; Martinez-Valdez et al., 2017), the root mean square EMG amplitude was significantly greater at 20% MVC force for both young and older adults. Despite the increases in EMG amplitude, differences in the coefficient of variation for force were not associated with either the mean or the coefficient of variation for ISI. However, the high-density EMG signals were decomposed to identify the discharge times of many concurrently active motor units (Merletti et al., 2001; Holobar and Zazula, 2007; Negro et al., 2016b) and to derive meaningful estimates of the population dynamics of the motor units involved in each task, such as estimates of the variability in common synaptic input received by motor neurons (Farina & Negro, 2015; Farina et al., 2016; Feeney et al., 2017).

Our results are consistent with previous reports that single motor unit characteristics do not explain differences in force steadiness (Barry et al., 2007). This is likely due to the nonlinear input-output relation of individual motor neurons (Farina and Negro, 2015; Powers and Heckman, 2017), the relatively small amount of force contributed by a single motor unit to the cumulative sum of the motor output (Fuglevand et al., 1993), and the low-pass filtering effect of muscles (Partridge, 1965; Baldissera, 1998) and motor neurons themselves (Farina et al., 2014). Force fluctuations, however, are strongly associated with the common, low-frequency components in motor unit discharge rates when many units are recorded concurrently (Negro et al., 2009). As it is not possible to infer the population dynamics of a motor pool from single motor units, contemporary methods, such as state-space models (Feeney et al., 2017) and the cumulative spike train approach (Farina and Negro, 2015; Farina et al., 2014), estimate the common synaptic input to all motor neurons from the discharge times of multiple concurrently active units. In this way, the estimate of variance in common input provides information that is obscured when analyzing single motor unit characteristics, such as the mean or coefficient of variation for ISI.

The variability in common synaptic input—not individual motor unit discharge characteristics—is responsible for a significant portion of the force fluctuations observed during steady isometric contractions. Variability in common synaptic input was significantly greater during double- than single-action tasks for young adults in our study, which was associated with differences in the coefficient of variation for force between the two actions. Although differences in common synaptic input in older adults did not reach statistical significance between actions, the coefficient of variation for force in both age groups was significantly related to the estimated variability in common synaptic input. Our results are consistent with the hypothesis of Farina

and Negro (2015) that only the low-frequency oscillations in common synaptic input influence the net force (Farina and Negro, 2015; Farina et al., 2014; Negro et al., 2016a). Although we did not find a main effect of target force on the variability in common synaptic input, we only tested two target forces (10 or 20%) whereas Castronovo et al. (2015) found that the proportion of common synaptic input relative to common noise decreased with greater target forces (up to 70% MVC).

A critical feature of our study is the use of a state-space model to estimate common synaptic input, which does not assume linearity of the motor unit pool (Boonstra et al., 2016; Powers and Heckman, 2017) and does not apply principal component analysis to point processes, such as instantaneous discharge rates (Kuhn et al., 2003). Therefore, we extend the work of Farina, Negro, and colleagues (Farina et al., 2014; Farina and Negro, 2015; Negro et al., 2016a) with a robust mathematical model of common synaptic input to the motor pool (Feeney et al., 2017).

In addition, we found that the estimated variance in common synaptic input to motor neurons innervating the wrist extensor muscles was greater during the double-action task relative to the single action task, but only for young adults. Although the wrist-extension target force was the same for both actions and there were no differences in the mean and coefficient of variation for ISI across actions, the estimated variance in common synaptic input was greater at the 20% target force relative to the 10% target force, consistent with a difference in the control strategy for the two actions (Dideriksen et al., 2017). The absence of an effect for the older adults was presumably due to the greater difficulty they had with these novel tasks, as indicated by their more variable force trajectories, especially during the double-action tasks. Although additional practice of the double-action tasks may have lessened the variability, we were concerned that the

adjustments would compromise our evaluation of the relation between the coefficient of variation for force during the double-action tasks and pegboard times as measured in a single trial. Alternatively, our study may not be sufficiently powered to detect the changes in common synaptic input to older adults during these tasks.

Grooved pegboard test. Significant amounts of the variance in the time to complete the grooved pegboard test was be explained by an expanded set of steadiness tasks (Almuklass et al., 2016; Hamilton et al., 2017) and the variability in common synaptic input (Feeney et al., 2017) during these tasks. A multiple-regression model explained 57% of the variance in pegboard times for all participants, which included age and the coefficient of variation for force during the double-action pinch at the 20% target force as the primary explanatory variables. These predictor variables are similar to those found by Marmon et al. (2011a) in which 36% of the variance in pegboard times of the participants (18-89 yrs) was explained by the coefficient of variation for force during index finger abduction at a 5% target force and handgrip strength.

A subsequent multiple-regression model for the data obtained from older adults (n = 25) by Marmon et al. (2011a), however, explained 59% of the variance in pegboard times with three predictor variables: age (partial $r = 0.66$), the coefficient of variation for force during index finger abduction at a 5% target force (partial $r = -0.31$), and pinch-grip strength (partial $r = 0.20$). In our study, 45% of the variance in pegboard times of older adults was explained by the estimated variance in common synaptic input derived from the discharge times of motor units in the wrist extensor muscles during the double-action task at the 20% target force. Moreover, there was a strong association between the estimated variance in common synaptic input (Q) and the coefficient of variation for force during wrist extension at 20% MVC ($r^2 = 0.6$). Our results are consistent with Marmon et al. (2011a) who demonstrated that the ability to exert a steady

submaximal force during an isometric contraction involves a control strategy that is critical to the time it takes to complete the grooved pegboard test, but we provide a mechanism (variability in common synaptic input) responsible for the differences in force steadiness.

Our results for young adults indicated that 47% of the variance in grooved pegboard time could be explained by a single variable: coefficient of variation for force during single-action wrist extension at the 10% target force. Similarly, Almuklass et al. (2016) found that one of the predictor variables in a multiple-regression model ($R^2 = 0.70$) for the pegboard times of young adults (n = 30) was also the coefficient of variation for force during single-action wrist extension at 10% target force. However, the directionality of this relation differed between the two studies; it was positive in our study ($r = 0.69$) and negative (partial $r = -0.48$) in Almuklass et al. (2016). Thus, young adults in our study with faster pegboard times had lower values for the coefficient of variation for force during the wrist-extension task, whereas the converse relation was reported by Almuklass et al. (2016).

A major difference between the two studies was the instructions given to the subject for the steady contractions. In our study, subjects were asked to match the target line displayed on the monitor and to maintain a steady contraction. Although Almuklass et al. (2016) used a similar instruction, their subjects were also required to reach the target force as quickly as possible. In their regression model, time to match the target force was the stronger of the two predictor variables (partial $r = 0.78$), which indicates that the rapid force-matching task explains more of the variance in pegboard times for young adults. Consistent with our hypothesis, Q did not emerge as a significant predictor of pegboard times in young adults ($r^2 = 0.09$ for Q during 10% wrist extension) likely due to their pegboard times depending more on decision-making

strategies than rather than being constrained by neuromuscular capabilities (Almuklass et al., 2016).

Chapter V

ELECTRICAL NERVE STIMULATION MODULATES FORCE STEADINESS OF THE WRIST EXTENSOR MUSCLES IN OLDER ADULTS, BUT NOT YOUNG ADULTS

ABSTRACT

The purpose of our study was to compare force steadiness during voluntary and electrically evoked contractions performed with hand and forearm muscles by young and older adults. Thirteen young (25 ± 4 yrs) and 12 older (78 ± 5 yrs) adults participated in a protocol that involved five types of isometric contractions to match a target of 10% of the maximal voluntary contraction force. The voluntary contractions involved wrist extension and pinch grip performed independently (single action) and concurrently (double action). The evoked contractions comprised wide-pulse, high-frequency (1 ms pulses at 100 Hz) neuromuscular electrical stimulation (NMES), narrow-pulse, low-frequency (0.2 ms pulses at 50 Hz) NMES, and a voluntary contraction with superimposed transcutaneous electrical nerve stimulation (TENS). The coefficient of variation for force was less for young adults (1.82 ± 0.43%) than older adults (2.80 ± 1.08%) during single-action wrist extension ($P = 0.03$) and was greater during the double-action tasks for both young and older adults. The coefficient of variation for force did not differ between the two groups during the three types of electrical nerve stimulation, but was only significantly reduced relative to single-action wrist extension for older adults. Moreover, older adults exhibited significant correlations between the coefficient of variation for force during single-action wrist extension and its decrease with each type of electrical nerve stimulation. This association was only significant in young adults for wide-pulse, high-frequency NMES. Modulation of force steadiness across conditions was greatest for the older adults who were least steady during the voluntary contraction.

INTRODUCTION

When an individual performs a submaximal isometric contraction to match a constant target force, the applied force typically fluctuates about the target. The magnitude of the force

fluctuations can be quantified as either the standard deviation (SD) or the coefficient of variation for force and is used as a measure of force steadiness (Galganski et al. 1993; Laidlaw et al. 2000; Salonikidis et al. 2009). Despite the simplicity of the measurement, force steadiness during isometric contractions is strongly associated with the time it takes young, middle-aged, and older adults to perform a pegboard test of manual dexterity (Almuklass et al. 2016, Hamilton et al. 2017, Marmon et al. 2011ab), chair-rise and stair-climbing times in older women (Seynnes et al. 2005), training-induced changes in stair-climbing ability and balance in older adults (Kobayashi et al. 2014), walking speed and balance in persons who have had a stroke (Hyngstrom et al. 2014), and declines in walking performance exhibited by persons with multiple sclerosis (Arpin et al. 2016).

The fluctuations in force during steady isometric contractions are strongly associated with the common modulation of discharge rate for concurrently active motor units (Farina et al. 2016; Farina and Negro 2015; Negro et al. 2009). The critical role of the integration of synaptic inputs by motor neurons in contributing to the modulation of force steadiness was demonstrated by Jones et al. (2002) when they compared the standard deviation of the force fluctuations at a range of target forces during voluntary contractions and those evoked by neuromuscular electrical stimulation (NMES). Although the standard deviation of the force fluctuations increased with target force during voluntary contractions, it remained relatively constant across target forces when the contractions were evoked by eliciting action potential in intramuscular axons with NMES. This finding underscored the importance of the synaptic inputs received by motor neurons in modulating force steadiness during voluntary contractions.

The specific intramuscular axons engaged by electrical stimulation depend on the intensity of the applied current and the pulse duration and frequency of the stimulus trains (Amiridis et al. 2015;

Chipchase et al. 2011; Collins 2007; Maffiuletti 2010; Martin et al. 2016). Conventional NMES protocols evoke contractions by activating motor axons with currents of less than 100 mA, frequencies in the range of 40 to 80 Hz, and pulse durations of 0.2 to 0.5 ms (Colson et al. 2009; Jones et al. 2002; Vanderthommen and Duchateau 2007). In contrast, longer pulse durations and greater frequencies, such as 1 ms and 100 Hz, can elicit action potentials in both motor and sensory axons and thereby involve a central contribution to the evoked force (Bergquist et al. 2011; Clair-Auger et al. 2012; Lagerquist et al. 2009; Wegrzyk et al. 2015). Moreover, transcutaneous electrical nerve stimulation (TENS) involves the application of weaker currents that activate sensory axons exclusively without evoking a muscle contraction (Sluka and Walsh, 2003). Although both conventional NMES (Jones et al. 2002) and TENS (Kouzaki et al. 2012) can reduce the coefficient of variation for force during steady isometric contractions, the influence of wide-pulse, high-frequency NMES on force fluctuations is unknown.

The purpose of our study was to compare force steadiness during voluntary and electrically evoked contractions performed with hand and forearm muscles by young and older adults. The protocol involved two types of voluntary contractions and three forms of electrical nerve stimulation, during which force steadiness was quantified as the coefficient of variation for force. The voluntary contractions involved wrist extension and index finger-thumb (precision) pinch, both independently (single-action task) and concurrently (double-action task) (Almuklass et al. 2016; Hamilton et al. 2017). The three types of electrical nerve stimulation manipulated the amount of sensory feedback that contributed to the force applied by the wrist extensors. We hypothesized that the coefficient of variation for force for both groups of participants would be greater during the double-action task and less during the two types of NMES-evoked

contractions than during voluntary contractions, but that it would be less during the application of TENS for older adults only.

METHODS

Thirteen young (25 ± 4 yrs; 8 women) and 12 older (78 ± 5 yrs; 7 men) adults met the inclusion criteria and provided informed consent to participate in our study. The experimental procedures were approved by the Institutional Review Board at the University of Colorado Boulder (Protocol #17-0064) and were in accordance with the Declaration of Helsinki. All participants were free of neuromuscular disease, reported no orthopedic problems that impacted the arms, hands, or fingers, and were not taking medications known to influence neuromuscular or cognitive function. All subjects participated in one experimental session that lasted approximately 1 hr.

Grooved pegboard test. The protocol began with one trial of the grooved pegboard test in which 25 keyhole-shaped pegs were inserted into similarly shaped holes on a rectangular board (Lafayette Instruments; Lafayette, IN). Prior to performing the timed trial of the test, participants familiarized themselves with the task by inserting pegs into the first row (5 holes) of the 5x5 grid. Pegboard performance was quantified as the time from a verbal command to start the test until the insertion of the final peg. Participants were encouraged to perform the grooved pegboard test as quickly as possible.

Muscle strength. The strength of the muscles that contributed to wrist extension and to a thumb-index finger pinch was quantified as the peak force reached during a maximal voluntary contraction (MVC). Subjects were seated comfortably with the right arm abducted by ~0.79 rad from the trunk, the elbow flexed to 1.57 rad with the pronated forearm resting on a metal stand,

and the wrist secured on a padded brace (Figure 1A). Each MVC trial involved an increase in force from rest to maximum over 3 s and then sustaining it for 3 s. In addition to verbal encouragement during each MVC, visual feedback of the force was provided on a monitor (43.2 cm) located at eye level ~60 cm in front of the subject. The average peak force from two trials that were within 5% of each other was designated as the MVC force, and this value was used to calculate the target forces for the subsequent tasks. Participants also performed an MVC at the end of the protocol to provide a measure of performance fatigability.

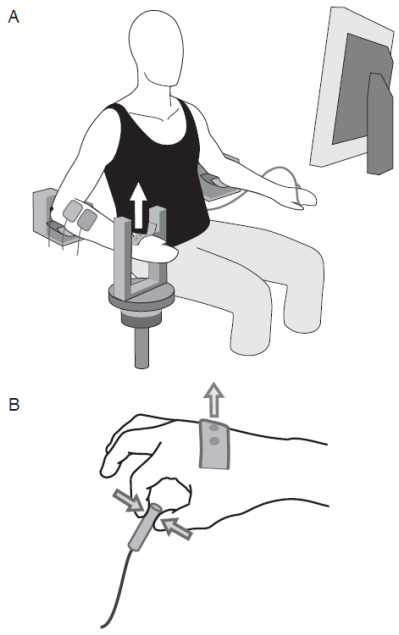

Figure 1. A. Position of the subject and location of the electrodes through which a current was applied to the wrist extensor muscles. B. Position of the transducer to measure force during the pinch and the location of the contact between the back of the hand and the rigid bar during the wrist-extension task.

The force exerted during wrist extension (both the voluntary and evoked contractions) was measured with a JR3 multi-axis force transducer that was attached to a rigid restraint (900 N range, 176 N/V; Woodland, CA). The subject was positioned so that the back of the hand, just proximal to the knuckles, could push up against a rigid restraint that was attached to the JR3

transducer during the wrist extension MVC. The precision pinch force was measured by placing a Sealed Super Mini load cell (2,000 N range, 250 N/V, Temecula, CA) between the index finger and thumb (Figure 1B). The force signals were digitized with a Power 1401 (Cambridge Electronic Design, CED; Cambridge, UK) at 1,000 samples/s and stored on a computer.

Force steadiness. Participants performed submaximal isometric contractions with the wrist-extensor and pinch-grip muscles to match the target force (10% MVC force) displayed on the monitor. The visual display was normalized to provide low-gain feedback with a visual angle of 0.75 degrees (Baweja et al. 2010; Baweja et al. 2012; Park et al. 2017). The steadiness tasks required participants to perform each action (wrist extension and precision pinch) independently (single-action task) and concurrently (double-action task) and to maintain a steady contraction for 30 s. The subjects practiced each task before performing the steadiness trial. The force exerted by the subject was displayed as a horizontal line in real-time over the course of a trial, which subjects were asked to match to the horizontal target line. The double-action task required subjects to move the horizontal line for each action concurrently to its target line.

In addition to the applied force, electromyographic (EMG) signals were recorded from the wrist extensors and flexors during the steadiness tasks with high-density grid electrodes (Sessantaquattro, OT Bioelettronica; Torino, IT) that comprised 32 recording sites (10 mm apart) arranged in 4 columns and 8 rows. To minimize stimulus artifacts, a 1.5 cm-wide stainless steel, braided cable was attached to a ground source and held by the participant. To ensure optimal contact between the skin and the electrode, the electrode grids were held in place with adhesive foam and conductive paste (Ten20, Weaver, Aurora, CO). A reference electrode (2 x 3.5 cm, conductive hydrogel, Kendall, Covidien, Mansfield, MA) was placed over either the olecranon process or ulnar head.

Electrical nerve stimulation. After completing the steadiness tasks with voluntary contractions, the high-density grid electrodes were removed and replaced with conductive stimulating electrode pads (PALS Platinum Neurostimulation Electrodes, 5 cm^2; model 895220, Axelgaard Manufacturing Co., Ltd.; Lystrup, Denmark) through which currents were applied to the wrist extensor muscles. A constant-current stimulator (DS7A 129, Digitimer; Welwyn Garden City, UK) was used to provide an NMES current with monophasic, rectangular pulses. The cathode was placed near the proximal end of the wrist extensors with the anode located distal to the cathode (Figure 1). Two combinations of pulse width and frequency were investigated: wide-pulse NMES (1 ms) at 100 Hz and narrow-pulse NMES (0.2 ms) at 40 Hz. The currents were set to evoke contractions that matched the 10% MVC target force. Subjects were asked to relax and allow the stimulation to evoke a contraction for 30 s during which no visual feedback was provided. Participants completed a single trial of each NMES protocol in a randomized order.

Subsequently, participants performed a voluntary contraction with the wrist extensors to match a 10% target force while concurrently receiving a TENS current (LG-TEC Elite, LGMedSupply, LLC; Cherry Hill, NJ). The current was set at 1 mA less than the intensity required to evoke a consistent visible contraction in a forearm muscle, but which produced a tingling sensation. The stimulus parameters for TENS was 50 Hz with 0.2 ms pulses. The task was to match the 10% MVC force target and maintain a steady contraction for 30 s.

Data analysis. The magnitude of the force fluctuations about the target force was quantified as the coefficient of variation for force (ratio of standard deviation relative to the mean) to provide a measure of force steadiness (Galganski et al. 1993). A moving 10-s window (100-ms increments) was used to find the steadiest 10 s (lowest coefficient of variation for force) of each

30-s trial. The force recorded during the NMES trials was detrended prior to quantifying the force fluctuations.

EMG amplitude (mV) was quantified as the root mean square of the rectified and averaged single differential signals from all adjacent pairs of recording sites on the high-density electrode. The signals were averaged for the wrist extensors and flexors over the middle 10-s of the steady, voluntary contractions. Coactivation was quantified as the ratio (%) of the EMG amplitude of the wrist flexors relative to the average amplitude of the wrist extensors and wrist flexors (Falconer and Winter 1985).

Statistical analysis. After confirming the normality of the data with the Shapiro-Wilk test, a 2 x 5 (age by condition) analysis of variance (ANOVA) was implemented to compare the influence of condition (voluntary single-action task, voluntary double-action task, two types of NMES, and augmented sensory stimulation on force steadiness). Two-tailed paired t-tests with Bonferroni corrections to the P-values were applied post-hoc to compare the coefficient of variation for force between groups. A repeated-measures ANOVA was used to compare the influence of condition within age groups. Effect sizes for ANOVA was estimated with η^2 and Cohen's d was used for post-hoc pairwise comparisons. An alpha level of $P < 0.05$ was used to identify significant differences and statistical analyses were performed using R (CRAN, R version 3.4.1). Data are presented in the text as mean ± SD.

RESULTS

The report comprises the results on force steadiness—coefficient of variation for force—during voluntary and evoked contractions and global EMG recordings obtained with the high-density grid electrodes during the voluntary contractions performed by 25 individuals (13 young and 12

older adults). All participants were right-handed, as verified by the laterality quotient (0.9 ± 0.2) of the Edinburgh Handedness Inventory (Oldfield 1971). There were no statistically significant differences between young and older adults for any of the descriptive characteristics, except that the time to complete the grooved pegboard test was longer for older adults (Table 1).

Table 1. *Subject characteristics.*

	Young	Older
Men/Women	5/8	7/5
Age (yrs)	25 ± 4	78 ± 5
Height (cm)	175 ± 8	175 ± 7
Mass (kg)	63 ± 13	73 ± 7
Handedness (1 = right)	0.8 ± 0.2	0.9 ± 0.2
Grooved pegboard test (s)	51 ± 6	73 ± 19*
Wrist extensor MVC force (N)	106 ± 27	118 ± 46
Pinch MVC force (N)	42 ± 14	32 ± 10

Values are mean ± SD. MVC = maximal voluntary contraction. NMES = neuromuscular electrical stimulation. TENS = transcutaneous electrical nerve stimulation. *$P < 0.05$ relative to young adults.

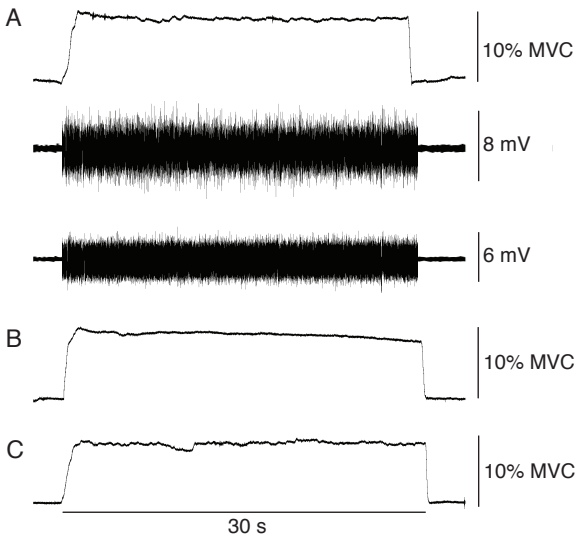

Figure 2. Representative force and high-density EMG recordings during the 30-s wrist-extension tasks. The target force was 10% MVC for all conditions. A. Wrist-extension force, EMG recording for the wrist extensors, and EMG recording for the wrist flexors during a voluntary contraction. B. Wrist-extension force during wide-pulse, high-frequency NMES. C. Wrist-extension force during augmented sensory stimulation (TENS).

As a foundation for interpreting the influence of electrical nerve stimulation on force steadiness, we measured the coefficient of variation for force when the two groups of participants performed single- and double-action tasks involving wrist extension and precision pinch. The target force for all tasks was 10% MVC. Representative records for a single participant are shown in Figure 2. An ANOVA between the two age groups and five contraction conditions revealed significant effects of age ($P = 0.037$, $\eta^2 = 0.05$) and contraction condition ($P = 2.8 \times 10^{-9}$, $\eta^2 = 0.37$). There was a significant effect of contraction condition within the young group ($P = 2.75 \times 10^{-4}$, $\eta^2 = 0.25$) and the older group ($P = 2.3 \times 10^{-7}$, $\eta^2 = 0.44$).

Both age groups had significantly greater coefficients of variation for force during the double-action tasks (young: $P = 0.004$, Cohen's $d = 0.8$; older: $P = 0.004$, Cohen's $d = 1.1$). Notably, there was greater variability across both groups of subjects, as indicated by the SD values, in the coefficient of variation for force during the double-action tasks relative to the single-action tasks,

and for the older adults during single-action wrist extension, but not precision pinch, compared with young adults. Despite these differences in the coefficient of variation for force and its variability between groups and actions, there were no statistically significant differences in EMG amplitude for either the wrist extensors or flexors across conditions (Table 2). There was a main effect for muscle group, which indicated that EMG amplitude for the wrist extensors was greater than that for the wrist flexors (young: P = 0.004; older: P = 0.04). However, there was no statistically significant difference in the coactivation ratio between age groups (P = 0.62), but there was less coactivation during the double-action task than the single-action task for both young (P = 0.008, Cohen's d 0.52) and older (P = 0.013, Cohen's d = 0.32) adults.

Table 2. *Coefficient of variation (CV) for force and EMG amplitudes of young and older adults during submaximal isometric contractions when performing single- and double-action steady contractions*

	Young		Older	
	Single	Double	Single	Double
Wrist extensor CV for force (%)	1.8 ± 0.3	3.3 ± 1.7†	2.8 ± 1.1*	4.3 ± 1.8†
Pinch CV for force (%)	2.5 ± 0.7	4.0 ± 2.1†	2.7 ± 1.6	5.3 ± 2.5†
Extensor EMG (mV)	4.3 ± 1.5	4.6 ± 1.3	3.8 ± 1.3	5.0 ± 1.8
Flexor EMG (mV)	3.3 ± 1.7	2.9 ± 1.4	2.7 ± 1.2	3.2 ± 1.4
Coactivation ratio (%)	42 ± 8	38 ± 8†	40 ± 9	38 ± 7†

Values are means ± SD. *$P < 0.05$ relative to young adults. †$P < 0.05$ relative to single action.

The current required to evoke a contraction in the wrist extensors to match the target force with wide-pulse, high-frequency NMES was not statistically different (P = 0.24) between young (6.3 ± 4.7 mA) and older adults (8.5 ± 4.2 mA). Similarly, the required current for narrow-pulse,

low-frequency NMES was not statistically different (P = 0.06) between young (19.0 ± 6.9 mA) and older adults (25.0 ± 6.7 mA). However, the current applied to augment sensory stimulation (TENS) was significantly less (P = 0.04, Η² = 0.20) for young (9.8 ± 1.4 mA) than older adults (11.0 ± 1.3 mA).

Table 3. Coefficient of variation for force (%) for young and older adults during the three types of electrical nerve stimulation.

	Young	Older
Evoked contractions		
Wide-pulse NMES (%)	1.93 ± 0.68	2.01 ± 0.67†
%Δ voluntary	12 ± 47	-19 ± 33
r (*P* value)	-0.57 (0.04)	-0.53 (0.03)
Narrow-pulse NMES (%)	1.83 ± 0.59	1.69 ± 0.62†
%Δ voluntary	2 ± 33*	-30 ± 30
r (*P* value)	-0.30 (0.32)	-0.60 (0.04)
Augmented sensory stimulation		
TENS (%)	2.41 ± 1.02†	2.29 ± 0.76
%Δ voluntary	33 ± 45*	-6 ± 38
r (*P* value)	-0.07 (0.81)	-0.62 (0.03)

Values are mean ± SD. NMES = neuromuscular electrical stimulation. TENS = transcutaneous electrical nerve stimulation. %Δ voluntary = difference in the coefficient of variation for force during the electrical nerve stimulation condition from that for the voluntary contraction at the 10% MVC target force. The correlation coefficient (*r*) indicates the association between the coefficient of variation for force during the voluntary contraction and the change produced by electrical nerve stimulation. *$P < 0.05$ relative to older adults. †$P < 0.05$ relative to single-action wrist-extension task.

The three types of electrical nerve stimulation elicited mixed effects in the two groups of participants (Table 3). The coefficient of variation for force for the young adults was not statistically different during either wide-pulse, high-frequency NMES (1.93 ± 0.68%) or narrow-pulse, low-frequency NMES (1.83 ± 0.59%) compared with the single-action voluntary contraction with the wrist extensors (1.8 ± 0.3%). In contrast, the coefficient of variation for force was reduced in older adults by both wide-pulse, high-frequency NMES (2.01 ± 0.67%) and narrow-pulse, low-frequency NMES (1.69 ± 0.62%) relative to the value during single-action wrist extension (2.8 ± 1.1%). The application of TENS to augment sensory feedback had the converse effect in that it increased the coefficient of variation for force in young adults (2.41 ± 1.02%), but had no statistically significant effect in older adults (2.29 ± 0.76%).

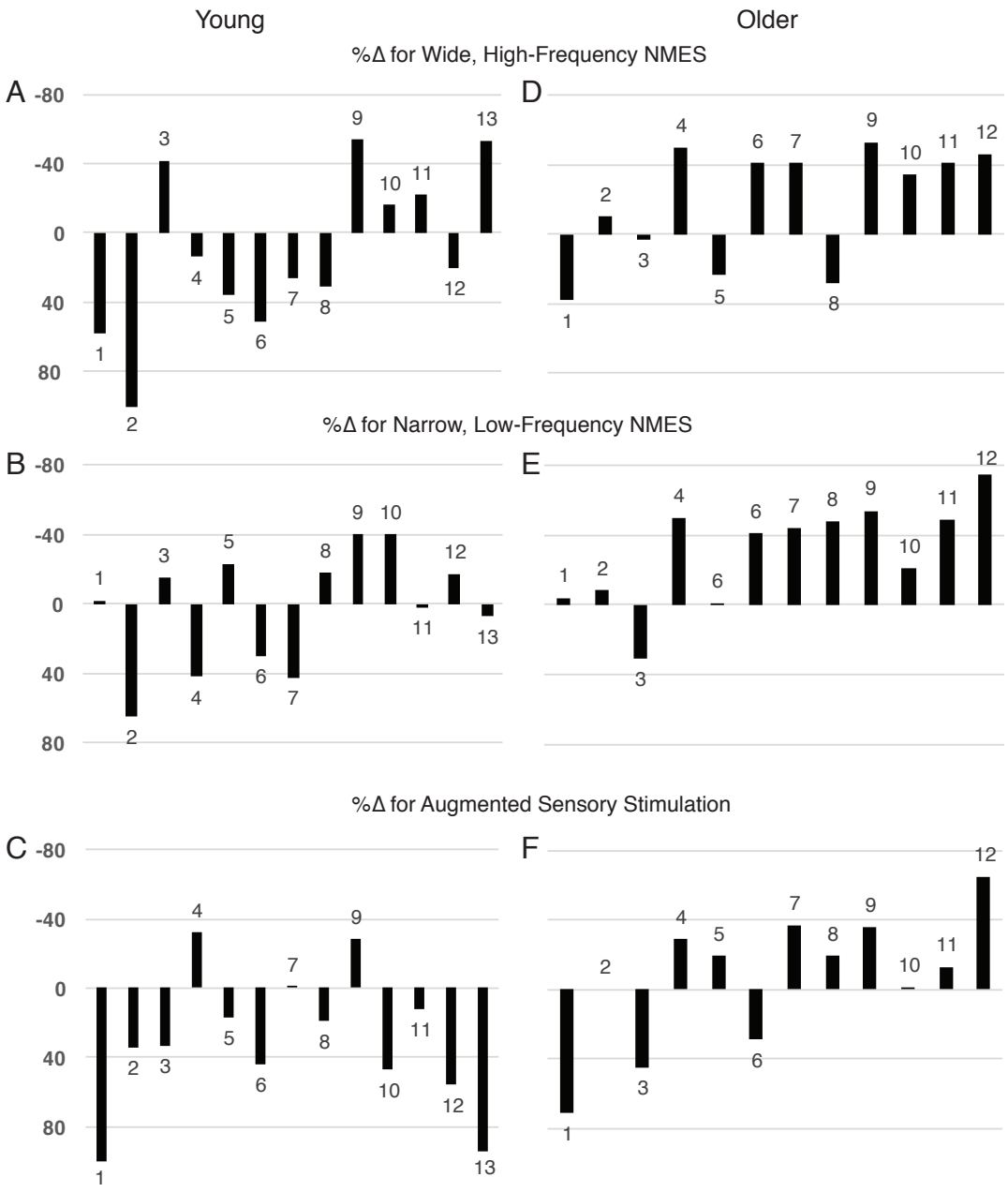

Figure 3. Percent change in the three electrical nerve stimulation conditions relative to the value during single-action wrist extension for young (A-C) and older (D-F) adults. Participants are listed in order of increasing coefficient of variation for force during single-action wrist extension. A, D. Percent change between voluntary wrist extension and wide-pulse, high-frequency NMES. B, E. Percent change between voluntary wrist extension and narrow-pulse, low-frequency NMES. C, F. Percent change between voluntary wrist extension and augmented sensory stimulation condition.

As indicated in Figure 3, however, there was considerable variability across subjects in the influence of electrical nerve stimulation on the coefficient of variation for force relative the value observed in the reference voluntary contraction (single-action wrist extension). Nonetheless, there were statistically significant effects within each group for some conditions when the relative change was compared with the reference value. For all three types of electrical nerve stimulation, there statistically significant correlations ($P < 0.05$) for older adults between the change in the coefficient of variation for force and the value observed during single-action wrist extension (Table 3). The negative correlations indicate that greater values for the coefficient of variation for force during the voluntary contraction were associated with greater changes during electrical nerve stimulation. In contrast, only one of the conditions exhibited a statistically significant association for young adults and that was for wide-pulse, high-frequency NMES.

MVC force during wrist extension at the end of the protocol was 97 ± 27 N for young adults and 114 ± 47 N for older adults, neither of which was statistically different (young: $P = 0.43$; older: $P = 0.61$) from that measured at the beginning of the experiment (Table 1).

DISCUSSION

The main findings of our study were that older adults exhibited worse force steadiness than young adults during only one of the four voluntary contractions and that the influence of electrical nerve stimulation on force steadiness differed for the two groups of participants. Both types of NMES reduced the coefficient of variation for the evoked force in older adults compared with the value observed during single-action wrist extension, whereas superimposed TENS during a voluntary contraction increased the coefficient of variation for force in young adults but not older adults. Critically, all three types of electrical nerve stimulation improved

force steadiness—reduced the coefficient of variation for force—in older adults, but the effect was significantly and negatively correlated with the value observed during single-action wrist extension. A similar association was observed for young adults, but only during wide-pulse, high-frequency NMES.

Voluntary contractions. Since the original observation that older adults are less steady than young adults during submaximal isometric contractions (Galganski et al. 1993), several studies have confirmed that force steadiness is usually worse in older adults during low-force isometric contractions (Barry et al. 2007; Carville et al. 2006; Laidlaw et al. 2000; Tracy and Enoka 2002). In our current study, however, we found that the coefficient of variation for force during single-action wrist extension at 10% MVC force was greater for the older adults than the young adults, but the difference between groups during single-action precision pinch was not statistically significant. In contrast, Hamilton et al. (2017) reported greater coefficients of variation for force during both single-action tasks, also at 10% MVC force, for older adults (74 ± 7 yrs) compared with middle-aged adults (51 ± 7 yrs). Older adults appear to be consistently less steady than young adults during low-force isometric contractions for some actions (e.g., index finger abduction, wrist extension), but the relation is more variable for other actions (e.g., precision pinch).

Although the single- and double-action tasks involved the same target force (10% MVC force), the coefficient of variation for force was greater during double-action wrist extension and precision pinch for both groups of participants. Similar findings have been reported previously (Almuklass et al. 2016; Hamilton et al. 2017). Despite the greater force fluctuations during the double-action, wrist-extension task, the difference in absolute EMG amplitude for the wrist extensors was not statistically significant between the single- and double-action tasks for either

group of subjects. This result is consistent with the evidence that the magnitude of the force fluctuations during steady isometric contractions is strongly associated with the variability in the common modulation of motor unit discharge rate (Farina and Negro, 2015; Negro et al. 2009) and not the cumulative amount of motor unit activity (Barry et al. 2007).

The decline in the coactivation ratio between the wrist extensors and flexors during the double-action task for both groups of subjects likely reduced the influence of the wrist flexors on the stability of the joint, leading to a greater coefficient of variation for force. Previous studies have demonstrated that increases in the coactivation of antagonistic muscles augments joint stability and reduces force fluctuations (Dideriksen et al. 2015). For example, Arellano et al. (2016) found that an increase in coactivation after a fatiguing contraction with the wrist extensors was accompanied by no change in coefficient of variation for force during steady contractions. This finding suggests that the older adults used coactivation to maintain force steadiness. Our study revealed that older adults reduced coactivation during double-action tasks, which led to greater coefficients of variations for force. The decrease in coactivation during the double-action task by both young and older adults was likely due to need to focus the wrist flexor activity on producing the precision pinch, which reduced the level of coactivation.

Electrical nerve stimulation. Part of the motivation for our study was the report by Jones et al. (2002) that the standard deviation for force during voluntary contractions scales linearly with target force (20-70% MVC) for young adults, whereas the standard deviation for force is constant during contractions evoked by NMES. Jones and colleagues used an NMES protocol (pulse width: 300 μs; frequency: 25-30 Hz) that was similar to our narrow-pulse, low-frequency condition. Their results indicate that most of the force fluctuations during voluntary isometric contractions are attributable to differences in central factors that influence motor unit activity,

whereas there are constant, low-level force fluctuations associated with the peripheral signal transduction. The application of NMES generates a current field that elicits action potentials in intramuscular motor axons, but, largely due to varying distances from the stimulating electrodes to the motor axons, that activation of muscle fibers is asynchronous and results in an irregular evoked force (Baldwin et al. 2006; Bergquist et al. 2011) that does not appear to change with the intensity of the NMES current (Jones et al. 2002).

We found that the coefficient of variation for force during the NMES-evoked contractions was not significantly less than that during voluntary contractions in young adults, whereas it was significantly reduced for older adults. This finding indicates that the force fluctuations exhibited by young adults during voluntary contractions were equivalent in amplitude to those produced by the asynchronous activation of intramuscular motor axons by NMES. In contrast, the force fluctuations caused by the common modulation of motor unit discharge rates during voluntary contractions was greater than those produced by the asynchronous activation of motor axons for older adults. Moreover, the coefficient of variation for force during the NMES contractions was similar for young and older adults, indicating a comparable effect of the asynchronous activation of motor axons in the two groups.

The relative difference in force fluctuations between the NMES-evoked and voluntary contractions varied across older adults during both NMES conditions and for young adults during wide-pulse, low-frequency NMES. There was a significant negative correlation between the magnitude of the decrease in the coefficient of variation for force during the NMES contractions and the coefficient of variation for force during voluntary contractions. This finding indicates variability across participants in the extent to which the influence of the common modulation of motor unit discharge rates on force fluctuations exceeded that of asynchronous

activation of motor axons. However, there was no such relation for young adults during narrow-pulse, low-frequency NMES, even though there was no statistically significant difference in the coefficient of variation for force between the two NMES conditions for young adults. Given that there was a moderate correlation ($r = 0.57$) between the reduction in the coefficient of variation for force during the two NMES conditions, it is not clear why the young adults did not exhibit a significant negative correlation for the percent change during the narrow-pulse, low-frequency condition.

In contrast to the influence of NMES on force steadiness, the concurrent application of TENS during the voluntary contraction (single-action, wrist extension) significantly increased the coefficient of variation for force in young adults, but not in older adults. The current applied during TENS was just below motor threshold, which elicits action potentials in a wide range of sensory axons (Gomes-Osman et al. 2017; Moran et al. 2011; Walker et al. 2014). The increase in the coefficient of variation for force exhibited by young adults suggests that the additional sensory feedback during the voluntary contraction increased the variability in the common modulation of motor unit discharge rates by increasing the afferent synaptic input onto motor neurons. This finding differs methodologically from that of Jones et al. (2002) when they found that the superimposition of NMES on a voluntary contraction increased the standard deviation for force; the resulting force fluctuations were due to the combined effects of common modulation of motor unit discharge rates and the asynchronous activation of intramuscular motor axons.

The absence of a main effect for concurrent TENS during a voluntary contraction on the coefficient of variation for force in older adults suggests that the central effects of sensory feedback were saturated in this group. The mechanisms responsible for the decrease in

responsiveness of the older adults could include a reduction in the numbers of sensory receptors, a decline in the responsiveness of the receptors, or an increase in the level of presynaptic inhibition (Baudry 2016). This result is consistent with the findings of others that older adults tend not to rely on sensory feedback when managing conditions that challenge stability (Baudry et al. 2010; Baudry et al. 2014). Despite the lack of a main effect in older adults, however, there was a negative correlation between the reduction in the coefficient of variation for force during TENS and the value observed during the voluntary contraction. Those older adults with worse force steadiness—greater force fluctuations—presumably experienced a reduction in the common modulation of motor unit discharge rates due to the additional sensory feedback, which was opposite to the effect observed in young adults. The concurrent application of TENS, therefore, attenuated at least one major source of the common input to motor neurons, but only in these older adults who were least steady during the submaximal, isometric contraction with the wrist extensors.

The force fluctuations exhibited by young adults during a steady, voluntary contraction with the wrist extensors were equivalent in amplitude to those observed during NMES-evoked contractions. In contrast, the force fluctuations of older adults were greater during the voluntary contraction than during the evoked contractions. The superimposition of TENS during a voluntary contraction, which provided additional sensory feedback, increased the force fluctuations in young adults, but had no main effect in older adults. Nonetheless, the effects elicited by the three types of electrical nerve stimulation in older adults were negatively correlated with the amplitude of the force fluctuations (coefficient of variation for force) during the voluntary contraction. The differences between the two groups of participants were

interpreted in terms of the relative influence of the common modulation of motor unit discharge rates and the asynchronous activation of intramuscular motor axons.

Chapter VI

PEG MANIPULATION CAPABILITIES DURING A TEST OF MANUAL DEXTERITY DIFFER FOR PERSONS WITH MULTIPLE SCLEROSIS AND HEALTHY INDIVIDUALS

Abstract
Manual dexterity declines with advancing age and the development of neurological disorders. Changes in manual dexterity are frequently quantified as the time it takes to complete the grooved pegboard test, which requires individuals to manipulate 25 pegs. The manipulation of each peg involves four phases: selection, transport, insertion, and return. The purpose of the study was to compare the times to complete the four phases of manipulating each peg and the forces applied to the pegboard during peg selection and insertion in persons with multiple sclerosis (MS) and age- and sex-matched healthy adults. Multiple-regression models that could explain the variance in pegboard times for each group of participants were compared to assess the relative significance of the peg-manipulation attributes. The performance of 17 persons with MS (52.2 ± 8.3 yrs) was compared with 17 control subjects (52.2 ± 11.5 yrs). The grooved pegboard test was performed on a force plate. Pegboard times for the MS group (104 ± 40 s) were longer than those for the Control group (61 ± 15 s). Regression analysis indicated that the pegboard times for the MS group could be predicted by the time for the peg-selection phase (R^2 = 0.78), whereas the predictors for Control group (R^2 = 0.77) were the times for the peg-transport (partial r = 0.80) and selection (partial r = 0.58) phases. The variance in the time it took the MS participants to complete the grooved pegboard test was strongly related to the time required to select each peg, whereas the pegboard times for the Control subjects depended mostly on the duration of the transport phase but also on the time to select each peg.

Introduction

Manual dexterity is the ability to manipulate objects through coordination of the hands and fingers, and is a key indicator of motor function (Gershon et al. 2010; Wang et al. 2011). It combines elements of cognitive acuity, tactile sensation, muscle strength, and force control.

Manual dexterity can be quantified as the time to complete a pegboard test, such as the grooved pegboard test or the nine-hole peg test.

Tests of manual dexterity are more sensitive to changes in upper extremity function than other methods used to quantify disability in persons with multiple sclerosis (MS), such as the Expanded Disability Status Scale (EDSS) (Goodkin et al. 1988; van Winsen et al. 2010). The most frequently administered pegboard test for persons with MS is the nine-hole test (Alusi et al. 2000; Fischer et al. 1999; Kragt et al. 2006), which requires subjects to insert and then remove nine cylindrical pegs as quickly as possible from nine holes arranged in 3 rows by 3 columns on a board. Average time to complete the nine-hole test is slower for persons with MS (25.2 ± 10.0 s) than for healthy age- and sex-matched healthy subjects (18.0 ±1.4 s) (Yozbatiran et al. 2006). Moreover, time to complete the nine-hole peg test is strongly correlated with disease-related costs over a six-month period (Koch et al. 2014) and a 20% increase in the time to complete the nine-hole test is associated with a worsening of disability (Kragt et al. 2006). Nonetheless, the greater discriminative capabilities of the grooved pegboard test might provide more insight into the functional significance of the declines in upper extremity strength and hand sensation associated with the progression of MS (Guclu-Gunduz et al. 2012).

The grooved pegboard test requires greater tactile acuity and visuomotor coordination than the nine-hole pegboard test and provides greater discrimination of dexterity among healthy adults (Wang et al. 2011; Bowden et al. 2013; Bryden and Roy 2005; Thompson-Butel et al. 2014). A study of 75 healthy adults demonstrated that the time to complete the grooved pegboard test is fastest for young adults (mean ± SD: 59 ± 6 s), slowest for old adults (89 ± 16 s), and intermediate for middle-aged adults (66 ± 9 s) (Marmon et al. 2011a). Measures of muscle strength, force steadiness during submaximal isometric contractions, and decision-making

strategies explain much of the variance among healthy adults in time to complete the grooved pegboard test (Marmon et al. 2011a; Almuklass et al. 2016; Hamilton et al. 2017). In contrast, essentially nothing is known about which aspects of the pegboard task contribute to differences in pegboard times between healthy individuals and those who are burdened with a neurological disorder.

The purpose of the current study was to compare the times to complete the four phases of manipulating each peg and the forces applied to the pegboard during peg selection and insertion by persons with MS and age- and sex-matched healthy adults. Peg-manipulation capabilities were quantified in terms of the times and forces of the four phases associated with inserting individual pegs into the 25-hole pegboard. The four phases comprised: (1) select a peg; (2) transport it to the specified hole; (3) insert it into the hole; and (4) move the hand back to the well to obtain another peg. The four phases corresponded to the behavioral tasks that are need to be completed with each peg in the pegboard test. Due to declines in cutaneous sensation exhibited by person with MS (Cuypers et al. 2010; Guclu-Gunduz et al. 2012; Kalron et al. 2013), the hypothesis was that significant amounts of the variance in time to complete the grooved pegboard test for the MS and Control subjects would be explained by different phases of peg manipulation. It was not possible to predict *a priori* which phases would emerge as the explanatory variables due to the potential pervasive influence of cutaneous sensation on at least three of the peg-manipulation phases (selection, transport, and insertion).

Methods

Seventeen persons with MS (52.2 ± 8.3 yrs; 10 women; Patient Determined Disease Steps score 3.6 ± 1.0) and 17 age- and sex-matched healthy adults (52.2 ± 11.5 yrs) met the inclusion criteria and participated in the study after informed consent was obtained (Table 1). All procedures were

approved by the Institutional Review Board (Protocol #13-0720 for the persons with MS; Protocol #15-0719 for the healthy individuals) and conducted in accordance with the Declaration of Helsinki.

Table 1. Descriptive statistics for the two groups of participants.

	Number	**Age (yrs)**	**GPT (s)**
Multiple sclerosis	17	52 ± 8 (31-60)	104 ± 40 (56-202)
Control	17	52 ± 12 (31-69)	61 ± 15 (42-100)

Mean ± SD (range). GPT= grooved pegboard test.

All participants performed the tests with the dominant hand, which was determined by self-report for the persons with MS and by the Edinburgh Handedness Inventory – Short Form for the healthy participants (Veale 2014).

Grooved pegboard test. The pegboard was secured to a plate and placed on top of a force transducer (0.0056 V/N, Model 45E15A-U760-A; JR3, Woodland, CA) (Fig. 1A). Force was sampled at 5 kHz, low-pass filtered (second-order bidirectional Butterworth filter, cutoff 12 Hz), and stored on a computer for offline analysis. The force signal was used to determine the time taken for the four phases of each peg-manipulation cycle and forces applied to the board when inserting a peg (Fig. 1B). Each subject performed the grooved pegboard test three times with the dominant hand.

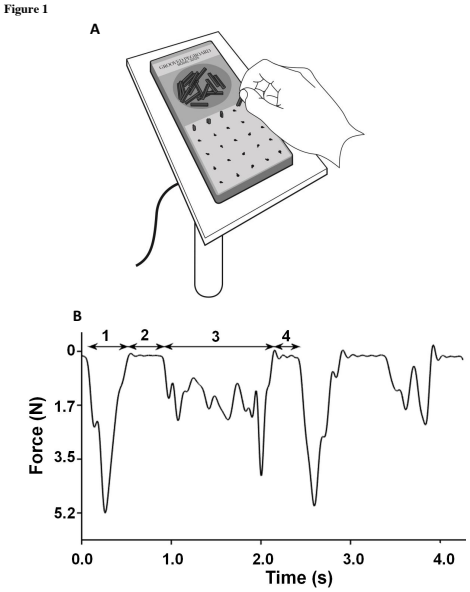

Figure 1. Measurement of the times and force applied to the grooved pegboard during a single peg-manipulation phase. A: Pegboard on a force plate. B: An example of the force-time trajectory showing the four peg-manipulation phases: (1) selecting the peg, (2) transporting it to the hole, (3) inserting it into the hole, and (4) moving the hand back to the well. Subjects were instructed to fill the board one row at a time, from left to right (right-handers) or right to left (left-handers) and from top to bottom.

In addition to the grooved pegboard test, the MS participants performed tests of walking endurance and maximal walking speed. Walking endurance was quantified as the distance walked in 6 min when walking around a 160-m track while being encouraged to walk as briskly as possible. Maximal walking speed was measured with two trials of 25-ft walk test in which participants were encouraged to walk as fast as possible. Maximal walking speed is reported as the average of the two trials.

Data analysis. A custom MATLAB script (Version 2015a, Mathworks, Natik, MA) was used to analyze the force (mean ± SD) applied to the board during peg selection and insertion and the

times for the four phases (Fig. 1B). The analysis was based on a synchronized event marker that denoted the moment the participant began to retrieve a peg from the well. The peg selection and insertion phases were identified when three criteria were met: the first force record prior to the event mark with a value of zero, the derivative of a 100-ms overlapping window (by 99 ms) was less than -0.01 V/s, and the standard deviation of the subsequent window was greater than the preceding one. The transportation and return phases were defined as the intervals of zero force between the force deflections associated with the selection and insertion phases. Subsequently, all phases were visually inspected by the same investigator to ensure that the force profiles were similar to the one shown in Figure 1. Any traces with additional force deflections, such as due to dropping a peg, were discarded and replaced with the data for the next or a previous peg.

The SD of force during peg insertion was measured as an index of force steadiness. Previous studies have found that the normalized measure of force steadiness (coefficient of variation for force) during submaximal isometric contractions can explain significant amount of the variance in pegboard times for young, middle-aged, and older adults (Almuklass et al. 2016; Hamilton et al. 2017; Marmon et al. 2011a).

To assess the potential influence of fatigability on pegboard performance, the data were averaged across three sets of pegs (each set comprised 3 pegs; pegs 2-4, 12-14, and 22-24) for each trial of the grooved pegboard test. Due to the absence of statistically significant differences in timing characteristics between the three sets of pegs, the times for the phases and the applied forces were averaged across nine pegs for each trial. As each subject performed 3 trials of the pegboard test, the data comprised 51 sets of peg-manipulation measurements for each group of participants.

The Shapiro-Wilk test was used to assess normality. The data obtained for the MS participants and the Control group were not normally distributed and were examined with nonparametric tests. Friedman's test was used to assess differences in the timing of the phases within each group and the Mann-Whitney U test used to compare the two groups. The effect size between the four phases was quantified as φ for non-parametric data, which was obtained from $\left(\sqrt{\frac{x^2}{N}}\right)$. The effect size when comparing two values was obtained from $(\frac{z}{\sqrt{n1+n2}})$.

Spearman (non-parametric data) correlations were used to examine the associations between the time to complete the grooved pegboard test with the phase times and the force applied to the board during peg insertion. Based on the correlation results, a stepwise multiple-regression analysis was used to construct a model that explained significant amounts of the variance in the times to complete the grooved pegboard test for each group. Multicollinearity was estimated with the variance inflation factor. Normality tests were performed on the residuals and outliers were removed based on Cook's Distance criterion (Cook 1977). All statistical procedures were performed with SPSS (version 22.0; SPSS, Chicago, IL) and R (version 3.3.2) with α set to 0.05. Within-group post-hoc comparisons with the Wilcoxon Signed Rank test were made between the 4 phases involved 6 statistical comparisons with an adjusted significance set at 0.0083.

Results

Results were obtained for 34 individuals who were assigned to one of two groups (Table 1). The data obtained for the MS group and the Control group were not normally distributed and were examined with nonparametric tests.

Grooved pegboard test. Pegboard times for persons with MS (104 ± 40) were slower ($P <$ 0.0001, effect size = 0.68) than those for age- and sex-matched healthy subjects (61 ± 15 s).

Phase times. Persons with MS were slower than the Control group ($P < 0.0001$, effect sizes range 0.47-0.66) across all phases of peg manipulation (Table 2, Fig. 2). Within-group analysis indicated statistically significant differences between the times for the phases for each group ($P < 0.0001$, effect sizes = 0.82 for MS, 0.88 for control), except between the select and transport phases for age- and sex-matched Control group ($P = 0.014$) (Table 2). Although the MS group took longer to complete each peg-manipulation phase (% increase ± SD), there was considerable variability among these participants in the time for each phase: select, 87 ± 90 %; transport, 99 ± 96%; insert, 63 ± 72 %; return, 84 ± 97% (Fig. 2).

Table 2. Times for the grooved pegboard test (GPT), the four phases of peg manipulation, and force (mean ± SD) applied to the board during peg insertion for the two groups of participants.

	GPT	**Select (s)**	**Transport (s)**	**Insert (s)**	**Return (s)**	**Force (N)**
Multiple sclerosis	104.2 ± 40.3	0.86 ± 0.39	1.04 ± 0.38	1.26 ± 0.4	0.69 ± 0.4	1.9 ± 0.9
Control	61.2 ± 14.8*	0.51 ± 0.21*	0.57 ± 0.19*	0.84 ± 0.3*	0.40 ± 0.2*	2.00 ± 0.9
Effect size	0.68	0.54	0.66	0.56	0.47	0.05

Mean ± SD. * $P < 0.05$ relative to MS group. Within-group analysis found statistically significant differences between the times for the phases for each group (effect sizes in last column), except between the select and transport phases for the Control group ($P = 0.014$).

Figure 2.

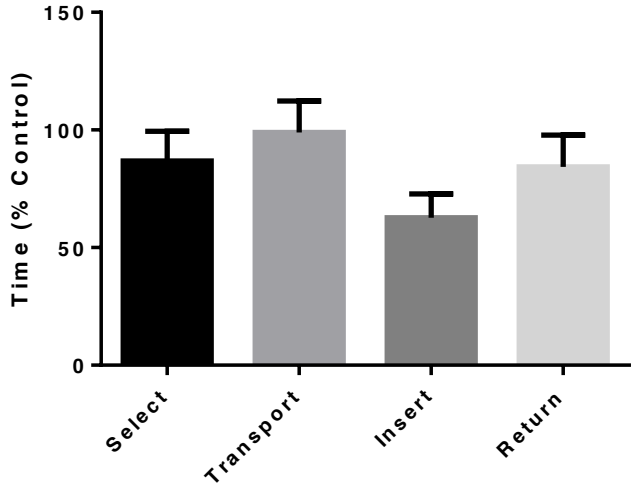

Figure 2. Mean ± SE for the times of each phase for individuals with Multiple Sclerosis (MS) relative to the average values for healthy control.

Force during peg insertion. There were no statistically significant differences between the two groups in the mean force applied to the board during peg insertion ($P = 0.58$, effect size 0.05*)*. However, the standard deviation (SD) of force was less for persons with MS (0.73 ± 0.31 N) than for the Control group (0.92 ± 0.46 N) ($P = 0.02$, effect size = 0.23) (Table 2).

Regression models. There were significant correlations between the time for the grooved pegboard test and the timing of the phases for each group. There were no statistically significant correlations between grooved pegboard time and either mean or SD of force applied to the board during the peg-insertion phase (Table 3).

Table 3. Spearman correlation coefficients between time to complete the grooved pegboard test with the times for the four phases of peg manipulation and the force (mean ± SD) applied during peg insertion.

	Select (s)	Transport (s)	Insert (s)	Return (s)	Force (N)	SD force (N)
Multiple sclerosis (n = 51)	**0.79** [0.88]	**0.68**	**0.69**	**0.77**	0.08	0.01
Control (n = 51)	**0.56** [0.58]	**0.56** [0.80]	**0.32**	**0.65**	-0.23	-0.21

n = number of trials. Bold font indicates statistically significant correlations ($P < 0.05$). Data in brackets denote partial r values for significant predictor variables from the regression models.

The variables that were significantly correlated with the pegboard times were entered into a stepwise, multiple-regression analysis for each group. Regression analysis revealed a significant model for each group with at least one dependent variable, and the residuals for each model were calculated. Normality tests were then performed on the residuals and outliers were removed when the Cook's distance was greater than 4/n, where n is the number of trials for the group (Cook 1977). Based on this criterion, four trials were removed from the analysis for each group. Collinearity was assessed using the variance inflation factor (VIF).

A regression model for individuals with MS explained 78% of the variance in the grooved pegboard time with only one predictor variable: peg-selection time (partial $r = 0.88$; VIF = 1.00; $P < 0.001$) (Fig. 3A). Regression analysis for the Control group produced a model with two predictor variables that explained 77% of the variance in the grooved pegboard time:

transport time (partial r = 0.80; VIF = 1.16; $P < 0.001$) and peg-selection time (partial r = 0.58; VIF = 1.16; $P < 0.001$) (Fig. 3B).

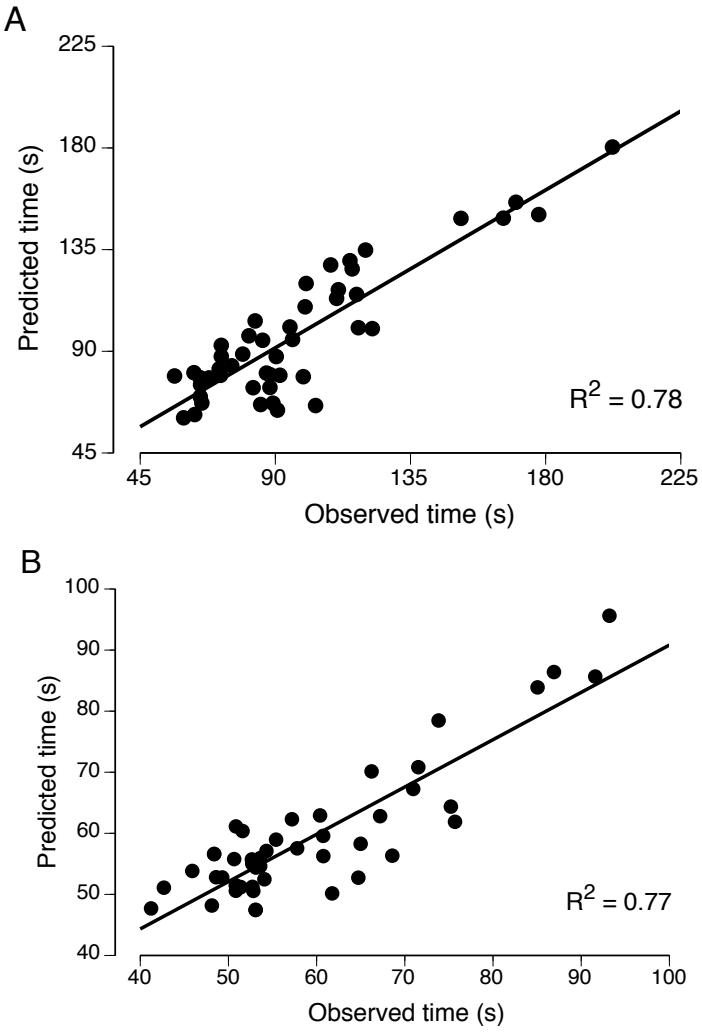

Figure 3. Association between observed and predicted times to complete the grooved pegboard test. A: MS individuals. The predictor variables were identified with a stepwise, multiple regression analysis and comprised only one predictor variable; selection phase (partial r = 0.88; VIF = 1.00; P < 0.001). B: Healthy Control. The predictor variables were identified with a stepwise, multiple regression analysis and comprised peg-selection time (partial r = 0.58; VIF = 1.16; P < 0.001) and transport time (partial r = 0.0.80; VIF = 1.16; P < 0.001).

To further assess the functional significance of the regression model for the MS group, correlations were calculated for the pegboard time and the four peg-manipulation phases with two tests of walking performance (6-min walk and 25-ft walk). As indicated in Table 4, time to

complete the grooved pegboard test was negatively correlated with the distance walked in 6 min (361 ± 140 m) and positively correlated with the time taken to walk 25-ft (8.6 ± 10.6 s). Moreover, the only peg-manipulation phase to be significantly correlated with the two walking tests was peg-selection time, which emerged from the regression analysis as the strongest predictor of the variance in pegboard time for the MS group.

Table 4. Spearman correlation coefficients between walking performance tests with time to complete the grooved pegboard test and the times for the four phases of peg manipulation.

	GPT (s)	**Select (s)**	**Transport (s)**	**Insert (s)**	**Return (s)**
6-min walk (m)	**-0.49**	**-0.55**	-0.21	-0.32	-0.26
25-ft walk (s)	**0.55**	**0.65**	0.15	0.30	0.24

Bold font indicates $P < 0.05$.

Discussion

The main finding of the study was that differences in the time to complete a test of manual dexterity—the grooved pegboard test—for the two groups of individuals depended on the timing of only one or two of the four peg-manipulation phases. The critical phases overlapped for persons with MS (peg selection) and the age- and sex-matched Control group (peg selection and transport). The proportion of the variance in grooved pegboard time explained by the predictor variables was similar for the two groups (R^2=0.77 and 0.78; Control and MS groups respectively). The results were consistent with the hypothesis in that the time it took the two groups of participants to complete the grooved pegboard test was strongly associated with different aspects of peg manipulation.

The average pegboard time for the MS group was longer than those for the healthy adults. Others have similarly reported that pegboard times are slower for persons with MS than for healthy individuals (van Winsen et al. 2010; Yozbatiran et al. 2006; Bertoni et al. 2015; Kierkegaard et al. 2012).

Times to complete all four peg-manipulation phases were strongly correlated with grooved pegboard times for persons with MS (Table 3). Nonetheless, the regression analysis identified a single predictor variable, time to select each peg from the well (*partial r* = 0.88), to explain most of the variance in the grooved pegboard times. Peg selection requires the participant to pick up one of many pegs from the well, which challenges tactile acuity in individuals with reductions in cutaneous sensation. Persons with MS have impaired light touch-pressure, reduced two-point discrimination, and impaired vibration sensations of the hand compared with healthy controls (Guclu-Gunduz et al. 2012; Cuypers et al. 2010). Furthermore, individuals with MS take longer to complete the Action Research Arm Test, which measures the ability to handle and transport small and large objects. Compared with control subjects, persons with MS exhibited less smooth movements, especially during the manipulation components of the test. The strong correlations between the times of the four peg-manipulation phases and time to complete the pegboard test (Table 3) suggest that the deficits in manipulation responsible for the prolonged peg-selection phase also influenced the times for the other three phases.

The associations between the grooved pegboard time and walking performance tests for persons with MS, suggest that pegboard tests provide a systemic indication of disability status, consistent with prior reports of associations between manual dexterity and both activities of daily living (Paltamaa et al. 2007; Kierkegaard et al. 2012; Poole et al. 2010) and measures of walking performance (Kieseier & Pozzilli 2012). The current study showed the peg-selection phase is the

only phase out of four phases that was associated with walking performance in persons with MS. Although there was no *a priori* prediction of which phase might have the greatest influence on pegboard time, it is somewhat surprising that the transport phase—during which the peg is oriented to the hole—did not emerge as a predictor variable for the MS group.

The two predictors for the grooved pegboard times for the Control group were the peg-selection and transport phases. The transport phase, which includes the time from the end of peg selection to the beginning of peg insertion, was the stronger of the two predictor variables (partial r = 0.80). The transport phase is used to detect and align the orientation of the peg held in a pinch between the index finger and thumb to the orientation of the target hole. This task has been reported to require greater tactile acuity and visuomotor coordination than inserting cylindrical pegs for the 9-hole pegboard test (Wang et al. 2011; Thompson-Butel et al. 2014). However, deteriorations in cutaneous sensation and tactile acuity observed in healthy aging do not appear to explain much of the variance in measures of manual dexterity (Bowden et al. 2013; Hamilton et al. 2017; Cole et al. 1998; Voelcker-Rehage et al. 2010). Instead, manipulation of the peg during the transport phase likely relies on various aspects of cognitive function. For example, Ashendorf et al. (2009) reported that the time it took old adults (55-74 yrs) to complete the grooved pegboard test was significantly correlated with scores on tests of psychomotor function, memory, attention, visuospatial ability, and executive function. An independent component analysis by Hamilton et al. (2017) found the grooved pegboard times of old adults (65-89 yrs) to be significantly correlated with age and scores on a test of working memory, but no test of motor function such as those found for middle-aged adults. Consequently, the emergence of time to select a peg as the second predictor variable (*partial r* = 0.58) for the

pegboard times for the Control group may be related to a decline in working memory (Hamilton et al. 2017).

There was no significant difference in the force applied to the plate between the two groups. However, the Control group had significantly greater SD of the force when inserting a peg. The SD of force exhibited by the Control group during the insertion phase was significantly correlated with the times for the transport phase ($r = -0.32$, $P = 0.02$) and the insertion phase ($r = -0.33$, $P = 0.017$). The negative correlations indicate that those participants with faster times for these two phases produced greater force SD during peg insertion. In contrast, there were no significant associations between SD of force and any of the phases in persons with MS. The significant correlations for the Control group are partially consistent with a previous report in which healthy participants with faster pegboard times exhibited worse force steadiness during the force-matching task (Almuklass et al. 2016). This association suggests that decision-making strategies related to the speed-accuracy tradeoff may account for some of the differences in grooved pegboard times of healthy individuals.

In conclusion, times to complete the four phases involved in manipulating each peg during the performance of the grooved pegboard test were all significantly correlated with the time to complete the pegboard test for both groups of participants. Moreover, most of the variance in grooved pegboard times for each group of participants was explained by the timing of one or two of the peg-manipulation phases: peg selection for both groups and peg transport for the Control group. These findings indicate that the most consistently challenging aspect of the grooved pegboard test for the MS participants was selecting a peg, whereas it was transporting the peg for the Control group.

Chapter VII

INDIVIDUALS WITH SACROILIAC JOINT DYSFUNCTION LACK A MUSCLE SYNERGY BETWEEN THE CONTRALATERAL GLUTEUS MAXIMUS AND LATISSIMUS DORSI WHEN WALKING

ABSTRACT

Sacroiliac (SI) joint dysfunction is a debilitating condition that involves pain in the lower back. In healthy individuals, the combined actions of gluteus maximus and contralateral latissimus dorsi likely stabilize the joint and minimize displacement of the involved joint surfaces. The purpose of our study was to compare the contributions of individual muscles to identified synergies between individuals with SI joint dysfunction and control subjects during walking. We hypothesized that individuals with SI joint dysfunction would exhibit significantly less involvement of gluteus maximus and contralateral latissimus dorsi. Electromyographic (EMG) signals were recorded from 16 muscles when individuals with SI joint dysfunction and control subjects walked at 1 m/s on a force-measuring treadmill. Non-negative matrix factorization (NMF) was used to identify patterns of EMG activity (muscle synergies). The output from the NMF analysis comprised information about the timing of each synergy and the relative contribution (weight) of each muscle. Individuals with SI joint dysfunction lacked a muscle synergy between gluteus maximus on the affected side and contralateral latissimus dorsi, which was present in control subjects. Moreover, the timing of this muscle synergy was more variable for individuals with SI joint dysfunction than healthy controls. The results are consistent with the hypothesis that individuals with SI joint dysfunction fail to coactivate gluteus maximus and contralateral latissimus dorsi to help stabilize the sacrum and ilium during walking.

INTRODUCTION

Sacroiliac (SI) joint dysfunction is the etiology for 15-30% of lower back pain (Bernard et al., 1987; Sembrano and Polly, 2009) and causes debilitating pain that impairs mobility (Cher et al., 2014). Symptoms of SI joint dysfunction often include pain in the low back and hip, in

addition to pain at the actual joint, all of which can alter gait patterns and muscle activation strategies.

The SI joint assists in load transfer from the spine to the lower extremities (Sturesson et al., 1988). As such, it must provide the necessary stability for this force transfer while maintaining a degree of mobility for activities of daily living. The joint experiences up to 4800 N of shear force, translates 1.6 mm in the anterior-posterior plane, and may rotate up to 4 degrees while ambulating[4]. Moreover, when laying supine and performing a straight leg raise, the ilium of the rested leg rotates 0.8 degrees backwards and 0.3 degrees inward (Kibsgård et al., 2017).

The function of this joint has been described by Vleeming and colleagues (Vleeming et al., 1992; 2012) with the principles of form and force closure. Form closure refers to the alignment of the concave surface of the sacrum with the convex surface of the ilium, whereas force closure is provided by surrounding muscles, ligaments, and fasciae. The most notable component of force closure is the gluteus maximus and its connection through the thoracolumbar fascia to the contralateral latissimus dorsi. Although the etiology of SI joint dysfunction is unknown, one potential cause of the disorder is the absence of coactivation between these muscles to support force closure of the joint (Kibsgård et al., 2017; Vleeming et al., 1992; 2012; Barker et al., 2014).

Our study is the first to apply a muscle synergy analysis to the electromyographic (EMG) signals during walking to quantify the relative activities of the gluteus maximus and latissimus dorsi muscles in individuals with SI joint dysfunction. A muscle synergy comprises a group of muscles that perform complimentary actions and can be activated with simple control strategies (Lee, 1984; Olree and Vaughan, 1995; Tresch and Jarc, 2009; Clark et al., 2010). Muscle synergies can be quantified by applying a factorization analysis, such as non-negative matrix

factorization (NMF) (Lee and Seung, 1999; 2001), to EMG data recorded during a cyclic task and identifying muscles with similar activation patterns (Tresch and Jarc, 2009; Clark et al., 2010, Cappellini et al., 2006; Ting et al., 2005). The NMF algorithm factors the original EMG signals into two vectors: a timing vector and muscle weighting vector. Muscles that are activated with similar spatiotemporal patterns are grouped into a synergy with the relative contribution of each muscle indicated by its weight.

Locomotion studies have found that three to five muscle synergies can account for 90% of the variance in EMG signals from many limb and trunk muscles during walking and running (Olree and Vaughan, 1995; Cappellini et al., 2006). For example, Olree and Vaughan (1995) characterized the muscle synergies required to reconstruct the original EMG signals as contributing to either a propulsion or loading function during walking. The propulsion synergy, which occurred in late stance, involved the gastrocnemius, adductor magnus, and hamstring muscles. The loading synergy, which appeared in early stance, involved gluteus maximus, gluteus minimus, and erector spinae muscles. Although multiple studies suggest pain in the low back region alters muscle activation patterns (Falla and Hodges, 2017; van Dieen et al., 2017; van den Hoorn et al., 2015; Hanada et al., 2011), no studies to date have examined muscle activation strategies of individuals with SI joint dysfunction during gait. This information could provide clinicians with insight into how patients with SI joint dysfunction adapt to the pain, and could lead to improved treatment plans.

The purpose of our study was to compare the muscle weights of identified synergies between individuals with SI joint dysfunction and control subjects when they walked at the same speed. We hypothesized that individuals with SI joint dysfunction would lack a significant

muscle synergy that included gluteus maximus on the affected side and contralateral latissimus dorsi when walking and that the timing of this muscle synergy would be more variable.

METHODS

Participants

Six women (age = 37.2 ± 5.9 yrs, BMI = 29.5 ± 5.0) who were diagnosed with unilateral SI joint dysfunction, free of neurological disorders, without surgery to the lower limbs or back, and otherwise in good health were compared with six healthy sex- and age-matched control subjects (age: 38.8 ± 7.0 yrs, BMI = 21.3 ± 5.9). Inclusion criteria for the SI joint cohort included a positive result on at least three of five physical examination maneuvers, relief on injection, and pain for at least six months. All individuals were diagnosed by a single physician to ensure diagnostic consistency. The protocol was approved by the IRB at the University of Colorado Boulder (approval number 15-0586). Written informed consent was obtained from all participants.

Experimental procedure

Participants walked at 1 m/s for 30 s on a dual-belt, force-measuring treadmill (Bertec Corp, Columbus, OH). Muscle activity was recorded with bipolar wireless (Noraxon, USA) electrodes from the following muscles, bilaterally: tibialis anterior (TA), medial gastrocnemius (MG), vastus lateralis (VL), biceps femoris (BF), gluteus maximus (GM), erector spinae (ES), and latissimus dorsi (LD). Electrodes were attached to the skin using SENIAM guidelines. Force and muscle activation signals were recorded synchronously at 1 kHz. The positions of 32 reflective markers were recorded at 100 Hz using a 3D 10-camera system (VICON, Centennial, CO). All data were collected in Vicon (Centennial, CO) and exported to MATLAB for

processing (Mathworks version 2015a, Natik, MA). Statistical analyses were performed using R (version 2.14.0).

Data analysis

EMG signals were recorded during 15 strides (left heel strike to left heel strike) for each subject. Left heel strike was defined as the index (i) with a local minimum for the position of the left heel marker, vertical ground reaction force equal to 0 N, and the vertical ground reaction force at the index (i + 10) being at least 5 N greater than the force at index i. The EMG activity from each muscle was then resampled to 0.1% of stride duration to obtain 1000 samples for each stride. EMG signals were band-pass filtered (10-490 Hz) and rectified. A linear envelope was created by low-pass filtering (Butterworth, 4^{th} order, cutoff frequency 10 Hz) and normalizing the signal to the peak value during the stride for each subject[12]. Data were averaged across the 15 strides for each muscle to produce the original EMG (EMG_o) matrix, an **m** x **t** matrix (16 muscles by 1000 samples) for each subject.

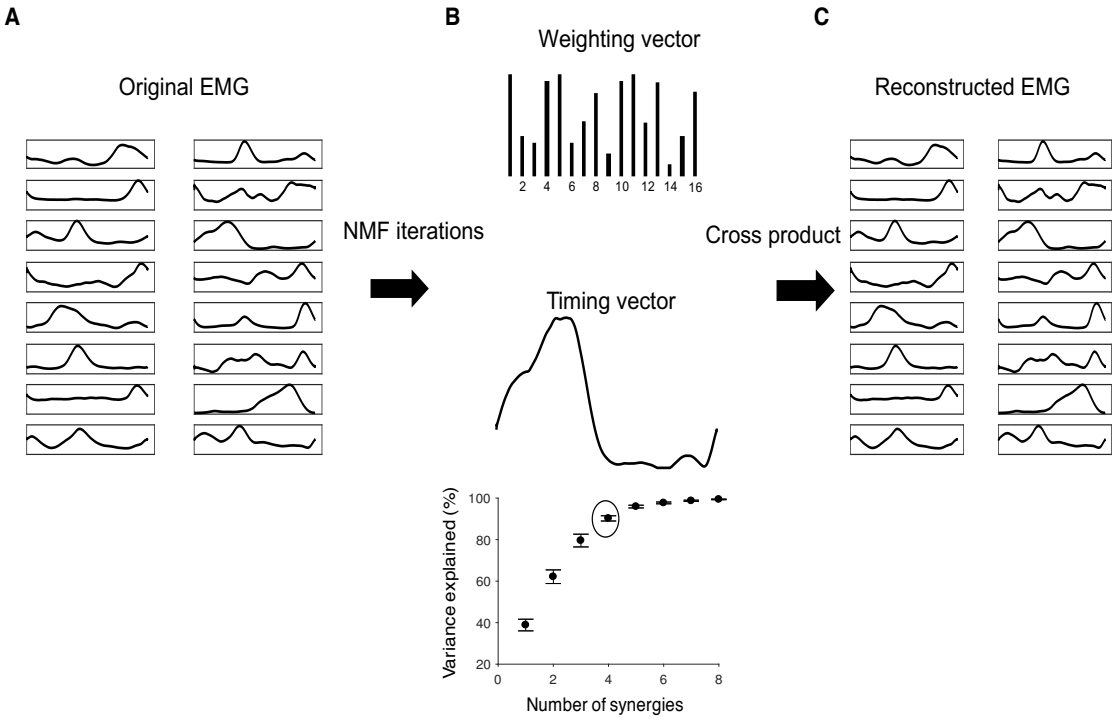

Figure 1. Schematic diagram of the NMF procedure. The rectified and filtered EMG signals (left panel) averaged across 15 strides were concatenated and a non-negative matrix factorization was performed for each subject with 1-8 factors (muscle synergies). Each factor comprised a weighting vector and a timing vector for the 16 muscles (middle panel). The criterion for the number of synergies required for each subject was the value when ≥ 90% of the variance in the original EMG signals was explained and no additional synergies accounted for > 5% of the unexplained variance. The cross product of the total weighting and timing matrices approximate the original 16 EMG signals (right panel).

Non- negative matrix factorization

Figure 1 depicts the NMF approach used to decompose the EMG signals (left panel) into timing and weighting matrices for each muscle synergy (middle panel), and the subsequent estimation of the original EMG signals by cross multiplication of the two vectors (right panel). The filtered, rectified, and normalized EMG signals were entered into a 16 x 1000 matrix (16 muscles at 1000 time points) as shown in the left panel of Figure 1. An iterative NMF algorithm (Lee and Seung, 1999; 2001) was then applied with a progressive increase in the number of factors until a criterion was met. The NMF algorithm decomposed the original **m** x **t** EMG matrix into an **m** x **n** matrix encoding the weights of each muscle on a factor (synergy) and an **n**

x **t** matrix encoding the activation timing of that factor during the stride. The product of the timing and weighting matrices should approximate the original signals (Clark et al., 2010; Lee and Seung, 1999; Ting et al., 2005).

$$EMG_o \approx \boldsymbol{W}\, x\, \boldsymbol{T}$$

An NMF may be performed with the number of factors ranging from 1 to the number of input signals (16 in our study). The number of factors was deemed sufficient when three criteria were met (Tresch et al., 2006): first, the variability accounted for (VAF) in the reconstructed EMG signals (EMG_r) exceeded 90% of the original EMG recordings (EMG_o); second, the plot of the VAF as a function of number of synergies (scree plot, bottom of middle panel in Figure 1) was concave down for the number of factors accepted; and third, subsequent synergies did not explain more than 5% of the variance in the original EMG signals.

$$VAF = 1 - \frac{(EMG_o - EMG_r)^2}{EMG_o^2}$$

The weights of each muscle in the m x n matrix were normalized to the maximal weight within that factor (synergy) so each muscle received a weight between 0 and 1. NMF requires this normalization procedure so that weights across different factors can be compared (Clark et al., 2010; Lee and Seung, 2001; Lawrence et al., 2015).

Once the number of factors had been determined, they were organized into functional groups[23]. This was accomplished by aligning the timing matrix of each factor with a functionally relevant event in the gait cycle, such as heel strike and toe off. The approach used in our study was to identify the factors with a peak in their timing vectors closest to heel strike and toe off bilaterally for each individual, and then ordering the factors from left heel strike to right toe off. Subsequently, the synergies for each participant were compared by finding the peak correlation in the timing vectors.

Statistics

Data were tested for normality using the Shapiro-Wilk test. Because the number of factors was not normally distributed, the Mann-Whitney U test was used to compare the number of factors required to reconstruct the EMG_o signals between groups with alpha = 0.05. Similarly, the muscle weights within each muscle synergy were non-normally distributed. Due to non-normality and our *a priori* hypothesis of a difference in the muscle weights of gluteus maximus and latissimus dorsi, a Mann-Whitney U test was used to evaluate differences in muscle weights for gluteus maximus and contralateral latissimus dorsi during the synergies for a loading response (early stance). Effect size was calculated as $Z/\sqrt{N}$. The time series of the muscle synergies were compared within each group using Pearson correlation coefficients for each participant. Differences between groups were examined with correlation coefficients for the all synergies with a Mann-Whitney U test and the effect size was calculated with Hedge's g.

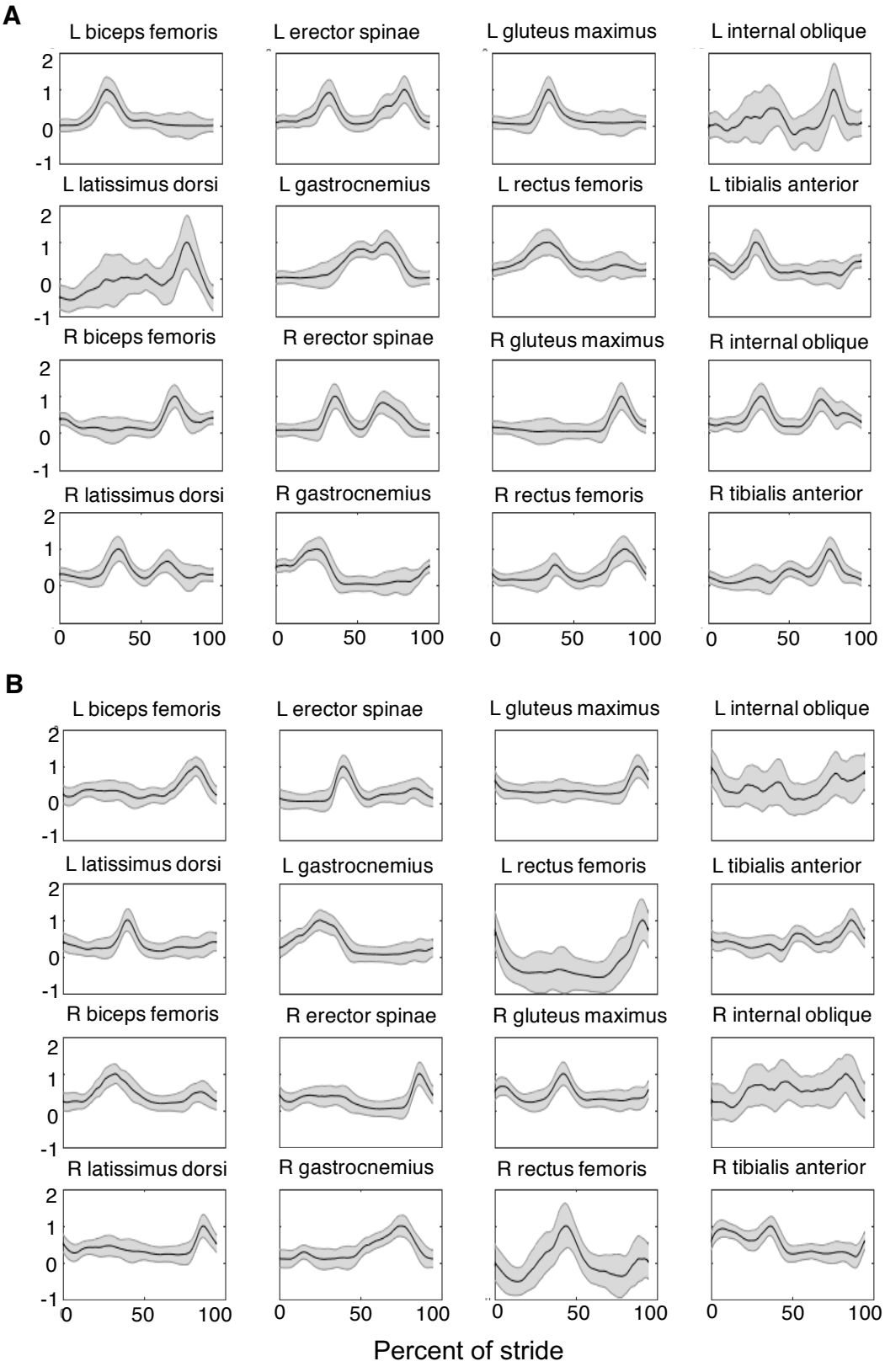
A
L biceps femoris
L erector spinae
L gluteus maximus
L internal oblique
L latissimus dorsi
L gastrocnemius
L rectus femoris
L tibialis anterior
R biceps femoris
R erector spinae
R gluteus maximus
R internal oblique
R latissimus dorsi
R gastrocnemius
R rectus femoris
R tibialis anterior
2
1
0
-1
0
50
100
B
L biceps femoris
L erector spinae
L gluteus maximus
L internal oblique
L latissimus dorsi
L gastrocnemius
L rectus femoris
L tibialis anterior
R biceps femoris
R erector spinae
R gluteus maximus
R internal oblique
R latissimus dorsi
R gastrocnemius
R rectus femoris
R tibialis anterior
Percent of stride

Figure 2. Rectified and filtered EMG signals recorded with bipolar surface electrodes from control subjects (A) and individuals with SI joint dysfunction (B). Black lines represent the average across 15 strides for each subject with grey lines denoting the standard deviation. The EMG amplitudes for each muscle were normalized to maximal amplitude during a gait cycle.

RESULTS

Figure 2 shows ensemble averaged EMG data for the six participants in each group, with the values for each person representing the average for 15 strides. The grey bars represent the standard deviation. The averaged EMG from each participant was decomposed using the NMF approach (Lee and Seung, 1999;2001).

Number of synergies

The number of muscle synergies required to reconstruct the original EMG signals with the stated criteria (Tresch and Jarc, 2009) ranged from 3-5. There was no significant difference in the number of synergies required to reconstruct the EMG patterns between control subjects and individuals with SI joint dysfunction ($p = 0.64$, $r = 0.008$). A scree plot was calculated for each participant and then averages were calculated for each group. Figure 3 depicts scree plots of the average variance accounted for by each synergy for individuals with SI joint dysfunction (Figure 3A) and control subjects (Figure 3B). The average number of synergies was 4.2 ± 0.4 for control subjects and 4.0 ± 0.7 for individuals with SI joint dysfunction.

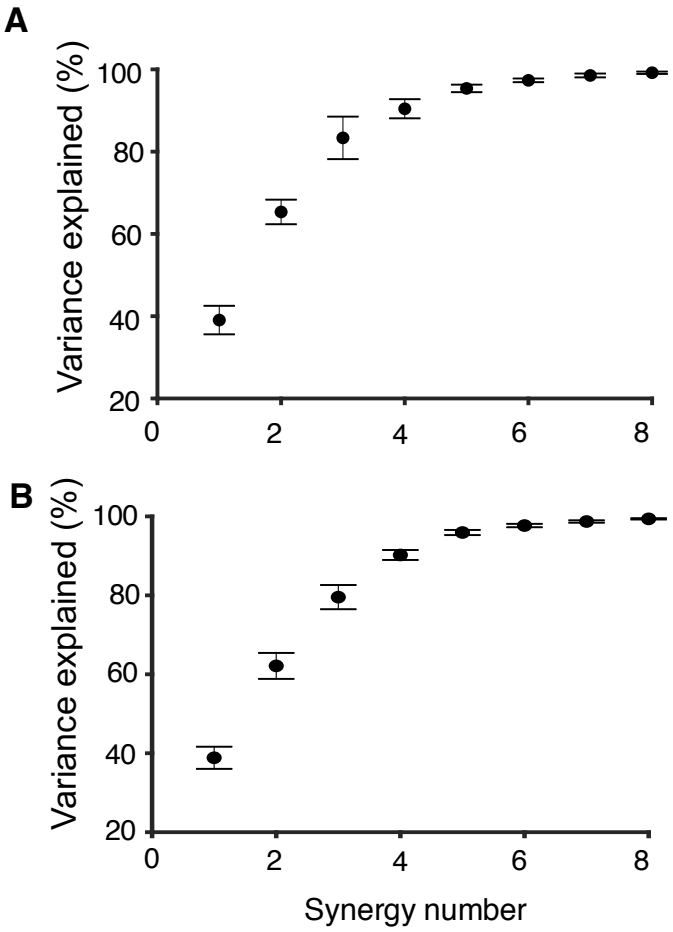

Figure 3. Scree plots for control subjects (A) and individuals with SI joint dysfunction (B) with the variance explained by the reconstructed EMG (from multiplying the W and T matrices) on the y-axis and the number of synergies on the x-axis.

Muscle activation timing

Figure 4 shows the average (dark lines) and individual (grey lines) timing data for each muscle synergy in control subjects and individuals with SI joint dysfunction. The correlation coefficient for the timing of the third muscle synergy was significantly less ($p = 0.002$, Hedge's $g = 1.7$) for individuals with SI joint dysfunction ($r = 0.54 \pm 0.09$) than healthy control subjects ($r = 0.83 \pm 0.05$). These results indicate that the timing of this synergy was more variable for individuals with SI joint dysfunction.

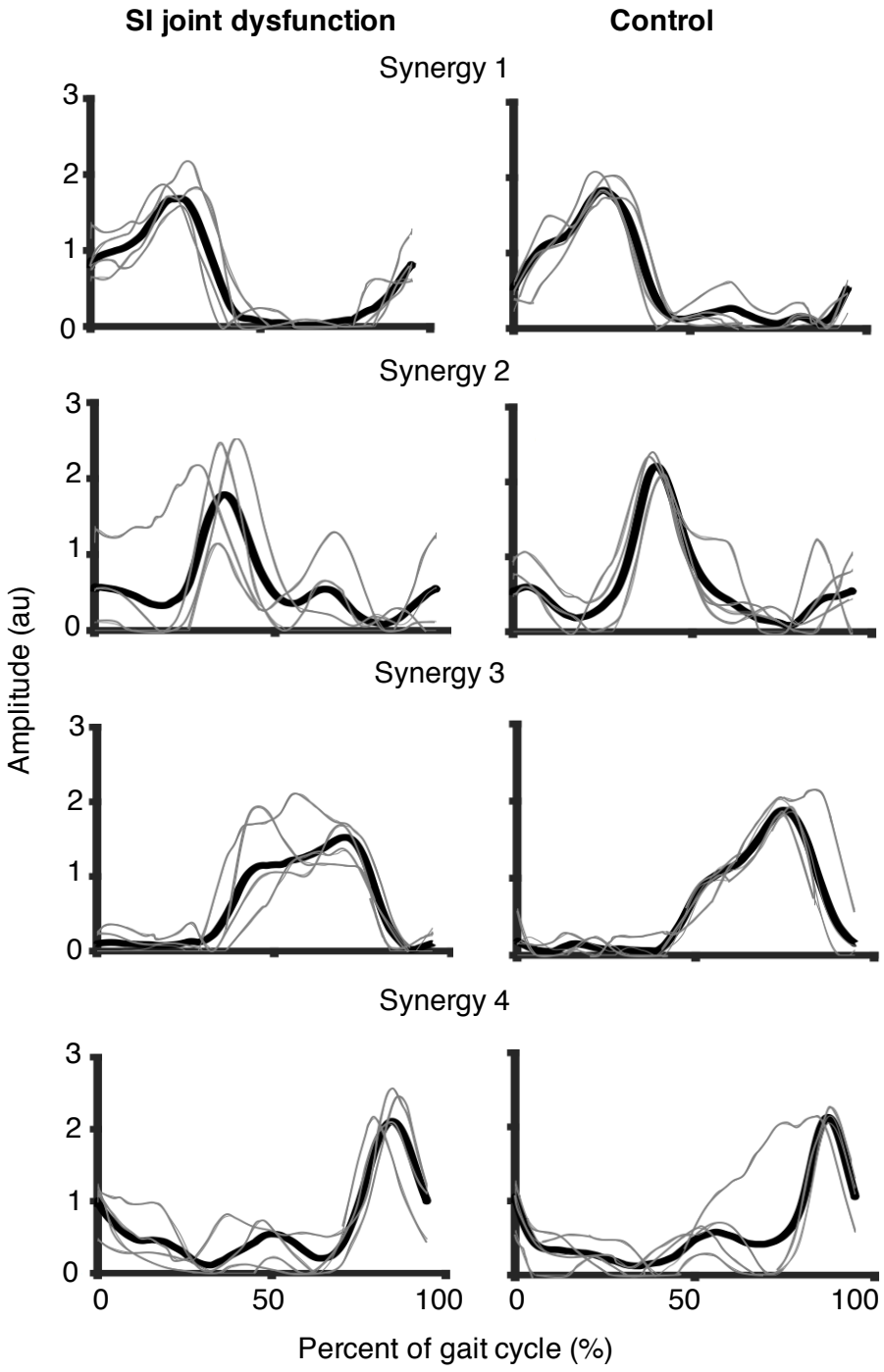

Figure 4. Averaged timing vectors for controls (A) and SI joint dysfunction (B). Black lines represent the average and grey lines are individual subject data. The synergies are most associated with relevant portions of the gait cycle (starting with heel-strike) as denoted on each figure.

Muscle synergies

Figure 5 displays the muscles that contributed to each synergy for the two groups of participants. Each muscle synergy comprises muscles that are activated at similar times. The muscles shown in the plots had confidence intervals that did not contain 0 after 1000 bootstraps of the NMF procedure (Sawyers et al., 2017), which indicates these muscles were significantly active for a given synergy. The muscles involved in the synergies were functionally related; for example, Synergies 2 and 4 for control subjects (Figure 4) were activated from late stance to toe off and included gastrocnemius and biceps femoris of the stance leg as well as the contralateral tibialis anterior. Synergies 1 and 3 comprised muscles involved with trunk and hip stabilization (erector spinae, latissimus dorsi) as well as hip extension (gluteus maximus). These synergies are consistent with the two synergies for propulsion and two for the loading response described by Olree and Vaughan[10].

Table 1 shows mean ± SD muscle weights for the muscle synergies 1 and 3 (loading response) for the two groups of participants. The muscle weights for gluteus maximus on the affected side ($p = 0.014$, effect size = 0.70) and contralateral latissimus dorsi ($p = 0.009$, effect size = 0.74) in the loading response were significantly less than those for control subjects. There was no difference between muscle weights (gluteus maximus, $p = 0.82$; latissimus dorsi, $p = 0.76$) for the loading on the other side; that is, the unaffected side for individuals with SI joint dysfunction.

fd

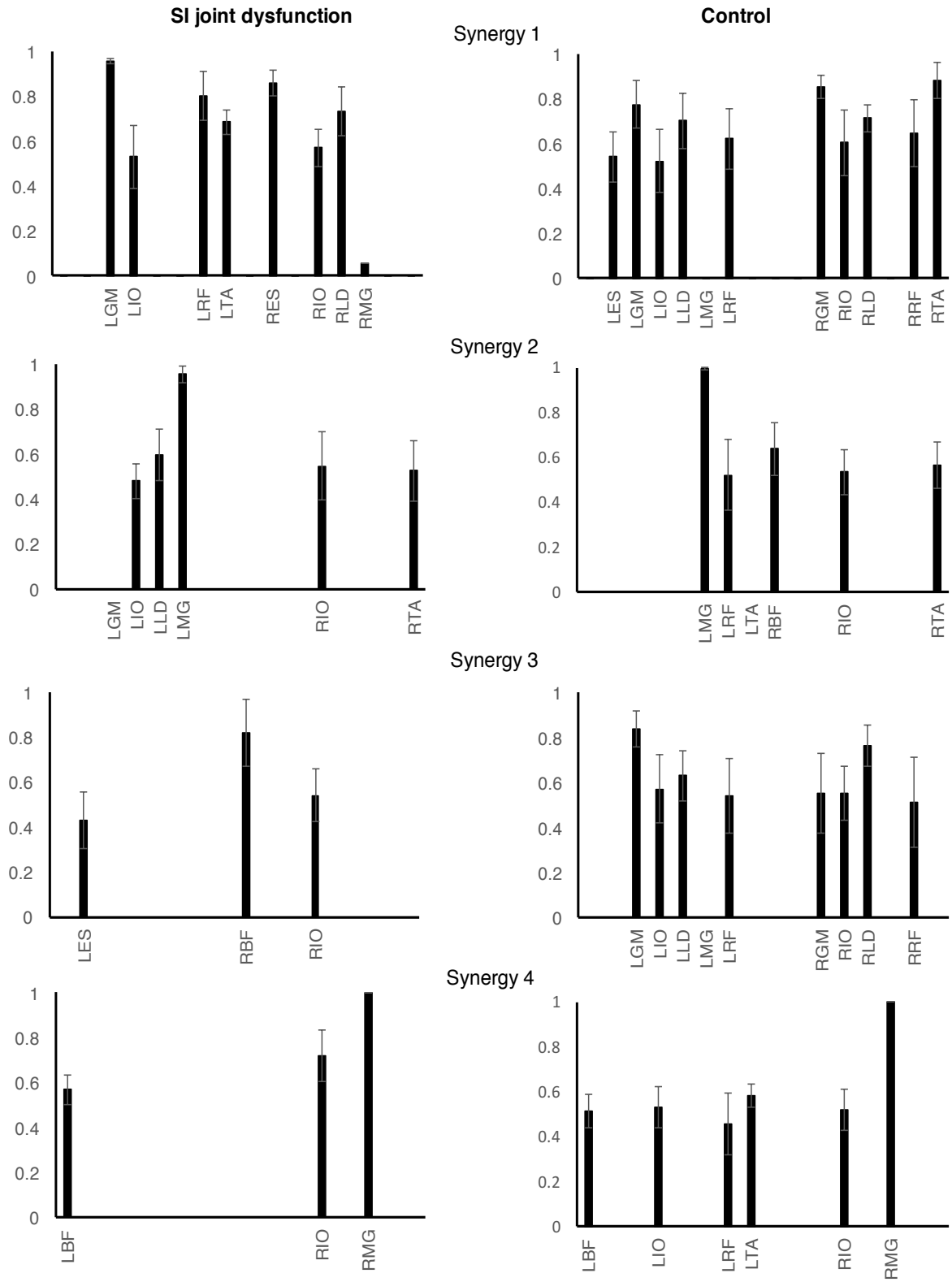
SI joint dysfunction
Control
Synergy 1
1
0.8
0.6
0.4
0.2
0
LGM
LIO
LRF
LTA
RES
RIO
RLD
RMG
LES
LGM
LIO
LLD
LMG
LRF
RGM
RIO
RLD
RRF
RTA
Synergy 2
LGM
LIO
LLD
LMG
RIO
RTA
LMG
LRF
LTA
RBF
RIO
RTA
Synergy 3
LES
RBF
RIO
LGM
LIO
LLD
LMG
LRF
RGM
RIO
RLD
RRF
Synergy 4
LBF
RIO
RMG
LBF
LIO
LRF
LTA
RIO
RMG

Figure 5. Mean ± SD normalized muscle weights for each muscle synergy for control subjects (A) and individuals with SI joint dysfunction (B). LBF: left biceps femoris, LES = left erector spinae, LGM = left gluteus maximus, LIO = left internal oblique, LLD = left latissimus dorsi, LMG = left medial gastrocnemius, LRF = left rectus femoris, LTA = left tibialis anterior, RBF = right biceps femoris, RES = right erector spinae, RGM = right gluteus maximus, RIO = right internal oblique, RLD = right latissimus dorsi, RMG = right medial gastrocnemius, RRF = right rectus femoris, RTA = right tibialis anterior)

Table 1. Mean ± SD Pearson correlation coefficients between the time series for each muscle synergy for control subjects and persons with SI joint dysfunction. Synergies are ordered from left heel strike (Synergy 1) to right toe off (Synergy 4). * $P < 0.05$ between the two groups.

Synergy	Control	SI
1	0.93 ± 0.01	0.90 ± 0.04
2	0.94 ± 0.02	0.69 ± 0.11
3	0.87 ± 0.05	0.58 ± 0.09†
4	0.84 ± 0.04	0.76 ± 0.12

DISCUSSION

Individuals with SI joint dysfunction exhibit significantly reduced muscle weights between gluteus maximus on the affected side with contralateral latissimus dorsi in a synergy during walking (Figures 4 and 5). This muscle synergy was present on both sides (1st and 3rd) in control subjects during the loading response, similar to the findings of Olree and Vaughan (1995). Moreover, the timing of this synergy was more variable in individuals with SI joint dysfunction than control subjects, which could indicate less stability in the timing of this synergy across subjects and steps. Nonetheless, there were no differences in the number of muscle synergies needed to account for 90% of the original EMG data between SI joint subjects and controls (Figure 3) using established criteria (Tresch and Jarc, 2009).

The absence of a synergy involving gluteus maximus on the affected side and contralateral latissimus dorsi may compromise pelvic stability and contribute to SI joint dysfunction by not providing force closure of the joint (Vleeming et al., 1992;2012). For example, Kibsgård and colleagues (2017) used surgically implanted markers to measure small backward rotation of the ilium relative to the sacrum during straight leg raises. When in a supine position, the SI joint exhibits a backward rotation of up to 0.8 degrees and inward rotation of 0.3 degrees of the innominate bone relative to the sacrum. Additionally, Kibsgård and colleagues (2014) found a rotation of 0.5 degrees between the ilium and sacrum during single leg stance of individuals with SI joint dysfunction. Presumably, the actions of gluteus maximus and latissimus dorsi can provide stability across the SI joint (Vleeming et al., 1992; 2012; Barker et al., 2014). The lack of synergist activity on the affected side of individuals with SI joint dysfunction likely enables slight displacements between the two joint surfaces and contributes to the pain associated with the disorder.

Pain in the lower back or SI joint alters muscle activation patterns during gait (Falla and Hodges, 2017; van Dieen et al., 2017; Hanada et al., 2011; Arendt-Nelson et al., 1995). Consistent with the result of our study, Hanada and colleagues (2011) found significant differences in trunk EMG activity during gait in individuals with chronic low back pain and suggested the muscles were activated in subphases, which indicate different muscle synergies. Moreover, Arendt-Nelson and colleagues (1995) demonstrated that when injected with a hypertonic saline injection, individuals with chronic low back pain had significantly different EMG activity during gait when compared with healthy controls and suggested that noxious stimuli may alter reflex pathways causing different muscle activation patterns. Additionally, van dem Hoom and colleagues (2015) demonstrated differences in trunk—but not calf— muscle

synergies during gait after a hypertonic saline injection. This has led to the conclusion that muscle synergies involved in propulsion may be relatively stable in the presence of pain, whereas secondary synergies may be altered (Falla and Hodges, 2017). Taken together with the results of our study and a recent review by van Dieën and colleageus (2017), it appears that pain can modulate EMG activity during gait.

Consistent with previous studies that have examined muscle synergies during walking, our study found three to five muscle synergies were needed to recreate the original EMG waveforms (Olree and Vaughan, 1995; Clark et al., 2012; Cappellini et al., 2006). Additionally, the muscle synergies were associated with key events the gait cycle, as determined by functional sorting (Kristiansen et al., 2016). Based on the approach developed by Olree and Vaughan (1995), the identified muscle synergies contributed to either propulsion (gastrocnemius, tibialis anterior, biceps femoris) or the loading response (gluteus maximus, erector spinae, latissimus dorsi). These results provide evidence that a preprogrammed motor plan may be used for walking (Lee, 1984; Cappellini et al., 2006), and this motor plan may differ between individuals with SI joint dysfunction and healthy controls.

Although individuals with SI joint dysfunction exhibit the same number of synergies as healthy control subjects when walking at the same speed, the results of our study are consistent with the hypothesis that the synergy between gluteus maximus on the affected side and the contralateral latissimus dorsi is compromised in individuals with SI joint dysfunction. This information provides clinicians with evidence that SI joint dysfunction presents with altered patterns of EMG activity and may provide the basis for future rehabilitation approaches.

Chapter VIII

SACROILIAC JOINT DYSFUNCTION PATIENTS EXHIBIT ALTERED MOVEMENT STRATEGIES WHEN PERFORMING A SIT-TO-STAND TASK

ABSTRACT

Summary of background data: The ability to rise from a chair is a basic functional task that is frequently compromised in individuals diagnosed with orthopedic disorders in the low back and hip. There is no published literature that describes how this task is altered by SIJD. The purpose of this study is compare lower extremity biomechanics and muscle activity onset during rising from a chair in individuals with SIJD and healthy persons. Six women with unilateral sacroiliac joint dysfunction (SIJD) and six age-matched healthy controls performed a sit-to-stand task while we measured kinematics, kinetics, and muscle activity. Subjects stood up at a preferred speed from a seated position on an armless and backless adjustable piano stool. We measured movement using a 10-camera motion capture system, ground reaction forces for each leg with force plates, and muscle activity with surface electromyography. Joint angles and torques were calculated using inverse dynamics. Leg loading rate was quantified as the average slope of vertical ground reaction force during the 500-ms window preceding maximal knee extension. Between-leg differences in loading rates and peak vertical ground reaction forces were significantly greater for the SIJD than the control group. Maximal hip angles were significantly less for the SIJD group ($p = 0.001$). Peak hip moment in the SIJD group was significantly greater in the unaffected leg (0.75 ± 0.22 N•m/kg) than the affected leg (0.47 ± 0.29 N•m/kg, $p = 0.005$). There were no between-leg or between-group differences for peak knee or ankle moments. The onset of activity in the latissimus dorsi muscle on the affected side in the SIJD group was delayed and the erector spinae muscles were activated earlier than in Controls. Individuals with SIJD have a greater vertical ground reaction force on the unaffected leg, generate a greater peak hip moment in the unaffected leg, use a smaller range of motion at the hip joint of the affected leg, and delay the onset of a key muscle on the affected side when rising from a seated position.

INTRODUCTION

Sacroiliac (SI) joint dysfunction (SIJD) is a significant cause of low back pain, accounting for up to 40% of nonspecific low back pain cases (Bernard et al., 1987; Sembrano and Polly, 2009). The impact of SIJD on quality of life is comparable to that observed with other debilitating orthopedic conditions, such as hip osteoarthritis and spinal stenosis, and is higher than many cardiovascular-related medical conditions (Cher et al., 2014). Indirect health care expenditures associated with low back pain range from $7 - $28 billion per year and individuals lose an estimated 5.2 hours of work time per week (Koenig et al., 2016; Stewart et al., 2003). In a recent clinical trial on SI joint fusion, 19% of subjects were not working due to back pain (Sembrano and Polly, 2009).

The SI joint assists in transferring load from the spine to the lower extremities, and as such, it must provide the necessary stability to support this force transfer, as well as the enable mobility required to facilitate bipedal locomotion, postural changes, and expansion during parturition (Sturesson et al., 1988). The anatomical capabilities of the SI joint that enable these movements were characterized by Vleeming and colleagues with the principles of form and force closure (Vleeming etl al 1990). Form closure refers to the stability provided by the complimentary convex and concave surfaces of the iliac and sacral joint surfaces. In women, the joint surface is somewhat smaller, less curved, and more backward tilted than in men, possibly contributing to the greater incidence of SIJD in women (Vleeming et al., 2012). Force closure describes the function of ligaments and muscles acting across the joint to provide joint mobility and stability. The primary muscles responsible for force closure are the gluteus maximus and latissimus dorsi

as tension is transmitted from one side to the other through their connection into the superficial layer of the thoracolumbar fascia (Carvalhais et al., 2013; Pool-Goudzwaard et al., 1998).

Diagnosing SIJD can be challenging as associated symptoms include pain at the low back and hip, in addition to pain at the joint itself (Polly et al., 2016). The etiology of SIJD is unknown, but one hypothesis is that it results from inadequate force closure needed to stabilize the joint during movement. Possible explanatory mechanisms include inadequate muscle coordination, reduced muscle strength, and alterations in ligamentous tension (Pool-Goudzwaard et al., 1998).

Joint and muscle pain are known to alter muscle activation, muscle coordination, normative gait patterns, and basic function (Falla and Hodges, 2017; Graven-Nielsen et al., 1997). Joint loading, the control of joint movements through coordinated muscular contractions, and joint integrity and stability are critical factors that influence degenerative responses (Herzog et al., 2003). Load transfer through the pelvis with an unstable SI joint can produce excessive loads on surrounding tissues, resulting in pain (Pool-Goudzwaard et al., 1998). Changes in muscle activation may be an individual's attempt to splint the painful area or avoid movements that exacerbate pain (Hodges et al., 2015). The consequence of these changes may result in abnormal joint loading, which influences the control of muscle forces and limb coordination, and is associated with joint degeneration (or worsening thereof) (Herzog et al., 2003; McCrory et al., 2001). Moreover, leg-loading asymmetry, as a result of pain or injury on one side, has been linked to the pathogenesis of osteoarthritis in the knee or hip of the healthy leg (McCrory et al., 2001).

The ability to rise from a chair is a basic functional task that requires approximately 60% of the available lumbar flexion range of motion (Hsieh et al., 1994). Torque at the hip joint during this movement may exceed that occurring during walking or climbing stairs and therefore may exacerbate symptoms in individuals suffering from SI joint pain (Gross et al., 1998).

Patients with SIJD present similarly to individuals with hip and spine disorders. While studies investigating sit-to-stand mechanics have been performed on individuals with end stage hip osteoarthritis and low back pain, there are no published studies that have investigated this daily functional task in individuals with SIJD (Al-Obaidi et al., 2003; Arendt-Nielsen et al., 1996; Abujaber et al., 2015; Shum et al., 2005). The purpose of our study was to compare lower extremity biomechanics and muscle activity onset during rising from a chair in individuals with SIJD and healthy persons. We hypothesized that the unilateral discomfort experienced by this patient population would result in asymmetrical leg loading and altered muscle onset timing compared with healthy controls.

METHODS

Twelve women volunteered to participate in the study. Six individuals were diagnosed with unilateral SIJD by an orthopedic surgeon who completed a spine fellowship and is an expert in diagnosing and treating the disorder. Diagnostic criteria included a positive result on at least three out of five physical provocative testing maneuvers designed to target the SI joint and pain relief after localized steroid injections (Szadek et al., 2009). These criteria were used in a recent randomized controlled trial of SI joint fusion (Whang et al., 2015). Six healthy, age-matched (±5 yrs) women without back, SI joint, or hip pain, served as the control group (Control). Study exclusion criteria included: bilateral symptoms (SIJD group), severe back or hip pain from other

causes, prior spinal fusion at any level, major lower extremity surgery, difficulty walking due to conditions other than SIJD, severe arthritis, neurological disorders, vestibular or visual disturbance affecting balance, fibromyalgia, chronic rheumatologic condition, drug or alcohol abuse, or uncontrolled psychiatric disease. All study participants were asked to rate pain severity on a visual analog scale (VAS), measured from 0 to 10 cm, and complete the Oswestry Disability Index (ODI) to assess overall disability (Fairbank et al., 2000).

The study was approved by the Institutional Review Board (protocol #15-0586). Written informed consent was obtained from all participants before beginning study-related procedures.

Procedures

Sit-to-stand task

An armless, backless piano stool was placed on a dual-belt, force-measuring treadmill (Bertec Corp., Columbus, OH) with each foot on a separate force plate. The piano stool was adjusted so that the top of the stool was even with the back of the participant's knee joint line (popliteal fossa) (Abujaber et al., 2015). With arms placed across the chest, the participant stood up until fully upright, and then sat back down. This task, performed at a self-selected speed, was repeated three times. We simultaneously collected kinematic data at 100 Hz, and kinetic and electromyography data at 1000 Hz.

Motion analysis

Kinematic data were obtained with a 10-camera motion capture system (VICON, Centennial, CO). The data were recorded at 100 Hz and low-pass filtered (2^{nd} order bidirectional Butterworth, 10-Hz cutoff). Spherical reflective markers were placed on the sternal notch, C7

spinous process, and bilaterally on the acromioclavicular joint, scapula, fifth lumbar vertebrae, iliac crest, anterior superior iliac spine (ASIS), posterior superior iliac spine (PSIS), greater trochanter, medial femoral condyle, lateral femoral condyle, medial malleolus, lateral malleolus, head of the first metatarsal, head of the fifth metatarsal, and posterior heel. A rigid thermoplastic shell with four reflective markers was placed bilaterally on the thighs and shanks to track the motion of these segments.

Ground reaction forces were measured for each leg at 1000 Hz and then low-pass filtered (Bidirectional 2^{nd} order Butterworth, 30-Hz cutoff).

Wireless surface EMG signals (Noraxon USA, Scottsdale, AZ), sampled at 100 Hz, were used to monitor activity in seven muscles bilaterally. Electrodes were placed according to SENIAM guidelines over the following muscles: latissimus dorsi, erector spinae, gluteus maximus, biceps femoris, medial gastrocnemius, rectus femoris, and tibialis anterior (Hermens et al., 2000).

Data Analysis

Joint angles and moments were calculated using inverse dynamics with Visual 3D (C-Motion, Germantown, MD). Leg loading rate was calculated by taking the average slope of vertical force during the 500-ms window preceding peak knee extension. Initiation of the sit-to-stand task (movement onset) was defined as the time at which the total vertical ground reaction force first exceeded 105% of body weight.

EMG signals were band-pass filtered (10-490 Hz) and full-wave rectified. Independently, two investigators determined muscle onset using visual inspection (Jesunathadas et al., 2012). Muscle onset is reported as the percentage of time from movement onset to peak knee extension.

All data were processed and analyzed using a custom Matlab script (MathWorks, Inc., Natick, MA). Data were assessed for normality using the Shapiro-Wilk test. Normally distributed data were compared by group using an independent groups two-tailed Student's t-test. Within-subject data were compared using paired t-test. Group-by-leg interaction for muscle onset was assessed using a two-way ANOVA. Significance was set at $\alpha = 0.05$. Effect size was calculated using Hedge's g with small, medium, and large effect sizes are defined as 0.2, 0.5 and 0.8, respectively. Statistics were performed in R and the results are reported as mean ± SD [30].

RESULTS

Mean (± SD) participant age was 39 ± 7 yrs for the SIJD group and 37 ± 8 yrs for Controls. There were no statistically significant differences in height (168 ± 14 cm, 162 ± 6 cm, $p > 0.05$) or body mass (72 ± 14 kg, 59 ± 6 kg, $p = 0.07$), but BMI was greater for the SIJD group (27.7 ± 5.0) than for Controls (21.2 ± 2.0) ($p=0.02$). SIJD symptom duration was 24 ± 11 months and ODI score was 41 ± 18% (Table 1). The VAS pain scores for the SIJD group were: low back, 6.3 ± 1.5 cm; affected leg, 6.7 ± 1.9 cm; unaffected leg, 2.7 ± 2.3 cm. Control subjects reported 0 cm on VAS and 0% on ODI.

Table 1: Oswestry Disability Index (ODI) and pain scores measured on a visual analog scale (VAS)

Subject	ODI score (%)	VAS: Low Back	VAS: Affected leg	VAS: unaffected leg
1	44	7	5	3
2	16	3	4	0
3	54	7	7	3

4	52	8	8	6
5	58	8	7	4
6	22	7	7	0

VAS, 0 – 10 cm: 0 = no pain, 10 = maximal pain. ODI score: 0 - 20% minimal, 21 - 40% moderate, 41 - 60% severe

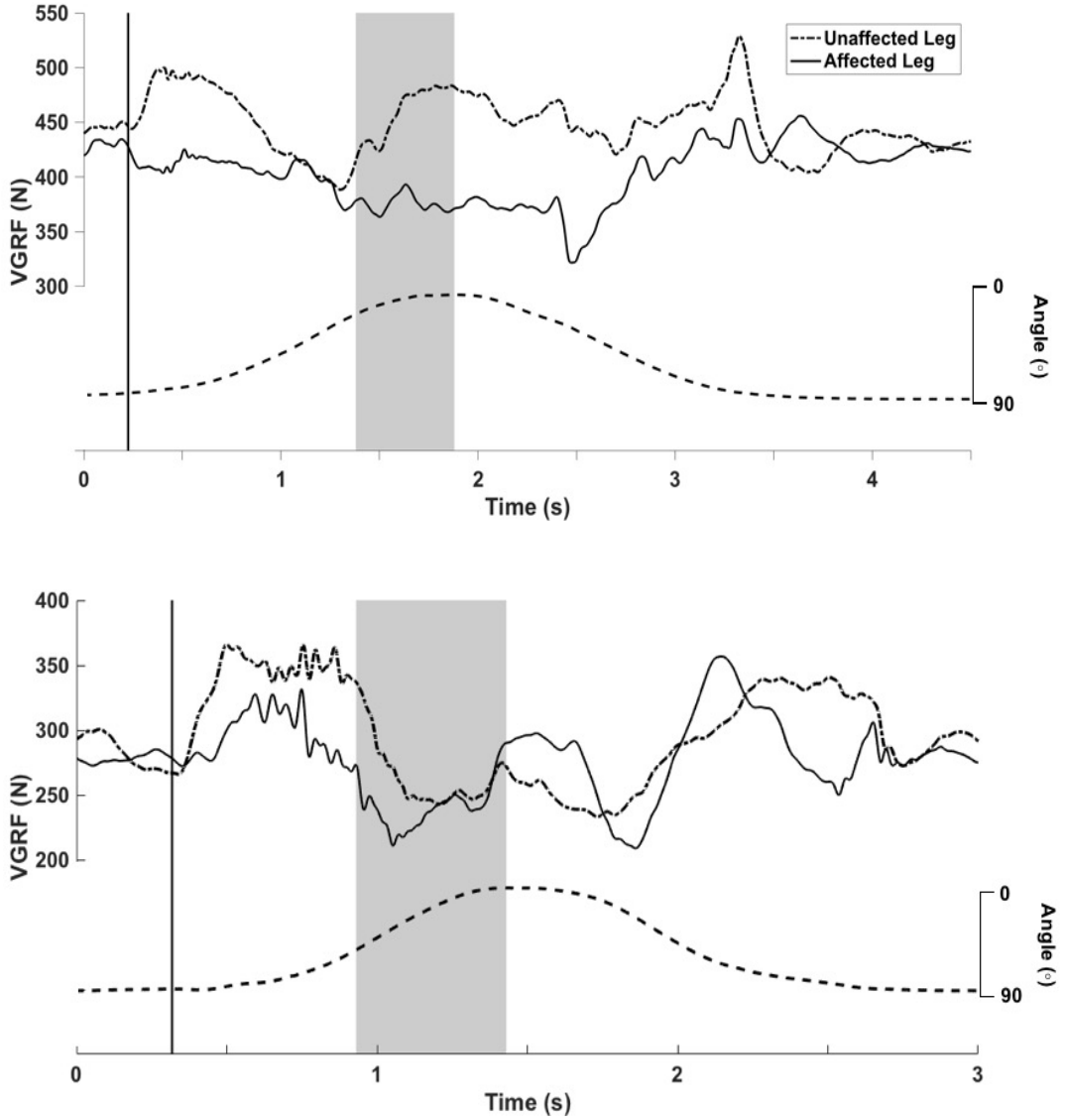

Figure 1.Vertical ground reaction forces (VGRF) for each side (above) and knee angle (dashed line below) for a subject in the SIJD group (a) and a control subject (b). The solid trace indicates the affected leg (A) and the right leg (B). The vertical line indicates movement onset when the summed VGRFs first exceeded 105% of body weight. Average loading rates for each leg were calculated from the 500-ms window preceeding peak knee extension (shaded area).

Average leg loading rate was symmetrical for the Control group (13 ± 11 N/s difference between sides), but was significantly different between legs for the SIJD group (112 ± 48 N/s difference) ($p = 0.008$, Hedge's $g = 1.07$) (Table 2, Figure 1). Although the difference in peak vertical ground reaction force between legs was negligible for the Control group (3 N), there was a significant difference (103 N) between legs for the SIJD cohort ($p < 0.000$, Hedge's $g = 1.17$).

Table 2: Results for the difference between legs in loading rate, peak vertical ground reaction force, and minimal and maximal hip flexion angles.

	Difference between sides		Hip angle	
	Leg loading rate (N/s)	Peak VGRF (N)	Minimal angle (°)	Maximal angle (°)
SIJD	112 ± 48*	103 ± 31*	-5.8 ± 7.5	59.9 ± 9.9*
Control	13 ± 11	3 ± 2	-3.2 ± 6.1	85.2 ± 9.9

* $p < 0.05$ between groups. VGRF = vertical ground reaction force. Maximal hip angle occurred during the seated position, whereas minimal hip angle corresponded to full extension when standing.

Table 3: Normalized peak hip moment (torque) and peak vertical ground reaction force (VGRF) results by side and group.

	Control		SIJD	
	Left	Right	Unaffected	Affected
Peak Hip Moment				
Normalized to body mass (N•m/kg)	0.83 ± 0.24	0.87 ± 0.19	0.75 ± 0.22	0.47 ± 0.29*
Normalized to body mass and height (N•m/kg•m)	0.49 ± 0.13	0.52 ± 0.10	0.47 ± 0.13	0.29 ± 0.18*
Peak VGRF (N/BW)	0.65 ±0.02	0.65 ± 0.05	0.65 ± 0.3	0.58 ± 0.02*

* $p < 0.05$ between legs. BW = body weight

Minimal and maximal hip angles were symmetric between legs for both groups, with no significant between-group differences for minimal hip angle (Table 2). However, maximal hip

angle was significantly less in the SIJD group (59.9 ± 9.9°) than the Controls (85.2 ± 9.9°; p = 0.001).

Peak hip-flexion moment in the sagittal plane was not statistically different between legs for Controls (p = 0.4) (Table 3), but was significantly greater on the affected side (0.47 ±0.29 N•m/kg) than the unaffected side (0.75 ± 0.22 N•m/kg) in the SIJD group (p = 0.005). The difference in peak hip moment between legs was significantly different between groups (p = 0.005, Hedges g = 0.87). There were no between-legs or between-group differences for peak knee or ankle moments.

Table 4: Muscle onset timing as a percentage of the time from movement onset to peak knee extension.

	Control (%)		SIJD (%)	
Muscle	Left leg	Right leg	Unaffected leg	Affected leg
Latissimus dorsi	12 ± 2	13 ±2	9 ± 3	12 ± 6
Erector spine	12 ± 3	11 ± 2	9 ± 3	8 ± 4
Gluteus maximus	18 ± 3	17 ± 5	14 ± 4	15± 5
Biceps femoris	21 ± 5	21 ± 6	18 ± 6	18 ± 3
Medial gastrocnemius	14 ± 4	14 ± 4	15 ± 9	15 ± 7
Rectus femoris	18 ± 7	19 ± 5	15 ±3	14 ± 2
Tibialis anterior	3 ± 6	2 ± 6	3 ± 5	2 ± 4

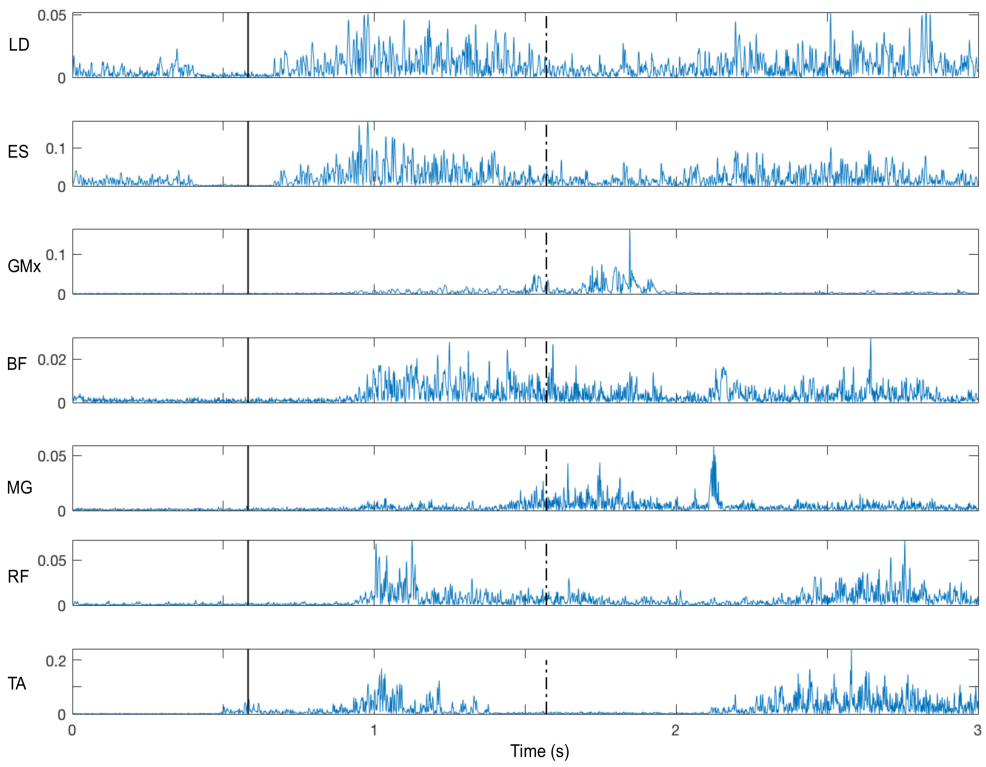

Figure 2. Representative EMG recordings for an SIJD subject for the right side. Solid vertical line indicates movement onset when the summed VGRFs first exceeded 105% of body weight. Dashed vertical line indicates time of peak knee extension.

Average onset times for the recorded muscles occurred after the VGRF first exceeded 105% of body weight, which indicates that other muscles contributed to the initial vertical acceleration of the center of mass (Figure 2). The onset of EMG activity for all muscles was symmetrical between sides for the Control group (Table 4). Latissimus dorsi was activated at the same time in both legs for the Control group, but the onset was delayed on the affected side (12 ± 6 %) relative to the unaffected side (9 ± 3 %) in the SIJD group. Additionally, SIJD subjects activated erector spinae earlier (unaffected: 9 ± 3%; affected: 8 ± 4%) than Controls (right: 12 ± 3%; left: 11 ± 2%). Two-way ANOVA revealed no interaction by group or by leg.

DISCUSSION

This is the first study to evaluate sit-to-stand kinematics, kinetics, and muscle activity onset in individuals with SIJD. Concordant with our hypothesis, individuals with SIJD preferentially loaded the unaffected leg when rising from a chair and when fully erect thereby reducing the load on the affected leg. Furthermore, they used a smaller range of motion at the hip joint of the affected leg and produced a greater peak hip moment on the unaffected side. These findings are similar to those reported for individuals with low back pain and with end-stage hip osteoarthritis(McCrory et al., 2001; Abujaber et al., 2015; Shum et al., 2005). Additionally, individuals with SIJD activated the erector spinae muscles (bilaterally) earlier than Controls, and had a delayed onset of the latissimus dorsi muscle on the affected side, indicating a potential disruption in the force closure mechanism between sides.

Our results illustrate that the compensatory movement patterns adopted by persons with SIJD are similar to those observed in individuals suffering from low back pain and end-stage hip osteoarthritis. Shum (2005) evaluated hip flexion in 60 individuals with low back pain during a sit-to-stand task and found values similar to those for our SIJD cohort: 64 ± 11° for LBP; 60 ± 10° for SIJD. In a study evaluating sit-to-stand performance in individuals with end-stage hip osteoarthritis, Abujaber et al. reported differences in peak hip moments (normalized to body mass and height) between the unaffected (0.48 N•m/kg•m) and affected sides (0.36 N•m/kg•m) (Abujaber et al., 2015). Our results were more asymmetric (unaffected: 0.47 N•m/kg•m; affected: 0.29 N•m/kg•m,) indicating a greater adjustment in our SIJD group. Similarly, peak vertical ground reaction forces were greater in the unaffected side in both our study and one on individuals prior to total hip arthroplasty (McCrory et al., 2001). As abnormal joint loading has been shown to result in joint degeneration on the healthy limb, it is possible that individuals with

SI joint dysfunction may develop early osteoarthritis in the hip of the unaffected side if left untreated (McCrory et al., 2001).

Muscle onset timing was variable between individuals and between our two groups. SIJD subjects activated their erector spinae muscles earlier than the Control subjects. This is consistent with our finding that SIJD individuals have smaller hip flexion angles and thus extend at hip earlier than Controls. However, variability within each group was high. In the presence of pain, individuals may adopt different motor strategies to accomplish the same task (Hug and Tucker, 2017; van Dieen et al., 2017). The delay in activation of the latissimus dorsi on the affected side of SIJD participants suggests a possible disturbance of the force-closure mechanism. Previous research has shown that individuals with low back pain exhibit decreased anticipatory responses in preparation for an impending perturbation (Hodges and Richardson, 2017; Nelson-Wong et al., 2013). Latissimus dorsi provides an essential component of the force-closure mechanism for the SI joint, important for stability during weight-bearing. These findings imply deficient movement preparation for rising from a chair in the SIJD group. Further studies, with larger sample sizes, to explore muscle activation differences in people with SIJD, are needed.

Our study has limitations. Subject recruitment was difficult due to rigorous inclusion criteria. However, this was necessary to ensure the study population had SIJD and not other back- or hip-related conditions. Although our sample size was small, the effect sizes are large. Additionally, our Control group values for peak hip flexion moment and maximal hip flexion angle are similar to those reported in the literature with larger sample sizes. Abujaber (2015) reported peak hip flexion moments of 0.48 and 0.47 N•m/kg•m, compared with our values of 0.49 and 0.52

N•m/kg•m. Maximal hip flexion values for Controls in our study (85 ± 10°) are similar to those reported by Shum (2005) 87 ± 11°. Participants were allowed to move at a self-selected speed which increased variability, but provided insights for natural movement patterns.

The data from our study represents the first step in understanding the kinematics and kinetics in individuals with SIJD. Many cases of SIJD are misdiagnosed as low back pain, perhaps due to poor diagnostic criteria or lack of understanding of the disease presentation (Sembrano et al., 2009; Bernard et al., 1987). More importantly, misdiagnosis of SIJD may lead to unnecessary lumbar spinal surgery (Cher et al., 2016). Katz et al. found that SIJD was the etiology of low back pain in 32% of patients treated with lumbar fusion surgery (Katz et al., 2003). Thus, it is imperative that we seek to further understand this disease and how to differentiate it from other lumbopelvic disorders.

We found that individuals diagnosed with SIJD adopt similar movement patterns to individuals with low back pain and end stage hip osteoarthritis when rising from a chair. They preferentially loaded the unaffected leg, maintained this asymmetry when fully upright, and experienced a larger peak hip moment on the affected side. Furthermore, muscle onset timing was disrupted in key muscles providing force closure of the joint.

References

Abujaber SB, Marmon AR, Pozzi F, Rubano JJ, Zeni JA. Sit-To-Stand Biomechanics Before and After Total Hip Arthroplasty. *J Arthroplasty* 10: 23-24, 2015.

Adam A, De Luca CJ. Firing rates of motor units in human vastus lateralis muscle during fatiguing isometric contractions. *J Neurophysiol* 99: 268-280, 2005.

Adrian ED, Bronk DW. The discharge of impulses in motor nerve fibres Part II. The frequency of discharge in reflex and voluntary contractions. *J Physiol* 67: 119-151, 1929.

Ahmadian Y, Pillow JW, Paninski L. Efficient Markov chain Monte Carlo methods for decoding neural spike trains. *Neural Comput* 23: 46–96, 2011.

Al-Obaidi SM, Al-Zoabi B, Al-Shuwaie N, Al-Zaabie N, Nelson RM. The influence of pain and pain-related fear and disability beliefs on walking velocity in chronic low back pain. *Int J Rehabil Res Int Z Für Rehabil Rev Int Rech Réadapt* 26:101–8, 2003.

Almuklass A, Price RC, Gould JR, Enoka RM. Force steadiness as a predictor of time to complete a pegboard test of dexterity in young men and women. *J Appl Physiol.* 120: 1410-1417, 2016

Alusi SH, Worthington J, Glickman S, Findley LJ, Bain PG. Evaluation of three different ways of assessing tremor in multiple sclerosis. *J Neurol Neurosurg Psychiatry* 68(6):756–60, 2000.

Ambike SS, Paclet F, Latash ML, Zatsiorsky VM. Grip-force modulation in multi-finger prehension during wrist flexion and extension. *Exp Brain Res* 227:509–522, 2013.

Amiridis IG, Mani D, Almuklass A, Matkowski B, Gould JR, Enoka RM. Modulation of motor unit activity in biceps brachii by neuromuscular electrical stimulation applied to the contralateral arm. *J Appl Physiol* 118: 1544-1552, 2015.

Ang KH, Chong G, Li Y. PID control system analysis, design, and technology. *IEEE Trans Control Syst Technol* 13:559–576, 2005.

Archer E, Koster U, Pillow J, Macke JH. Low- dimensional models of neural population activity in sensory cortical circuits. *Advances in Neural Information Processing Systems* 27: 28th Conference on Neural Information Processing Systems, 2014.

Arendt-Nielson L, Graven-Nielsen T, Svarre H, Svensson P. The influence of low back pain on muscle activity and coordination during gait: a clinical and experimental study. *Pain* 1995; 64: 231-240.

Arellano CJ, Caha D, Hennessey JE, Amiridis IG, Baudry S, Enoka RM. Fatigue-induced adjustment in antagonist coactivation by old adults during a steadiness task. *J Appl Physiol* 120:

1039-1046, 2016.

Arpin DJ, Davies BL, Kurz MJ. Multiple sclerosis influences the precision of the ankle plantarflexion muscular force production. *Gait Posture* 45: 170-174, 2016.

Ashendorf L, Vanderslice-Barr JL, Mccaffrey RJ. Motor tests and cognition in healthy older adults. *Appl Neuropsychol* 16(3):171–6, 2009.

Baldissera F, Cavallari P, Cerri G. Motoneuronal pre-compensation for the low-pass filter characteristics of muscle. A quantitative appraisal in cat muscle units. *J Physiol* 511:611–627, 1998.

Baldwin ERL, Klakowicz PM, Collins DF. Wide-pulse width, high-frequency neuromuscular electrical stimulation: implications for functional electrical stimulation. *J Appl Physiol* 101: 228-240, 2006.

Barker PJ, Hapuarachchi KS, Ross JA, Sambaiew E, Ranger TA, Briggs CA. Anatomy and biomechanics of gluteus maximus and the thoracolumbar fascia at the sacroiliac joint. *Clin Anat* 27: 234-240, 2014

Barry BK, Pascoe MA, Jesunathadas M, Enoka RM. Rate coding is compressed but variability is unaltered for motor units in a hand muscle of old adults. *J Neurophysiol* 97:3206–3218, 2007.

Baudry S. Aging changes the contribution of spinal and corticospinal pathways to control balance. *Exer Sport Sci Rev* 44: 104-109, 2016.

Baudry S, Maerz AH, Enoka RM. Presynaptic modulation of Ia afferents in young and old adults when performing force and position control. *J Neurophysiol* 103: 623-631, 2010.

Baudry S, Penzer F, Duchateau J. Input-output characteristics of soleus homonymous Ia afferents and corticospinal pathways during upright standing differ between young and elderly adults. *Acta Physiol* 210: 667-677, 2014.

Baweja HS, Kennedy DM, Vu J, Vaillancourt DE, Christou EA. Greater amount of visual feedback decreases force variability by reducing force oscillations from 0-1 and 3-7 Hz. *Eur J Appl Physiol* 108: 935-943, 2010.

Baweja HS, Kwon M, Christou EA. Magnified visual feedback exacerbates positional variability in older adults due to altered modulation of the primary agonist muscle. *Exp Brain Res* 222: 355-364, 2012.

Bays PM, Wolpert DM. Computational principles of sensorimotor control that minimize uncertainty and variability. *J Physiol* 578:387–96, 2007.

Bellumori M, Uygur M, Knight CA. High-speed cycling intervention improves rate-dependent mobility in older adults. *Med Sci Sports Exerc* 2017.

Berg RW, Ditlevsen S, Hounsgaard J. Intense synaptic activity enhances temporal resolution in spinal motoneurons. *PLoS One* 3: e3218, 2008.

Bergquist AJ, Clair JM, Lagerquist O, Mang CS, Okuma Y, Collins DF. Neuromuscular electrical stimulation: implications of the electrically evoked sensory volley. *Eur J Appl Physiol* 111: 2409-2226, 2011.

Bernard TN Jr, Kirkaldy-Willis WH. Recognizing specific characteristics of nonspecific low back pain. *Clin Orthop Relat Res* 217: 266-280, 1987.

Bernstein N. The problem of the interrelation of co-ordination and localization. *Arch Biol Sci* 38, 1935.

Bernstein N. The coordination and regulation of movements. Oxford: Pergamon, 1967

Bertoni R, Lamers I, Chen CC, Feys P, Cattaneo D. Unilateral and bilateral upper limb dysfunction at body functions, activity and participation levels in people with multiple sclerosis. *Mult Scler J* 21(12):1566–74, 2015.

Bessou P, Joffroy M, Montoya R, Pages B. Evidence of the co-activation of alpha-motoneurones and static gamma-motoneurones of the sartorius medialis muscle during locomotion in the thalamic cat. *Exp Brain Res* 82:191–198, 1990

Bigland B, Lippold OC. Motor unit activity in the voluntary contraction of human muscle. *J Physiol* 125: 322-335, 1954.

Boonstra TW, Farmer S, Breakspear M. Using computational neuroscience to define common input to spinal motor neurons. *Front Hum Neurosci* 10: 313, 2016.

Bourbonnais D, Vanden Noven S, Carey KM, Rymer WZ. Abnormal spatial patterns of elbow muscle activation in hemiparetic human subjects. *Brain* 112: 85-102, 1989.

Bowden JL, McNulty PA. The magnitude and rate of reduction in strength, dexterity and sensation in the human hand vary with ageing. *Exp Gerontol* 48(8):756–65, 2013.

Bremner FD, Baker JR, Stephens JA. Variation in the degree of synchronization exhibited by motor units lying in different finger muscles in man. *J Physiol* 432: 381-399, 1991.

Buesing L, Macke JH, Sahani, M. Spectral learning of linear dynamics from generalised-linear observations with application to neural population data. *NIPS* 00: 1691–1699, 2012.

Burge J, Ernst MO, Banks MS. The statistical determinants of adaptation rate in human reaching. *J Vis* 8:20.1-19, 2008.

Burke RE. Motor unit types of cat triceps surae muscle. *J Physiol* 193: 141-160, 1967.

Burke RE, Levine DN, Tsairis P, Zajac FE. Physiological types and histochemical profiles in motor units of the cat gastrocnemius. *J. Physiol* 234: 723–748, 1973.

Burke RE, Tsairis P. Anatomy and innervation ratios in motor units of cat gastrocnemius. *J Physiol* 234: 749-765, 1973.

Burke RE, Tsairis P. The correlation of physiological properties with histochemical characteristics in single muscle units. *Ana NY Acad Sci* 228: 145-159, 1974.

Bryden P, Roy E. A new method of administering the Grooved Pegboard Test: Performance as a function of handedness and sex. *Brain Cogn* 58(3):258–68, 2005.

Cappellini G, Ivanenko YP, Poppele RE, Lacquaniti F. Motor patterns in human walking and running. *J Neurophysiol* 95: 3426-3437, 2006.

Carpentier A, Duchateau J, Hainaut K. Motor unit behaviour and contractile changes during fatigue in the human first dorsal interosseus. *J Physiol* 534: 903-912, 2001.

Carlton LG. Processing visual feedback information for movement control. *J Exp Psychol Hum Percept Perform* 7:1019, 1981.

Carvalhais VO do C, Ocarino J de M, Araújo VL, Souza TR, Silva PLP, Fonseca ST. Myofascial force transmission between the latissimus dorsi and gluteus maximus muscles: an in vivo experiment. *J Biomech* 46: 1003–7, 2013.

Carville SF, Perry MC, Rutherford OM, Smith IC, Newham DJ. Steadiness of quadriceps contractions in young and older adults with and without a history of falling. *Eur J Appl Physiol* 100(5): 527-533, 2006.

Castronovo AM, Negro F, Conforto S, Farina D. The proportion of common synaptic input to motor neurons increases with an increase in net excitatory input. *J Appl Physiol* 119: 1337-1346, 2015.

Cher D, Polly D, Berven S. Sacroiliac joint pain: burden of disease. *Med Devices Auckl NZ* 7: 73–81, 2014.

Chipchase LS, Schabrun SM, Hodges PW. Corticospinal excitability is dependent on the parameters of peripheral electric stimulation: a preliminary study. *Arch Phys Med Rehabil* 92: 1423-1430, 2011.

Christou E. Aging and variability of voluntary contractions. *Exerc Sport Sci Rev* 39: 77-84, 2013.

Clair-Auger JM, Collins DF, Dewald JPA. The effects of wide pulse neuromuscular electrical stimulation on elbow flexion torque in individuals with chronic hemiparetic stroke. *Clin Neurophysiol* 123: 2247-2255, 2012.

Clark DL, Ting LH, Zajac FE, Neptune RR, Kautz SA. Merging of healthy motor modules predicts reduced locomotor performance and muscle coordination complexity post-stroke. *J Neurophysiol,* 103:844-857, 2010.

Cole KJ, Rotella DL, Harper JG. Tactile impairments cannot explain the effect of age on a grasp and lift task. *Exp Brain Res* 121(3):263–9, 1998.

Collins DF. Central contributions to contractions evoked by tetanic neuromuscular electrical stimulation. *Exercise Sport Sci Rev* 35: 102-109, 2007.

Colson SS, Martin A, Van Hoecke J. Effects of electromyostimulation versus voluntary isometric training on elbow flexor muscle strength. *J Electromyogr Kinesiol* 19: e311-e319, 2009.

Cook RD. Detection of influential observation in linear regression. *Technometrics* 19(1):15–8, 1977.

Craik KJW. Theory of the human operator in control systems. I. the operator as an engineering system. *Br J Psychol* 38:56–61, 1947.

Cunningham JP, Yu BM. Dimensionality reduction for large-scale neural recordings. *Nat Neurosci* 17: 1500–1509, 2014

Cuypers K, Levin O, Thijs H, Swinnen SP, Meesen RLJ. Long-term tens treatment improves tactile sensitivity in MS patients. *Neurorehabil Neural Repair* 24(5):420–7, 2010.

Dasen JS, Liu JP, Jessell TM. Motor neuron columnar fate imposed by sequential phases of Hox-c activity. *Nature* 425: 926-933, 2003.

Day SJ, Hulliger M. Experimental simulation of cat electromyogram: evidence for algebraic summation of motor-unit action-potential trains. *J Neurophysiol* 86: 2144-2158, 2001.

De Luca CJ, LeFever RS, McCue MP, Xenakis AP. Control scheme governing concurrently active human motor units during voluntary contractions. *J Physiol* 329*:* 129-42, 1982.

De Luca CJ, Erim Z. Common drive of motor units in regulation of muscle force. *Trends Neurosci* 17: 299-305, 1994.

De Luca CJ, Erim Z. Common drive in motor units of a synergistic muscle pair. *J Neurophysiol* 87:2200–2204, 2002.

De Luca CJ, Foley PJ, Erim Z. Motor unit control properties in constant-force isometric contractions. *J Neurophysiol* 76: 1503-1516, 1996.

Del Veccio A, Negro F, Felici F, Farina D. Association between motor unit action potential parameters and surface EMG features. *J Appl Physiol* 123: 835-843, 2017.

de Vries Ingmar EJ, Daffertshofer A, Stegeman DF, Boonstra TW. Functional connectivity in the neuromuscular system underlying bimanual coordination. *J Neurophysiol* 116: 2576-2585, 2016.

Demireva EY, Shapiro LS, Jessell TM, Zampieri N. Motor neuron position and topographic order imposed by β- and γ- catenin activities. *Cell* 147: 641-652, 2011.

Denny-Brown D, Pennybacker, JB. Fibrillation and fasciculation in voluntary muscle. *Brain* 61: 311-334, 1938.

Desmedt JE, Godaux E. Ballistic contractions in man: characteristic recruitment pattern of single motor units of the tibialis anterior muscle. *J Physiol* 264: 673-693, 1977a.

Desmedt JE, Godaux E. Fast motor units are not preferentially activated in rapid voluntary contractions in man. *Nature* 267: 717-719, 1977b.

Dempster AP, Laird NM, Rubin DB. Maximum likelihood from incomplete data via the EM algorithm. *J Royal Stat Soc* 39: 1–38, 1977.

Dideriksen JL, Farina D, Baekgaard M, Enoka RM. An integrative model of motor unit activity during sustained submaximal contractions. *J Appl Physiol* 108: 1550-62, 2010.

Dideriksen JL, Negro F, Enoka RM, Farina D. Motor unit recruitment strategies and muscle properties determine the influence of synaptic noise on force steadiness. *J Neurophysiol* 107:3357–3369, 2012.

Dideriksen JL, Negro F, Farina D. The optimal neural strategy for a stable motor task requires a compromise between level of muscle cocontraction and synaptic gain of afferent feedback. *J Neurophysiol* 114: 1895-1911, 2015.

Dideriksen JL, Feeney DF, Almuklass AW & Enoka RM. Control of force during rapid visuomotor force-matching tasks can be described by discrete time PID control algorithms. *Exp Brain Res* 235, 2561-2573, 2017.

Diedrichsen J, Shadmehr R, Ivry RB. The coordination of movement: optimal feedback control and beyond. *Trends Cogn. Sci*. 14:31–39, 2010.

Duchateau J., Enoka RM. Human motor unit recordings: Origins and insight into the integrated motor system. *Brain Res* 1409: 42-61, 2011.

Enoka, RM, Robinson GA, Kossev AR. A stable, selective electrode for recording single motor-unit potentials in humans. *Exp. Neurol* 99: 761-764, 1988.

Erim Z, De Luca CJ, Mineo K, Aoki T. Rank-ordered regulation of motor units. *Muscle Nerve* 19: 563-573, 1996.

Falla D, Hodges PW. Individualized exercise interventions for spinal pain. *Exerc Sport Sci Rev* 45 105-115, 2017.

Fairbank JC, Pynsent PB. The Oswestry Disability Index. *Spine* 25:2940–2952, 2000.

Falconer K, Winter DA. Quantitative assessment of co-contraction at the ankle joint in walking. *Electromyogr Clin Neurophysiol* 25: 135-149, 1985.

Farmer SF, Bremner FD, Halliday DM, Rosenberg JR, Stephens JA. The frequency content of common synaptic inputs to motoneurones studied during voluntary isometric contraction in man. *J Physiol* 470: 127-55, 1993.

Farina D, Negro F. Accessing the neural drive to muscle and translation to neurorehabilitation technologies. *IEEE Rev Biomed Eng* 5: 3-14, 2012.

Farina D, Negro F, Dideriksen JL. The effective neural drive to muscles is the common synaptic input to motor neurons. *J Physiol* 49:1–37, 2014.

Farina D, Negro F. Common synaptic input to motor neurons, motor unit synchronization, and force control. *Exerc Sport Sci Rev* 43: 23-33, 2015.

Farina D, Negro F, Muceli S, Enoka RM. Principles of motor unit physiology evolve with advances in technology. *Physiology* 31: 83-94, 2016.

Farina D, Vujaklija I, Sartori M, Kapelner T, Negro F, Jiang N, Bergmeister K, Andalib A, Principe J, Aszmann OC. Man/machine interface based on the discharge timings of spinal motor neurons after targeted muscle reinnervation. *Nat Biomed Eng* 1: 1–12, 2017.

Feeney DF, Meyer FG, Noone N, Enoka RM. A latent low-dimensional common input drives a pool of motor neurons: a probabilistic latent state-space model. *J Neurophysiol* 118: 2238-2250, 2017.

Feinstein B, Lindegard B, Nyman E, Wohlfart G. Morphologic studies of motor units in normal human muscles. *Acta Anat Basel* 23:127-42, 1955.

Fischer J, Rudick R, Cutter G, Reingold S. The Multiple Sclerosis Functional Composite measure (MSFC): an integrated approach to MS clinical outcome assessment. *Mult Scler J* 5(4):244–50, 1999.

Fuglevand AJ, Winter DA, Patla AE. Models of recruitment and rate coding organization in motor- unit pools. *J Neurophysiol* 70: 2470-2486, 1993.

Fuglevand AJ, Lester RA, Johns RK. Distinguishing intrinsic from extrinsic factors underlying firind rate saturation in human motor units. *J Neurophysiol* 113: 1310-1322, 2015.

Galganski ME, Fuglevand AJ, Enoka RM. Reduced control of motor output in a human hand muscle of elderly subjects during submaximal contractions. *J Neurophysiol* 69:2108–2115, 1993

Gawel M, Kostera-Pruszczyka. Effect of age and gender on the number of motor units in healthy subjects estimated by the multipoint incremental MUNE method. *J Clin Neurophysiol* 31:272-278, 2014.

Gawthrop P, Gollee H, Loram I. Intermittent Control in Man and Machine, 2014.

Gawthrop P, Loram I, Lakie M, Gollee H. Intermittent control: A computational theory of human control. *Biol Cybern* 104:31–51, 2011

Gazzoni M, Botter A, Vieira T. Surface EMG and muscle fatigue: multichannel approaches to the study of myoelectric manifestations of muscle fatigue. *Physiol Measurements* 38, 5, 2017.

Gershon RC, Cella D, Fox NA, Havlik RJ, Hendrie HJ, Wagster MV. Assessment of neurological and behavioural function: the NIH Toolbox. *Lancet* 9: 138-139, 2010.

Gomes-Osman J, Tibbett JA, Poe BP, Field-Fote EC. Priming for improved hand strength in persons with chronic tetraplegia: a comparison of priming-augmented functional task practicem, priming alone, and conventional exercise training. *Front Neurol* 242: 1-13, 2017.

Goodale M a, Pelisson D, Prablanc C. Large adjustments in visually guided reaching do not depend on vision of the hand or perception of target displacement. *Nature* 320:748–750, 1986.

Goodkin DE, Hertsgaard D, Seminary J. Upper extremity function in multiple sclerosis: improving assessment sensitivity with box-and-block and nine-hole peg tests. *Arch Phys Med Rehabil* 69(10):850–854, 1988.

Guclu-Gunduz A, Citaker S, Nazliel B, Irkec C. Upper extremity function and its relation with hand sensation and upper extremity strength in patients with multiple sclerosis. *Neurorehabilitation* 30(4):369-374, 2012.

Gustafsson B, Pinter MJ. An investigation of threshold properties among cat spinal alpha-motorneurones. *J Physiol* 357: 453-483, 1984.

Graven-Nielsen T, Svensson P, Arendt-Nielsen L. Effects of experimental muscle pain on muscle activity and co-ordination during static and dynamic motor function. *Electroencephalogr Clin Neurophysiol* 105:156–64, 1997.

Gross M, Stevenson P, Charette S, Pyka G, Marcus R. Effect of muscle strength and movement speed on the biomechanics of rising from a chair in healthy elderly and young women. *Gait Posture* 8:175–85, 1998.

Gydikov A, Kosarov D. Extraterritorial potential field of impulses from separate motor units in human muscles. *Electromyography* 12: 127-147, 1972

Gydikov A, Kosarov D, Kossev A, Kostov K, Trayanova N, Radicheva N. 1986 Motor unit potentials at high muscle activity recorded by selective electrodes. *Biomed. Biochem Acta* 45: S63–S68, 1967.

Gydikov A, Kossev A, Trayanova N, Radicheva N. Selective recording of motor unit potentials. *Electromyogr Clin Neurophysiol* 26: 273-281, 1986.

Hamill J, Palmer C, Van Emmerick REA. Coordinative variability and overuse injury. *Sports med arth rehab therapy tech* 4: 45:54, 2012.

Hamilton LD, Thomas E, Almuklass AM, Enoka RM. A framework for identifying the adaptations responsible for differences in pegboard times between middle-aged and older adults. *Exp Gerontol* 97:9-16, 2017.

Hanada EY, Johnson M, Hubley-Kozey C. A comparison of trunk muscle activation amplitudes during gait in older adults with and without chronic low back pain. *Phys Med and Rehab* 3: 920-928, 2011

Heckman CJ, Johnson M, Mottram C, Schuster J. Persistent inward currents in spinal motoneurons and their influence on human motoneuron firing patterns. *Neuroscientist* 14:264–275, 2008.

Heckman CJ, Enoka RM. Motor Unit. *Comp Physiol* 2: 2629-2682, 2012.

Henneman E. Relation between size of neurons and their susceptibility to discharge. *Science* 126: 1345–1347, 1957.

Henneman E, Olson CB. Relations between structure and function in the design of skeletal muscles. *J Neurophysiol* 28: 581–598, 1965

Henneman E, Somjen G, Carpenter DO. Functional significance of cell size in spinal motoneurons. *J Neurophysiol* 28: 560–580, 1965.

Hermens HJ, Freriks B, Disselhorst-Klug C, Rau G. Development of recommendations for SEMG sensors and sensor placement procedures. *J Electromyogr Kinesiol Off J Int Soc Electrophysiol Kinesiol* 10:361–74, 2000.

Herzog W, Longino D, Clark A. The role of muscles in joint adaptation and degeneration. *Langenbecks Arch Surg* 388:305–15, 2003.

Hodges PW, Richardson CA. Inefficient muscular stabilization of the lumbar spine associated with low back pain. A motor control evaluation of transversus abdominis. *Spine* 21:2640–50, 1996.

Hodges PW, Smeets RJ. Interaction Between Pain, Movement, and Physical Activity: Short-term Benefits, Long-term Consequences, and Targets for Treatment. *Clin J Pain* 31:97–107, 2015.

Holobar A, Zazula D. Correlation-based decomposition of surface electromyograms at low contraction forces. *Med Biol Eng Comput* 42: 487-95, 2004.

Hug F, Tucker K. Muscle Coordination and the Development of Musculoskeletal Disorders: *Exerc Sport Sci Rev, in press.*

Hsieh CY, Pringle RK. Range of motion of the lumbar spine required for four activities of daily living. J Manipulative *Physiol Ther* 17:353–8, 1994.

Hyngstrom AS, Kuhnen HR, Kirking KM, Hunter SK. Functional implications of impaired control of submaximal hip flexion following stroke. *Muscle Nerve* 49(2) 225-232, 2014.

Jesunathadas M, Aidoor SS, Keenan KG, Farina D, Enoka RM. Influence of amplitude cancellation on the accuracy of determining the onset of muscle activity from the surface electromyogram. *J Electromyogr Kinesiol Off J Int Soc Electrophysiol Kinesiol* 22:494–500, 2012.

Jo S, Massaquoi SG. A model of cerebellum stabilized and scheduled hybrid long-loop control of upright balance. *Biol Cybern* 91:188–202, 2004.

Johansson S, Ytterberg C, Classon IM, Lindberg J, Hillert J, Andersson M, Widen Holmqvist L, von Koch L. High concurrent presence of disability in multiple sclerosis. *J Neurology*. 254: 767-773, 2007.

Johnson MD, Thompson CK, Tysseling VM, Powers RK, Heckman CJ. The potential for understanding the synaptic organization of human motor commands via the firing patterns of motoneurons. *J Neurophysiol* 118:520-531, 2017.

Jones KE, Hamilton AF, Wolpert DM. Sources of signal-dependent noise during isometric force production. *J Neurophysiol* 88:1533–1544, 2002.

Kalron A, Greenberg-Abrahami M, Gelav S, Achiron A. Effects of a new sensory re-education on hand sensibility and manual dexterity in people with multiple sclerosis. *NeuroRehabil* 32: 943-948, 2013.

Katz B, Miledi R. Membrane noise produced by acetylcholine. *Nature* 226: 962-3, 1970.

Katz V, Schofferman J, Reynolds J. The sacroiliac joint: a potential cause of pain after lumbar fusion to the sacrum. *J Spinal Disord Tech* 16:96–9, 2003.

Kanda K, Hashizume K. Factors causing difference in force output among motor units in the rat medial gastrocnemius muscle. *J Physiol* 448: 677-695, 1992.

Keenan KG, Farina D, Maluf KS, Merletti R, Enoka RM. Influence of amplitude cancellation on the simulated surface electromyogram. *J Appl Physiol* 98: 120-131, 2005.

Kernell, D. The limits of firing frequency in cat lumbosacral motoneurones possessing different time course of after hyperpolarization. *Acta Physiol Scand 65*: 87–100, 1965.

Kernell D, Monster AW. Threshold current for repetitive impulse firing in motoneurones innervating muscle fibres of different fatigue sensitivity in the cat. *Brain Research* 229: 193-196, 1981.

Kibsgård TJ, Røise O, Sturesson B, Röhrl S, Stuge, B. Radiosteriometric analysis of movement in the sacroiliac joint during a single-leg stance in patients with long-lasting pelvic girdle pain. *Clin Biomech* 29: 406–411, 2014.

Kibsgård TJ, Röhrl SM, Røise O, Sturesson B, Stuge B. Movement of the sacroiliac joint during the active straight leg raise test in patients with long lasting severe sacroiliac joint pain. *Clin Biomech* 47: 40-45, 2017

Kierkegaard M, Einarsson U, Gottberg K, Koch LV, Holmqvist LW. The relationship between walking, manual dexterity, cognition and activity/participation in persons with multiple sclerosis. *Mult Scler J* 18(5):639–46, 2012.

Kieseier BC, Pozzilli C. Assessing walking disability in multiple sclerosis. *Mult Scler* 18(7):914-924, 2012.

Kirkwood PA, Sears TA, Westgaard RH. Recurrent inhibition of intercostal motoneurones in the cat. *J Physiol* 319:111–130, 1981.

Koch MW, Murray TJ, Fisk J, Greenfield J, Bhan V, Jacobs P, Brown M, Metz LM. Hand dexterity and direct disease related cost in multiple sclerosis. *J Neurol Sci* 341(1-2):51–4, 2014.

Koenig L, Saavoss J, Cher D. Productivity benefits of minimally invasive surgery in patients with chronic sacroiliac joint dysfunction. *Clin Outcomes Res* 77, 2016.

Kobayashi H, Koyama Y, Enoka RM, Suzuki S. A unique form of light-load training improves steadiness and performance on some functional tasks in older adults. *Scand J Med Sci Sports* 24: 98-110, 2014.

Körding KP, Wolpert DM. Bayesian integration in sensorimotor learning. *Nature* 427:244–247, 2004.

Kouzaki M, Kimura T, Yoshitake Y, Hayashi T, Moritani T. Subthreshold electrical stimulation reduces motor unit discharge variability and decreases the force fluctuations of plantar flexion. *Neurosci Lett* 513: 146-150, 2012.

Kornatz KW, Christou EA, Enoka RM. Practice reduces motor unit discharge variability in a hand muscle and improves manual dexterity in older adults. *J Appl Physiol* 98: 2072-2080, 2005.

Kline JC, De Luca CJ. Synchronization of motor unit firings: an epiphenomenon of firing rate characteristics not common inputs. *J Neurophysiol* 115: 178-92, 2015.

Kragt JJ, Linden FAVD, Nielsen JM, Uitdehaag BM, Polman CH. Clinical impact of 20%

worsening on Timed 25-foot Walk and 9-hole Peg Test in multiple sclerosis. *Mult Scler J* 12(5):594–8, 2006.

Kuhn A, Aertsen A, Rotter S. Higher-order statistics of input ensembles and the response of simple model neurons. *Neural Comput* 15: 67–101, 2003.

Kristiansen M, Samani A, Madeleine P, Hansen EA. Effects of 5-weeks of bench press training on muscle synergies: a randomized controlled study. *J Str Cond Res* 30: 1948-1959, 2016.

Lagerquist O, Walsh LD, Blouin JS, Collins DF, Gandevia SC. Effect of a peripheral nerve block on torque produced by repetitive electrical stimulation. *J Appl Physiol* 107: 161-167, 2009.

Laidlaw DH, Bilodeau M, Enoka RM. Steadiness is reduced and motor unit discharge is more variable in old adults. *Muscle and Nerve* 23:600–612, 2000.

Laine CM, Martinez-Valdes E, Falla D, Mayer F, Farina D. Motor neuron pools of synergistic thigh muscles share most of their synaptic input. *J Neurosci* 35: 12207-16, 2015.

Latash ML. Motor synergies and the equilibrium-point hypothesis. *Motor Control* 14: 294-322, 2007.

Lawrence EL, Dayanidhi S, Fassola I, Requejo P, Leclercq C, Winstein CJ, Valero-Cuevas, FJ. Outcome measures for hand function naturally reveal three latent domains in older adults: strength, coordinated upper extremity function, and sensorimotor processing. *Frontiers in Aging Neuroscience*, *7*, 108, 2015.

Lee WA. Neuromotor synergies as a basis for coordinated intentional action. *J Mot Behav* 16: 135-170, 1984.

Lee DD, Seung HS. Learning the parts of objects by non-negative matrix factorization. *Nature* 401: 788–791, 1999.

Lee DD, Seung HS. Algorithms for non-negative matrix factorization. *Adv Neural Inform Proc Syst* 13: 556–562, 2001.

Loram ID, Gollee H, Lakie M, Gawthrop PJ. Human control of an inverted pendulum: is continuous control necessary? Is intermittent control effective? Is intermittent control physiological? *J Physiol* 589:307–324, 2011.

Loram ID, Lakie M, Gawthrop PJ. Visual control of stable and unstable loads: what is the feedback delay and extent of linear time-invariant control? *J Physiol* 587:1343–65, 2009.

Loram ID, Van De Kamp C, Lakie M. Does the motor system need intermittent control? *Exerc Sport Sci Rev* 42:117–125, 2014.

Jenny AB, Inukai J. Principles of motor organization of the monkey cervical spinal cord. *J Neurosci* 3: 567-575, 1983.

Liddell EGT, Sherrington CS. Recruitment and some other factors of reflex inhibition. *Proc R Soc Lond Ser B* 97:488-518, 1925.

Macefield VG, Fuglevand AJ, Bigland- Ritchie B. Contractile properties of single motor units in human toe extensors assessed by intraneural motor axon stimulation. *J Neurophysiol* 75: 2509-2519, 1996.

Macke JH, Buesing L, Cunningham JP, Byron MY, Shenoy KV, Sahani M. Empirical models of spiking in neural populations. *NIPS*, pages 1350–1358, 2011.

Maffiuletti NA. Physiological and methodological considerations for the use of neuromuscular electrical stimulation. *Eur J Appl Physiol* 110: 223-234, 2010.

Maluf KS, Shinohara M, Stephenson JL, Enoka RM. Muscle activation and time to task failure differ with load type and contraction intensity for a human hand muscle. *Exp Brain Res* 167:165–177, 2005.

Mangion AZ, Yuan K, Kadirkamanathan V, Niranjan M, Sanguinetti G. Online variational inference for state-space models with point-process observations. *Neural Comput* 23: 1967–1999, 2011.

Manto M, Bower JM, Conforto AB. Consensus paper: Roles of the cerebellum in motor control-the diversity of ideas on cerebellar involvement in movement. *Cerebellum* 457–487, 2012.

Marmon AR, Pascoe MA, Schwartz RS, Enoka RM. Associations among strength, steadiness, and hand function across the adult life span. *Med Sci Sports Ex* 43(4):560-567, 2011a.

Marmon AR, Gould JR, Enoka RM. Practicing a functional task improves steadiness with hand muscles in older adults. *Med Sci Sports Exerc* 43: 1531-1537, 2011b.

Martin A, Grospretre S, Vilmen C, Guye M, Mattei AP, Le Fur Y, Bendahan D, Gondin J. The etiology of muscle fatigue differs between two electrical stimulation protocols. *Med Sci Sports Exerc* 48: 1474-1484, 2016.

Martinez-Valdez E, Negro F, Laine CM, Falla D, Mayer F, Farina D. Tracking motor units longitudinally across experimental sessions with high-density surface electromyography. *J Physiol* 595:1479-1496, 2017.

McCrory JL, White SC, Lifeso RM. Vertical ground reaction forces: objective measures of gait following hip arthroplasty. *Gait Posture* 14:104–9, 2001.

McPhedran AM, Wuerker RB, Henneman E. Properties of motor units in a homogeneous red muscle (soleus) of the cat. *J Neurophysiol* 28: 71–84, 1965.

McNaughton BL, Battaglia FP, Jensen O. Path integration and the neural basis of the "cognitive map." *Nat Rev Neurosci* 7:663–78, 2006.

Merletti R, Rainoldi A, Farina D. Surface electromyography for noninvasive characterization of muscle. *Exer Sport Sci Rev* 29: 20-25, 2001.

Merletti R, Botter A, Troiano A, Merlo E, Minetto MA. Technology and instrumentation for detection and conditioning of the surface electromyographic signal: state of the art. *Clinical Biomechanics* 24: 122-134, 2009.

Miall RC, Weir DJ, Stein JF. Manual tracking of visual targets by trained monkeys. *Behav Brain Res* 20:185–201, 1986.

Miall RC, Weir DJ, Stein JF. Intermittency in human manual tracking tasks. *J Mot Behav* 25:53–63, 1993.

Milner- Brown HS, Stein RB, Yemm R. The contractile properties of human motor units during voluntary isometric contractions. *J Physiol* 228: 285-306, 1973.

Mileusnic MP, Brown IE, Lan N, Loeb GE. Mathematical models of proprioceptors. I. Control and transduction in the muscle spindle. *J Neurophysiol* 96:1772–1788, 2006.

Monster AW, Chan H. Isometric force production by motor units of extensor digitorum communis muscle in man. *J Neurophysiol* 40: 1432-1440, 1977.

Moran F, Leonard T, Hawthrone S, Hughes CM, McCrum-Gardner E, Johnson MI, Rakel BA, Sluka KA, Walsh DM. Hypoalgesia in response to transcutaenous electrical nerve stimulation (TENS) depends on stimulation intensity. *J Pain* 12(8): 929-935, 2011.

Moritz CT, Barry BK, Pascoe MA, Enoka RM. Discharge rate variability influences the variation in force fluctuations across the working range of a hand muscle. *J Neurophysiol* 93: 2449-2459, 2005.

Mottram CJ, Jakobi JM, Semmler JG, Enoka RM. Motor-unit activity differs with load type during a fatiguing contraction. *J Neurophysiol* 93: 1381–1392, 2005.

Negro F, Holobar A, Farina D. Fluctuations in isometric muscle force can be described by one linear projection of low-frequency components of motor unit discharge rates. *J Physiol* 527: 5925- 5938, 2009.

Negro F, Muceli S, Castronovo AM, Holobar A, Farina D. Multi-channel intramuscular and surface EMG decomposition by convolutive blind source separation. *J Neural Eng* 13:1741-1758, 2016a.

Negro F, Yavuz US, Farina D. The human motor neuron pools receive a dominant slow-varying common synaptic input. *J Physiol* in press, 2016b.

Neilson PD, Neilson MD, O'Dwyer NJ. Internal models and intermittency: A theoretical account of human tracking behavior. *Biol Cybern* 58:101–112, 1988.

Nelson-Wong E, Bourgeois G, DeGrandis C, Hamilton N, Kirven I, Pieratt Kl. Lumbopelvic control and hip muscle activation in low back pain cases vs controls, Omaha, NE: 2013.

Nordstrom MA, **Fuglevand AJ, Enoka RM**. Estimating the strength of common input to human motoneurons from the cross-correlogram. *J Physiol* 453: 547-574, 1992.

O'Sullivan I, Burdet E, Diedrichsen J. Dissociating Variability and Effort as Determinants of Coordination. *PLoS Comput Biol* 5:e1000345, 2009.

Oldfield RC. The assessment and analysis of handedness: the Edinburgh inventory. *Neuropsychologia* 9: 97-113, 1971.

Oliveira AS, Gizzi L, Farina D, Kersting WG. Motor modules of human locomotion: influence of MG averaging, concatenation, and number of step cycles. *Front Hum Neurosci* 8, 2014.

Olree KS, Vaughan CL. Fundamental patterns of bilateral muscle activity in human locomotion. *Biol Cybern* 73L: 409-414, 1995.

Ostwald SK, Snowdon DA, Rysavy SDM, Keenan NL, Kane RL. Manual dexterity as a correlate of dependency in the elderly. *J Am Geriat Soc.* 37: 963-969.

Paninski L, Ahmadian Y, Ferreira DG, Koyama S, Rahnama Rad K, Vidne M, Vogelstein J, Wu W. A new look at state-space models for neural data. *J Comput Neurosci* 29: 107–126, 2010.

Paltamaa J, Sarasoja T, Leskinen E, Wikstrom J, Malkia E. Measures of physical functioning predict self-reported performance in self-care, mobility, and domestic life in ambulatory persons with multiple sclerosis. *Arch Phys Med Rehabil* 88(12):1649–1657, 2007.

Park SH, Kwon M, Christou EA. Motor output oscillations with magnification of visual feedback in older adults. *Neurosci Lett* 24: 647-648, 2017.

Partridge LD. Modification of neural output signals by muscles: a frequency response study. J Appl Physiol 20, 150-156, 1965.

Perkel DH, Gerstein GL, Moore GP. Neuronal spike trains and stochastic point processes. I. The single spike train. *Biophys J* 7: 391–418, 1967.

Person RS. Rhythmic activity of a group of human motoneurones during voluntary contraction of a muscle. *Electroencephalogr Clin Neurophysiol* 36: 585–595, 1974

Person RS, Kudina LP. Discharge frequency and discharge pattern of human motor units during voluntary contraction of muscle. *Electroencephalogr Clin Neurophysiol* 32:471–483, 1972.

Peterka RJ. Sensorimotor integration in human postural control. *J Neurophysiol* 88:1097–118, 2005.

Peterka RJ, Loughlin PJ. Dynamic regulation of sensorimotor integration in human postural control. *J Neurophysiol* 91:410–423, 2004.

Poole JL, Nakamoto T, McNulty T, Montoya JR, Weill D, Dieruf K, Skipper B. Dexterity, visual perception, and activities of daily living in persons with multiple sclerosis. *Occup Ther Health Care* 24(2):159-170, 2010.

Pool-Goudzwaard AL, Vleeming A, Stoeckart R, Snijders CJ, Mens JMA. Insufficient lumbopelvic stability: a clinical, anatomical and biomechanical approach to "a-specific" low back pain. *Man Ther* 3:12–20, 1998.

Powers RK, Binder MD. Summation of motor unit tensions in the tibialis posterior muscle of the cat under isometric and nonisometric conditions. *J Neurophysiol* 66; 1838-1846, 1991.

Powers RK, Heckman CJ. Synaptic control of the shape of the motoneuron pool input-output function. *J Neurophysiol* 117: 1171–1184, 2017.

Powers RK, Dai Y, Bell BM, Percival DB, Binder MD. Contributions of the input signal and prior activation history to the discharge behaviour of rat motoneurones. *J Physiol* 562: 707–724, 2005.

Pnevmatikakis EA, Soudry D, Gao Y, Machado TA, Merel J, Pfau D, Reardon T, Mu Y, Lacefield C, Yang W, Ahrens M, Bruno R, Jessell TM, Peterka DS, Yuste R, Paninski L. Simultaneous denoising, deconvolution, and demixing of calcium imaging data. *Neuron* 89: 285–299, 2016.

Proske U, Gandevia SC. The kinaesthetic senses. J Physiol 587:4139–4146, 2009.

Radebold A, Cholewicki J, Panjabi MM, Patel TC. Muscle response pattern to sudden trunk loading in healthy individuals and in patients with chronic low back pain. *Spine* 25:947–54, 2000.

Reuben DB, Magasi, S, McCreath, HE, Bohannon, RW, Wang, YC, Bubela, DJ, Rymer WZ, Beaumont J, Rine RM, Gershon, RC. Motor assessment using the NIH Toolbox. *Neurology*, *80*(11 Suppl 3), S65–S75, 2013.

Rudroff T, Justice JN, Matthews S, **Enoka RM**. Muscle activity differs with load compliance during fatiguing contractions with the knee extensor muscles. *Exp Brain Res* 203:307–316, 2010.

Ruff RM, Parker SB. Gender- and age-specific changes in motor speed and eye-hand coordination in adults: normative values for the Finger Tapping and Grooved Pegboard Tests. *Percept. Mot. Skills* 76**,** 1219–1230, 1993.

Salonikidis K, Amiridis IG, Oxyzoglou N, de Villareal ES, Zafeiridis A, Kellis E. Force variability during isometric wrist flexion in highly skilled and sedentary individuals. *Eur J Appl Physiol* 107: 715-722, 2009.

Sawyers A, Pai Y-C, Bhatt T, Ting LH. Neuromuscular responses differ between slip-induced falls and recoveries in older adults, *J Neurophysiol* 117: 509-522, 2017.

Scott SH. The computational and neural basis of voluntary motor control and planning. *Trends Cogn. Sci.* 16:541–549, 2012.

Sears TA, Stagg D. Short-term synchronization of intercostal motoneurone activity. *J Physiol* 263:357-81, 1976.

Sembrano JN, Polly DW. How often is low back pain not coming from the back? *Spine* 34: E27-32, 2009.

Seynnes O, Hue OA, Garrandes F, Colson SS, Bernard PL, Legros P, Fiatarone Singh MA. Force steadiness in the lower extremities as an independent predictor of functional performance in older women. *J Aging Phys Activity* 13(4): 395-408, 2005.

Shum GLK, Crosbie J, Lee RYW. Effect of low back pain on the kinematics and joint coordination of the lumbar spine and hip during sit-to-stand and stand-to-sit. *Spine* 30:1998–2004, 2005.

Slifkin AB, Vaillancourt DE, Newell KM. Intermittency in the control of continuous force production. *J Neurophysiol* 84:1708–1718, 2000.

Sluka KA, Walsh D. Transcutaneous electrical nerve stimulation: basic science mechanisms and clinical effectiveness. *J Pain* 4: 109-121, 2003.

Smith AC, Brown EN. Estimating a state-space model from point process observations. *Neural Comput* 15: 965–991, 2003.

Sosnoff JJ, Newell KM. Aging, visual intermittency, and variability in isometric force output. *J Gerontol B Psychol Sci Soc Sci* 61B:P117–P124, 2006.

Sosnoff JJ, Valantine AD, Newell KM. Independence between the amount and structure of variability at low force levels. *Neurosci Lett* 392:165–169, 2006.

Stein RB, French AS, Mannard A, Yemm R. New methods for analyzing motor function in man and animals. *Brain Research* 40:187-192, 1972.

Stewart WF, Ricci JA, Chee E, Morganstein D, Lipton R. Lost productive time and cost due to common pain conditions in the US workforce. *JAMA* 290:2443–54, 2003.

Sturesson B, Selvik G, Uden A. Movements of the sacroiliac joints. A roentgenstereophotogrammetric analysis. *Acta Orthop Scand Suppl* 59: 89, 1988.

Szadek KM, van der Wurff P, van Tulder MW, Zuurmond WW, Perez RSGM. Diagnostic validity of criteria for sacroiliac joint pain: a systematic review. *J Pain* 10:354–68, 2009.

Thompson-Butel AG, Lin GG, Shiner CT, Mcnulty PA. Two common tests of dexterity can stratify upper limb motor function after stroke. *Neurorehabil Neural Repair* 28(8):788–96, 2014.

Ting LH. and Macpherson JM. A limited set of muscle synergies for force control during a postural task. *J Neurophysiol* 93: 609–613, 2009.

Townsend BR, Paninski L, Lemon RN. Linear encoding of muscle activity in primary motor cortex and cerebellum. *J Neurophysiol* 96: 2578–2592, 2006.

Tracy BL, Enoka RM. Older adults are less steady during submaximal isometric contractions with the knee extensor muscles. *J Appl Physiol* 92: 1004-1012, 2002.

Tracy BL, Maluf KS, Stephenson JL, Enoka RM. Variability of motor unit discharge and force fluctuations across a range of muscle forces in older adults. *Muscle and Nerve* 32:533–540, 2005.

Tresch MC, Jarc A. The case for and against muscle synergies. *Curr. Opin. Neurobiol.* 19:601–607, 2009.

Truccolo W. Stochastic models for multivariate neural point processes: collective dynamics and neural decoding. Analysis of Parallel Spike Trains. New York: Springer, p. 321–341, 2010.

Van Cutsem M, Feiereisen P, Duchateau J, Hainaut K. Mechanical properties and behaviour of motor units in the tibialis anterior during voluntary contractions. *Can J Appl Physiol* 22(6):585-597, 1997.

van Dieën J, Herta F, Hodges PW. Low-back pain patients learn to adapt motor behavior with adverse secondary consequences. *Med Sci Sports Ex* 45: In Press, 2017.

van den Hoorn W, Hodges PW, van Dieen JH, Hug F. Effect of acute noxious stimulation to the leg or back on muscle synergies during walking. *J. Neurophysiol* 113: 244–54, 2014

van de Kamp C, Gawthrop PJ, Gollee H, Loram ID. Refractoriness in Sustained Visuo-Manual Control: Is the Refractory Duration Intrinsic or Does It Depend on External System Properties? *PLoS Comput Biol* 9:e1002843, 2013.

van Winsen LM, Kragt JJ, Hoogervorst EL, Polman CU, Uitdehaag BM. Outcome measurement in multiple sclerosis: detection of clinically relevant improvement. *Mult Scler J* 16(5):604–10, 2010.

Vanderthommen M, Duchateau J. Electrical stimulation as a modality to improve performance of the neuromuscular system. *Exerc Sport Sci Rev* 35: 180-185, 2007.

Veale JF. Edinburgh Handedness Inventory – Short Form: A revised version based on confirmatory factor analysis. *Laterality* 19(2):164–77, 2014.

Vila-Cha C, Falla D, Farina D. Motor unit behavior during submaximal contractions following six weeks of either endurance or strength training. J Appl Physiol 109, 1455-1466, 2010.

Vleeming A, Stoeckart R, Volkers AC, Snijders CJ. Relation between form and function in the sacroiliac joint. Part I: Clinical anatomical aspects. *Spine* 15:130–2, 1990.

Vleeming A, Buyruk HM, Stoeckart R, Karamursel S, Snijders CJ. An integrated therapy for peripartum pelvic instability: a study of the biomechanical effects of pelvic belts. *Am J Obstet Gynecol* 166: 1243–1247, 1992.

Vleeming A, Pool-Goudzwaard AL, Stoeckart R, van Wingerden JP, Snijders CJ. The posterior layer of the thoracolumbar fascia. Its function in load transfer from spine to legs. *Spine* 20:753–8, 1995.

Vleeming A, Schuenke MD, Masi AT, Carreiro JE, Danneels L, Willard FH. The sacroiliac joint: an overview of its anatomy, function and potential clinical implications. *J Anat* 221: 537–567, 2012.

Voelcker-Rehage C, Godde B. High frequency sensory stimulation improves tactile but not motor performance in older adults. *Motor Control* 14(4):460–77, 2010.

Walker ER, Hyngstrom AS, Schmit BD. Sensory electrical stimulation improves foot placement during targeted stepping post-stroke. *Exp Brain Res* 232(4): 1137-1143, 2014.

Wang YC, Magasi SR, Bohannon RW, Reuben DB, McCreath HE, Bubela DJ, Gershon RC, Rymer, ZW. Assessing Dexterity Function: A Comparison of Two Alternatives for the NIH Toolbox. *J. Hand Ther.* 24:313–321, 2011.

Watanabe RN, Magalhães FH, Elias LA, Chaud VM, Mello EM, Kohn AF. Influences of premotoneuronal command statistics on the scaling of motor output variability during isometric plantar flexion. *J Neurophysiol* 110: 2592-2606, 2013.

Wegrzyk J, Fouré A, Vilmen C, Ghattas B, Maffiuletti NA, Mattei JP, Place N, Bendahan D, Gondin J. Extra forces induced by wide-pulse, high-frequency electrical stimulation: occurrence, magnitude, variability and underlying mechanisms. *Clin Neurophysiol* 126: 1400-1412, 2015.

Welch TDJ, Ting LH. A feedback model reproduces muscle activity during human postural responses to support-surface translations. *J Neurophysiol* 99:1032–8, 2008.

Werremeyer MM, Cole KJ. Wrist action affects precision grip force. *J Neurophysiol* 78:271–280, 1997.

Whang PG, Cher D, Polly D, Frank C, Lockstadt H, Glaser J. Sacroiliac Joint Fusion Using Triangular Titanium Implants vs. Non-Surgical Management: Six-Month Outcomes from a Prospective Randomized Controlled Trial. *Int J Spine Surg* 9: Article 6, 2015.

Williams ER, Baker SN. Circuits generating corticomuscular coherence investigated using a biophysically based computational model. I. Descending systems. *J Neurophysiol* 101: 31–41, 200

Windhorst U. Do Renshaw cells tell spinal neurones how to interpret muscle spindle signals? *Prog Brain Res* 80:283–294, 1989.

Wolpert DM, Diedrichsen J, Flanagan JR. Principles of sensorimotor learning. Nat Rev Neurosci 12:739–751, 2011.

Wu HG, Miyamoto YR, Gonzalez- Castro LN, Ölveczky BP, Smith MA. Temporal structure of motor variability is dynamically regulated and predicts motor learning ability. *Nature Neuroscience* 17: 312-321, 2014.

Yozbatıran N, Baskurt F, Baskurt Z, Ozakbas S, Idiman E. Motor assessment of upper extremity function and its relation with fatigue, cognitive function and quality of life in multiple sclerosis patients. *J Neurol Sci* 246(1-2):117–22, 2006.

Yu WS, van Duinen H, Gandevia SC. Limits to the control of human thumb and fingers in flexion and extension. *J Neurophysio*l 103, 278-289, 2010.